Spring 1-1-2011

The Effects of Dissolved Organic Matter on Mercury-Sulfide Interactions in Aqueous Systems

Chase A. Gerbig
University of Colorado at Boulder, gerbig@colorado.edu

THE EFFECTS OF DISSOLVED ORGANIC MATTER ON MERCURY-SULFIDE INTERACTIONS IN AQUEOUS SYSTEMS

by

CHASE A. GERBIG

B.S., Clarkson University, 2005

M.S., University of Colorado, 2008

A thesis submitted to the

Faculty of the Graduate School of the

University of Colorado in partial fulfillment

of the requirement for the degree of

Doctor of Philosophy

Department of Civil, Environmental, and Architectural Engineering

2011

This thesis entitled:

The Effects of Dissolved Organic Matter on Mercury-Sulfide Interactions in Aqueous Systems

written by Chase A. Gerbig

has been approved for the Department of Civil, Environmental, and Architectural Engineering

_____

Joseph N. Ryan, committee chair

_____

George R. Aiken

_____

Diane M. McKnight

_____

R. Scott Summers

_____

Alexis S. Templeton

Date_____

The final copy of this thesis has been examined by the signatories, and we
Find that both the content and the form meet acceptable presentation standards
Of scholarly work in the above mentioned discipline.

Abstract

Gerbig, Chase A. (Ph.D., Civil, Environmental, and Architectural Engineering)

The Effects of Dissolved Organic Matter on Mercury-Sulfide Interactions in Aqueous Systems

Thesis directed by Professor Joseph N. Ryan,

Mercury speciation with sulfide and dissolved organic matter was characterized by extended X-ray absorption fine structure (EXAFS) spectroscopy under a variety of conditions, including a range of Hg:DOM ratios, sulfide concentrations, and equilibration times. Five different DOM isolates were used to elucidate the effects of DOM characteristics on mercury speciation in sulfidic environments. In the absence of sulfide, the mercury-DOM complex was characterized by thiol-like binding with 2.4 sulfur atoms at a distance of 2.35 Å from the mercury atom. In sulfidic systems, mercury existed as a very small (<10 nm) and/or poorly crystallized metacinnabar-like particle stabilized by DOM. Typically, the mercury-sulfur bond distance was representative of metacinnabar (2.53 Å), but changes in the number of sulfur atoms coordinating mercury were representative of changes in particle size and/or crystallinity. At high Hg:DOM ratios (> 4 nmol mg^{-1}) the nanocolloidal metacinnabar-like nanocolloids were significantly larger or more ordered than at low Hg:DOM ratios (< 4 nmol mg^{-1}) that are more representative of natural environments. The size and/or degree of crystallinity decreased as the specific UV absorbance (SUVA) of the DOM stabilizing the nanocolloidal metacinnabar-like particle increased. As the sulfide concentration decrease, at a fixed Hg:DOM ratio, the mercury-sulfide particle size/crystallinity decreased such that the smallest nanoparticles were modeled as less than 1 nm in diameter. The reactivity of the nanoparticles was tracked with a tin-reducible mercury assay. Sulfide-free systems indicated that kinetic limitations drive the fraction of reducible mercury and that mercury bound to thiol groups in DOM is substantially less reactive than mercury bound to weaker carboxyl groups. The fraction of reducible mercury in sulfidic systems was substantially higher when the particles were formed with high SUVA DOM compared to low SUVA DOM. The fraction of reducible mercury decreased rapidly with equilibration time, up to about 2 h, indicating that metacinnabar-like particles form rapidly. Poorly crystallized and/or nanocolloidal metacinnabar-like particle that are stabilized by DOM are relatively reactive and may be important mercury species in natural systems.

To baby Claire,

You deserve to inherit a clean world. May this be one step towards that goal.

With all my love,

Dad

Acknowledgements

My advisors, Joe Ryan and George Aiken, patiently supported the development of this research. They simultaneously pushed me towards a goal while also allowing me to explore a variety of projects with uncertain outcomes.

Thank you to the members of my committee, George Aiken, Joe Ryan, Diane McKnight, Scott Summers, and Alexis Templeton, for reviewing my work and serving on my committee.

This work was supported by NSF grant EAR-0447386.

Chris Kim (Chapman University) and John Stegemeier (Carnegie Mellon), co-authors of the published version of Chapter 2, provided technical and logistical support for the collection and analysis of EXAFS data in Chapters 2 and 3.

Mark Marvin-DiPasquale (US Geological Survey) and Le Kieu (US Geological Survey) provided technical and analytical support with the reducible mercury measurements in Chapter 4.

John Moreau (University of Melbourne) helped secure X-ray spectroscopy beam time at the Stanford Synchrotron Radiation Lightsource.

Mark Brigham (US Geological Survey), Jeff Writer (US Geological Survey), Rob Spencer (Woods Hole Research Center) and two anonymous reviewers critically reviewed Chapter 1.

Helen Hsu-Kim (Duke University), Blaine McCleskey (US Geological Survey), and three anonymous reviewers critically reviewed Chapter 2.

The Aiken lab at the USGS was critical to the completion of this work. In particular, Kenna Butler maintained instrumentation, provided advice, and generally made most of this work possible.

The Aiken and Ryan research groups – Alison Craven, Tim Dittrich, Jarrod Gasper, Ben Kamark, Doug Latch, Blaine McCleskey, Sanjay Mohanty, Audrey Norvell, Brett Poulin, Jack Webster, and Jeff Writer – provided moral and scientific support. Brett and Alison, especially, helped with analyses, advice, and editing. It was a pleasure working with all of you.

My parents and brother encouraged my academic pursuits from a young age. Thank you for continuing to encourage me to pursue what I enjoy.

None of this work would have been possible without the endless love and support of my wife, Meagan. She gambled coming out to Colorado with me six years ago. I hope she thinks that gamble paid off. I certainly think it has turned out well!

Contents

CHAPTERS

Tables

TABLE

Figures

FIGURE

Chapter 1

The Effects of Dissolved Organic Matter on Mercury Biogeochemistry

Chase A. Gerbig[*,‡], Joseph N. Ryan[‡], George R. Aiken[⊥]

[‡]Department of Civil, Environmental, and Architectural Engineering, University of Colorado Boulder, 428 UCB, Boulder, CO 80309, United States

[⊥]U.S. Geological Survey, 3215 Marine St., Suite E127, Boulder, CO 80303, United States

*Corresponding Author: phone (585) 704-8167, email chase.gerbig@colorado.edu

Chapter published in
Advances in Environmental Chemistry and Toxicology of Mercury
Yong Cai, Guangliang Liu, and Nelson O'Driscoll, N., editors

Citation:
Gerbig, C.A., Ryan, J.N., Aiken, G.R., 2011. The effects of dissolved organic matter on mercury biogeochemistry, in: Cai, Y., Liu, G., O'Driscoll, N. (Eds.), *Advances in Environmental Chemistry and Toxicology of Mercury*. Wiley, New York, pp 259-292.

1.1 INTRODUCTION

Improved understanding of the geochemistry, fate, and transport of mercury (Hg) in aquatic ecosystems is critical for assessing its ecological and human health effects. In particular, the need to understand factors controlling the bioavailability and reactivity of mercury under environmentally relevant conditions has increased as society strives to manage resources and restore ecosystems while ameliorating the effects of mercury. It has long been recognized that the chemical forms of mercury in the water column and sediments are intimately related to its overall effects on living organisms, but a number of important questions concerning processes that control mercury reactivity, especially with regard to bioavailability for methylation, remain to be addressed. Often, the key questions involve chemistry at the aqueous–geological–microbial interface in environments that are chemically complex, such as the sediment–water interface.

Dissolved organic matter (DOM), which is ubiquitous in water, soil, and sediment environments, frequently controls a number of important environmental processes that are relevant for the cycling of metals, including mercury, in aquatic ecosystems. These processes include mineral dissolution and precipitation (Hoch et al., 2000; Waples et al., 2005), photochemical oxidation and reduction reactions (Moran and Covert, 2003; Stubbins et al., 2008), and the speciation, transport, and fate of metals (Perdue, 1998; Haitzer et al., 2003). The compounds that comprise DOM also indirectly influence the fate of metals in aqueous systems by controlling ecological processes. Some of the indirect effects of DOM include influencing pH, serving as a substrate for microbially mediated reactions (Tranvik, 1998; Findlay, 2003), controlling the depth of the photic zone (Wetzel, 2001), and influencing the availability of nutrients (Qualls and Richardson, 2003).

The most significant processes to define for understanding the chemistries of organic matter and mercury are (i) the effects of DOM on the chemical speciation and bioavailability of mercury for methylation by microorganisms and (ii) the effects of DOM on the partitioning of mercury and methylmercury (MeHg) between dissolved and particulate phases and the biota in the water column.

Until recently, very low mercury concentrations in most ecosystems have masked the strength and mechanisms of mercury–DOM interactions, resulting in a poor understanding of important environmental processes. With advances in experimental design and analytical approaches, however, new insights are beginning to emerge. In this chapter, we describe the effects of DOM on mercury biogeochemistry by addressing field-based observations and fundamental chemical interactions that drive mercury and methylmercury reactivity in the aquatic environment.

1.2 DISSOLVED ORGANIC MATTER

DOM is a complex, heterogeneous continuum of low to high molecular weight organic compounds exhibiting different solubilities and reactivities. Organic compounds can be truly dissolved, aggregated into colloids, associated with inorganic colloids, or bound to filterable particles. Historically, organic matter in natural waters has been arbitrarily divided into dissolved and particulate organic carbon based on filtration, generally through 0.45- or 0.7-μm filters (Figure 1.1). No natural cutoff exists between DOM and particulate organic matter and the distinction is operational.

The study of the composition and environmental significance of organic matter in natural waters is hampered by its inherent chemical complexity, which poses a number of analytical

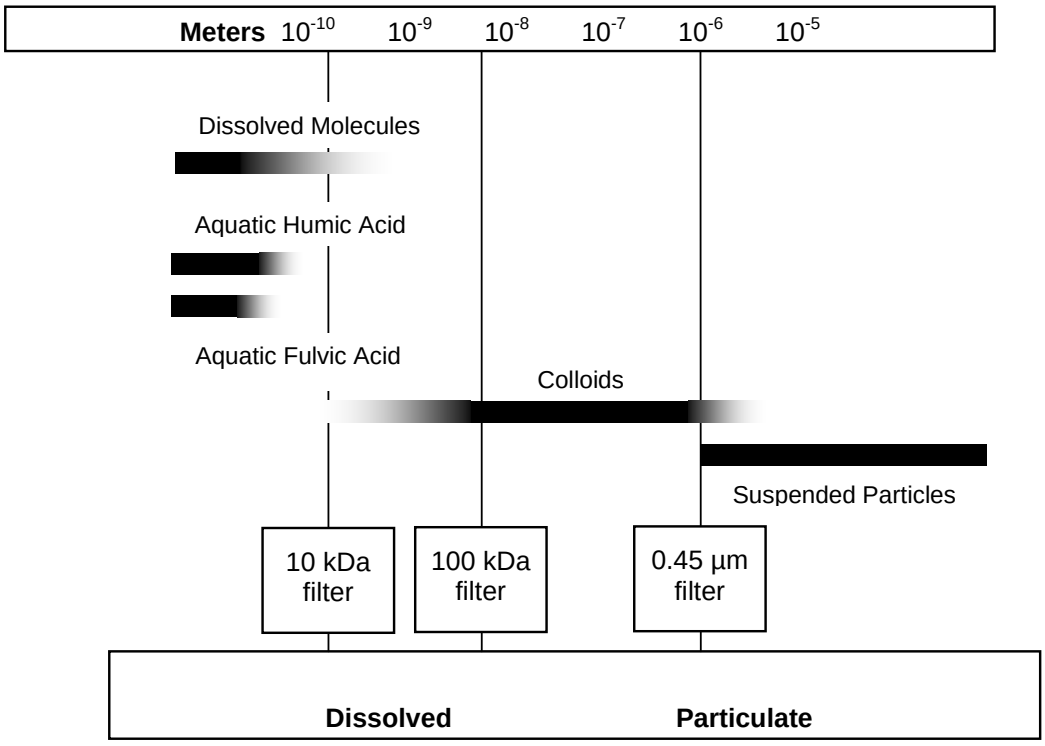

Figure 1.1. Conceptual diagram showing the size distribution of organic matter between particulate and dissolved organic carbon in natural waters.

problems in defining its reactivity (Aiken and Leenheer, 1993). Thousands of molecules are known to contribute to the composition of DOM in a given water sample (Stenson et al., 2003; Sleighter et al., 2010). The distribution of these compounds and, hence, the chemical characteristics of DOM in a water body, are influenced by the nature of source materials and the biogeochemical processes involved in carbon cycling within the entire ecosystem, including the terrestrial watershed (Aiken and Cotsaris, 1995; McKnight and Aiken, 1998; Fellman et al., 2010). In addition, for most rivers and streams, DOM concentration and composition vary as a function of hydrology (Aiken and Cotsaris, 1995; Saraceno et al., 2009; Dittman et al., 2010). The variability in the amount and nature of DOM among ecosystems, especially with respect to differences in polarity and aromatic carbon content, are significant factors in controlling DOM reactivity in a number of important environmental processes relevant to mercury biogeochemistry.

DOM is a complex mixture of molecules, and the various molecules comprising DOM react in different ways with mercury. For instance, studies of mercury binding to DOM have shown that only a small fraction of DOM molecules possess the necessary functional groups to bind Hg(II) very strongly (Haitzer et al., 2002). Other molecules that bind Hg(II) weakly can nonetheless interact with HgS(s), an important form of mercury in sulfidic environments and cinnabar mining regions, to inhibit HgS(s) precipitation or enhance HgS(s) dissolution (Ravichandran et al., 1998; Ravichandran et al., 1999; Slowey, 2010). Other molecules that may not directly interact with Hg(II) or HgS(s) can influence their fate by controlling photochemical reactions or fueling microbial activity. While certain fractions of DOM react with mercury, a large portion of DOM molecules may be inert with regard to interactions with mercury, especially under the common conditions where the concentration of DOM (milligrams per liter)

greatly exceeds that of mercury (nanograms per liter). Complicating the situation is that, for some processes, the pool of compounds comprising DOM may contain compounds that counteract each other with regard to a particular reaction. For instance, the presence of both dissolution-promoting and dissolution-inhibiting compounds has been noted for DOM interactions with bulk (Waples et al., 2005) and colloidal HgS(s) (Slowey, 2010).

Despite advances in methods to characterize DOM, serious challenges remain in defining its reactivity with mercury at the molecular level. A variety of approaches have been employed in the study of DOM in natural systems. The simplest of these, and the most common with regard to field-based studies, is the determination of dissolved organic carbon (DOC) concentration. DOC concentration alone, however, does not provide information on DOM composition. Methods used to learn more about DOM composition in field settings include the measurement of optical properties such as the absorbance of ultraviolet and visible (UV–vis) radiation and fluorescence. Optical properties are used to calculate specific ultraviolet absorbance (SUVA; Weishaar et al., 2003), spectral slope (Helms et al., 2008), and various fluorescence parameters (Fulton et al., 2004; Cory and McKnight, 2005; Fellman et al., 2010). This information is useful for assessing the nature and reactivity of DOM, although it only provides average data about the chromophores and fluorophores within a sample. Utilizing optical data is an attractive approach for studying DOM because data collection is straight forward, the data provide information about both the concentration and composition of DOM (Weishaar et al., 2003; Spencer et al., 2009), and detector systems can be employed for a variety of process-based studies and separation techniques to study DOM composition. In addition, optical data can be obtained *in situ*, allowing for the collection of high frequency environmental data in real time that can be used to better understand the influences of sources and processes

occurring within the ecosystem, even at watershed scales (Spencer et al., 2007; Saraceno et al., 2009).

A complementary approach to studying whole water samples is to isolate functionally distinct DOM fractions from whole water samples to determine the fundamental structural and chemical properties of each fraction. The properties of the fractions can be related to the biogenesis and environmental roles of these materials. Many of the methods used to characterize DOM lack sufficient sensitivity to obtain data on DOM samples at concentrations usually encountered in natural ecosystems; thus, isolation or concentration may be required (Aiken and Leenheer, 1993). Fractionation is often accomplished using solid phase extraction on hydrophobic sorbents such as XAD (Aiken et al., 1992), C_{18} (Green and Blough, 1994), and PPL resins (Dittmar et al., 2008). Fractionation on XAD resins has been employed to obtain large amounts of isolated organic matter (e.g., aquatic humic and fulvic acids; Figure. 1.1) for subsequent characterization and for use in experiments designed to elucidate chemical processes of interest. Detailed structural information has been obtained on fractionated samples by elemental analyses (Ma et al., 2001), ^{13}C nuclear magnetic resonance (^{13}C-NMR; Lu et al., 2003; Maie et al., 2006), mass spectrometry (Hatcher et al., 2001; Lu et al., 2003; Sleighter et al., 2010), and analyses for specific components of DOM such as lignin, carbohydrates, and phenols (Maie et al., 2006). Synchrotron-based techniques provide information related to chemical binding environments (i.e., extended X-ray absorption fine structure (EXAFS) spectroscopy; Xia et al. (1999), among others) or information about the redox status of key elements important for metal-binding interactions such as sulfur and nitrogen (i.e., X-ray adsorption near edge spectroscopy (XANES); Vairavamurthy et al., 1997; Vairavamurthy and Wang, 2002; Jokic et al., 2004; Prietzel et al., 2007). Finally, well-characterized, isolated fractions of DOM, such as

aquatic humic substances from different environments, have been employed in laboratory experiments designed to provide information on the chemical mechanisms driving DOM interactions with Hg(II) and HgS(s) (Ravichandran et al., 1998; Ravichandran et al., 1999; Haitzer et al., 2002, 2003; Waples et al., 2005; Deonarine and Hsu-Kim, 2009; Slowey, 2010). Application of new analytical approaches is expected to provide additional insights into the chemically complex processes driving interactions of DOM with mercury.

Ultrafiltration is another approach that has been applied to the study of both DOM (Benner et al., 1997) and mercury species in water samples (Cai et al., 1999; Babiarz et al., 2001; Choe and Gill, 2001). In this approach, dissolved samples (Figure 1.1) are fractionated based on molecular size. The resulting data provide information about the distribution of DOM, mercury, and methylmercury in the dissolved and colloidal size fractions, which is potentially useful in understanding dynamics driving export of mercury species under varying hydrologic and chemical conditions. As with all fractionation approaches, ultrafiltration is subject to potential artifacts and care is required in employing different membrane types, assigning molecular weight sizes without appropriate standardization (Aiken, 1984), and testing for suitability of membranes for mercury studies (Babiarz et al., 2001).

1.3 FIELD OBSERVATIONS

Some of the earliest articles addressing mercury in natural waters noted that DOM and mercury interact strongly to influence mercury behavior (Fitzgerald and Lyons, 1973; Andren and Harriss, 1975). In numerous studies since, strong correlations have been noted between the concentrations of total dissolved mercury and DOM in a variety of environmental settings

(Mierle and Ingram, 1991; Grigal, 2002; Balogh et al., 2004; Brigham et al., 2009; Dittman et al., 2010). Elevated fluxes of both mercury and DOM have been observed during high flow events for small catchments, which results in strong relationships between DOM (or DOC) and mercury concentrations (Figure 1.2). The relationship between mercury and DOM concentrations can vary greatly among different rivers and each system needs to be evaluated separately. Stronger correlations have been observed between mercury and hydrophobic portions of the organic matter pool (typically the fraction of DOM operationally defined as humic and fulvic substances) than between mercury and DOC concentration when hydrophobic fractions have been determined (Mierle and Ingram, 1991; Grigal, 2002; Shanley et al., 2008; Dittman et al., 2010).

For many streams and rivers, hydrologic factors controlling the export of DOM from upper soil horizons and wetlands within a watershed drive the export of mercury, and to a lesser degree, methylmercury. Changes in flow patterns in these systems are significant because upper soil horizons, riparian zones, and wetlands are rich in DOM (Cronan and Aiken, 1985) and also have greater mercury and methylmercury concentrations (Grigal, 2002). Indeed, discharge itself has been noted to be a good predictor of fluvial mercury export in numerous streams and rivers—total dissolved mercury concentrations increase as flow increases (Brigham et al., 2009; Dittman et al., 2010). Increased mercury concentrations during high flow can be attributed to the shift in soil runoff flow patterns to a more horizontal direction when soil is saturated as well as an increase in shallow subsurface and surface runoff. In addition, during periods of high flow, wetlands become inundated with water and become hydrologically connected to adjacent rivers and streams, resulting in the export of DOM, mercury, and methylmercury from these systems (Balogh et al., 2006). The importance of connectivity between organic-rich soil horizons, wetlands, and adjacent streams has been noted by Hinton et al. (1998). DOC concentrations

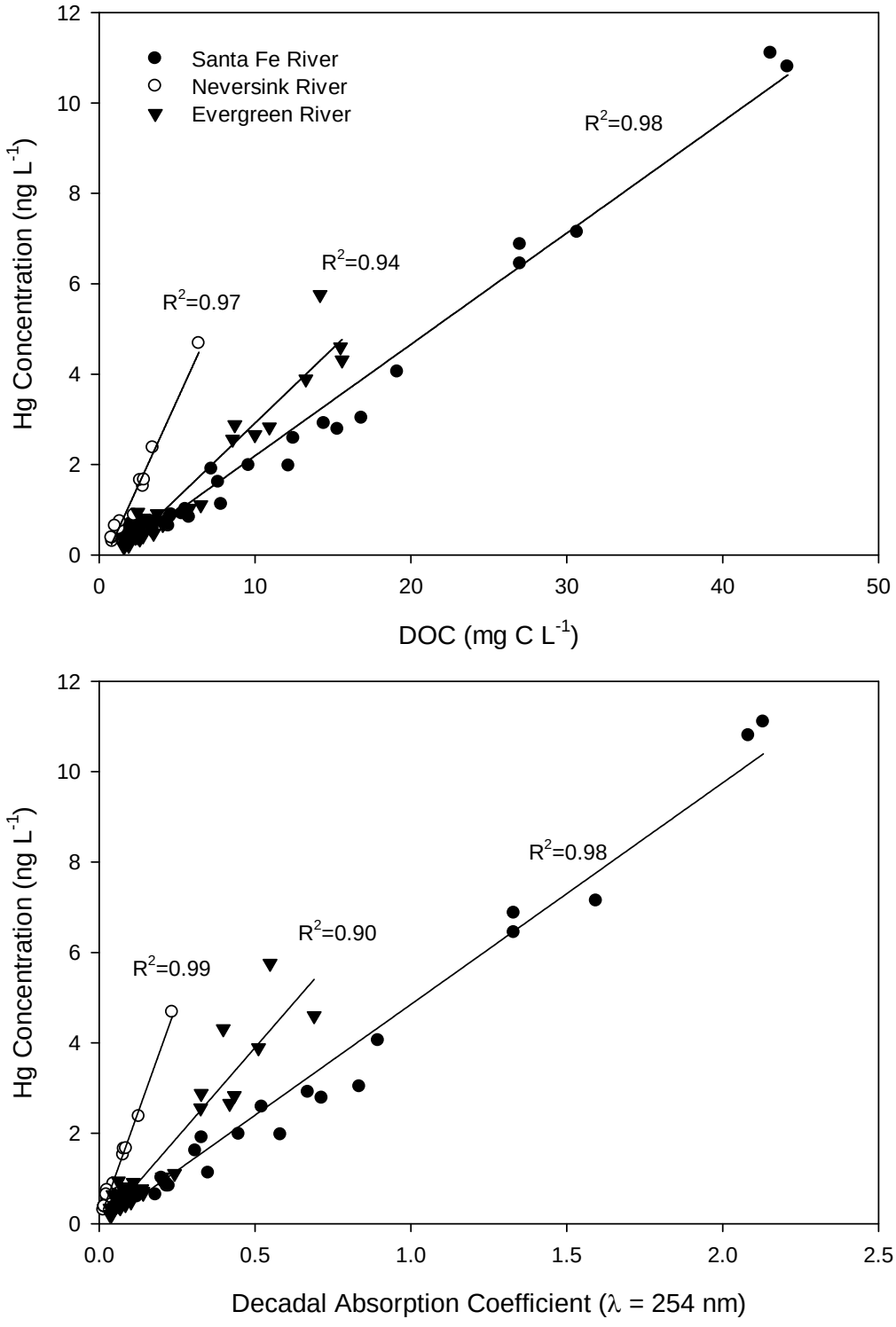

Figure 1.2. The relationship between DOC or UV absorbance (λ = 254 nm) and filtered mercury concentrations for the Neversink River, NY; Evergreen River, WI; and Santa Fe River, FL. Data from Brigham et al. (2008).

increase as higher proportions of runoff are derived from hydrologic flow paths that intersect shallow organic matter-rich soil layers and wetland ecosystems where soluble organic compounds, mercury, and methylmercury have accumulated. The shift in flow paths results in increasing DOC concentrations and compositional changes in the organic matter transported in rivers and streams. Storm events, the onset of the rainy season, or the melting of snowpack can all produce high flow conditions.

Given the strong correlations between DOM optical properties and the presence of aquatic humic substances, these optical properties are potentially useful indicators of mercury in rivers and streams. Mierle and Ingram (1991) first noted the correlation between mercury and color (Hazan units) associated with DOM in brown-water streams and were able to relate mercury export to DOM export. More recently, absorption coefficients determined at a wavelength of 254 nm were shown to be highly correlated to mercury export for a number of stream systems (Figure 1.2; Dittman et al., 2010). The use of DOM optical data to infer information about mercury concentrations in aquatic ecosystems offers some potentially important advantages. First, acquiring optical data is relatively inexpensive and requires minimal sample handling. Second, the development of optical sensors employing both absorption and fluorescence approaches permit *in situ* measurements of DOM concentrations, and by correlation, mercury, at greater frequency and during all portions of the hydrograph. For those systems where DOM and mercury concentrations are strongly correlated, *in situ* measurements can result in better determination of flux.

The relationship between DOM and mercury concentrations does not always hold. In the Everglades, for instance, correlations between DOM and dissolved mercury concentrations are weaker than those observed in northern riverine ecosystems (Hurley et al., 1998). This difference

is likely due to differences in the sources, cycling, and transport of these species in the Everglades compared to other ecosystems. The distribution of total mercury throughout the Everglades is complicated, varying spatially and seasonally (Liu et al., 2008), with concentrations of dissolved mercury generally <5 ng L^{-1} throughout the ecosystem (Hurley et al., 1998; Liu et al., 2008). DOM concentrations in the Everglades are generally greater than those found in most aquatic environments and can be generated *in situ* from existing vegetation, detritus, and peat soils or transported from other areas in the Everglades. In addition, correlations between DOM and mercury concentrations are weak-to-nonexistent for urban environments (Mason and Sullivan, 1998; Brigham et al., 2009). In these systems, wastewater discharge and urban runoff strongly influence the export and reactivity of DOM.

1.4 EFFECTS OF DOM ON MERCURY DISTRIBUTIONS BETWEEN SOLUTION AND PARTICLES

A consequence of strong interactions between DOM with Hg(II), HgS(s), and MeHg is that DOM influences the partitioning of mercury species to particles and soil organic matter such that concentrations of dissolved mercury and methylmercury increase in the presence of DOM. A number of studies have demonstrated that DOM is an important factor controlling the dissolution of mercury from

soils and sediments (Mierle and Ingram, 1991; Drexel et al., 2002). Factors that influence the concentration of dissolved mercury are significant because many of the processes (both abiotic and biotic) involved in mercury cycling in aquatic environments are hypothesized to be strongly dependent on the concentration of total dissolved mercury. For instance, Skyllberg et al. (2003)

showed that concentrations of methylmercury associated with soils and soil solutions correlated positively with the concentration of dissolved mercury in soil waters for a catchment in northern Sweden.

Field-based partitioning coefficients of mercury between the particulate and dissolved phase, described as the partitioning coefficient, are often given by an expression of the form:

$$K_d = \frac{P_{THg}/SS}{F_{THg}} \qquad \text{(Equation 1.1)}$$

where K_d is the concentration-based partition coefficient (liters per kilogram), P_{THg} is the concentration of total particulate mercury (nanograms per liter), SS is the concentration of suspended sediment (kilograms per liter), and F_{THg} is the concentration of total filterable mercury (nanograms per liter). A similar expression can be written to describe the distribution of methylmercury between dissolved and particulate forms. Reported field-based K_d values generally range from $10^{2.8}$ to $10^{6.6}$ for mercury in natural waters and from $10^{2.6}$ to $10^{5.9}$ for methylmercury (Babiarz et al., 2001; Brigham et al., 2009). The value of K_d depends, in part, on the DOM concentration. For instance, as shown in Figure 1.3a and 1.3c, K_d is generally weaker with increasing DOC concentration for a suite of rivers as reported by Brigham et al. (2009). It is assumed that at greater DOM concentrations there is less mercury association with suspended sediment.

In form, the field-based K_d is similar to traditional concentration distribution coefficients employed in the chemistry of separation science (Karger et al., 1973). The chemistry-based K_d, which is commonly employed in chromatography and other separation methods, is related to the thermodynamic distribution coefficient. As a consequence, sorption and desorption reactions

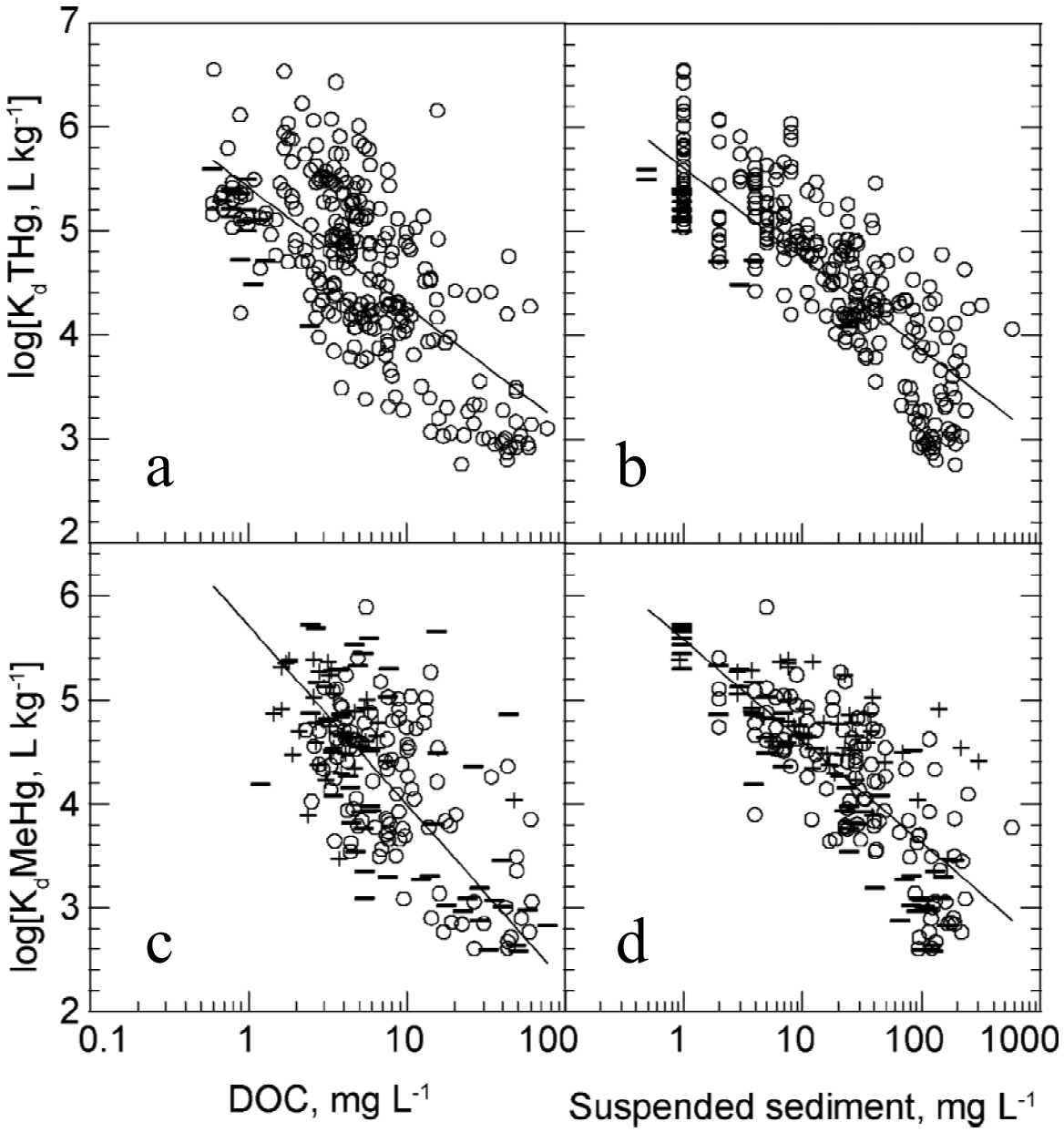

Figure 1.3. The relationship between distribution coefficients (K_d) for total mercury (THg) or methylmercury (MeHg) and DOC or suspended sediment load from a variety of stream ecosystems. Reproduced from Figure 5 of Brigham et al. (2009).

influencing K_d must be reversible. These constraints do not hold for field-based K_d values, which suffer from a number of complications. First, the nature of the particulate fraction is rarely defined. As a result, the mechanisms of interactions of mercury with the particulate surface are unknown or poorly defined. The organic matter content of the particles, soils, or sediments is a key factor controlling the ability of particles to adsorb mercury (Hammerschmidt and Fitzgerald, 2006; Marvin-DiPasquale et al., 2009); however, this parameter often goes unreported. Second, the particulate fraction, defined as the material retained on a filter (typically 0.45 μm; Figure 1.1), is a mixture of materials that interact differently with mercury. Liu et al. (2008) demonstrated different degrees of association of mercury with soils, floc, and periphyton in the Florida Everglades, whereas Marvin-DiPasquale et al. (2009) showed that the K_d values for total mercury and methylmercury in riverine sediments were a function of both DOM concentration and the amount of fine sediment material. Third, what is considered "dissolved" (<0.45 μm; Figure 1.1) also contains inorganic and organic colloidal materials that interact differently with both mercury and the surfaces of particulate materials compared to dissolved constituents (Babiarz et al., 2001; Choe and Gill, 2001). Babiarz et al. (2001) demonstrated that the colloidal phase exerted a strong control on the distribution of mercury between dissolved and particulate phases for a variety of surface waters resulting in underestimation of field-based K_d values. Lastly, K_d values are often dependent on the concentration of particles in solution, such as suspended sediment—this phenomena is known as the particle concentration effect (Figure 1.3b and 1.3d; Honeyman and Santschi, 1989; Babiarz et al., 2001). Given these factors, non-thermodynamic field-based K_d values—based only on the ratio of filterable versus particulate mercury—are not readily comparable between systems, or within the same system under

different hydrologic conditions. In addition, because the reactions driving observed K_d values are not reversible, the usefulness of these data is reduced for modeling purposes.

1.5 MERCURY BINDING STRENGTH

Mercury, a soft B-group metal, exhibits relatively weak interactions with oxygen containing ligands, moderate strength interactions with nitrogen-containing ligands, and strong interactions with sulfur-containing ligands. Consider the three ligands glycolic acid, glycine, and thioglycolic acid; they only vary in a single functional group (an alcohol, amine, and thiol group, respectively) and serve as an excellent example of the effect of a single functional group on Hg(II) binding strength. The Hg(II) binding constants *(β_2; HgL_2)* are $10^{7.05}$ (Rossotti and Whewell, 1977), $10^{19.3}$ (NIST, 2004), and $10^{43.8}$ (NIST, 2004), respectively (correcting for the slightly different temperatures and ionic strengths at which each constant was measured does not appreciably change the comparison). The oxidation state of the ligand in question is critical in predicting the strength of binding. The electron-dense binding sites created by reduced functionalities create a significantly stronger bond with Hg(II) than a binding site composed of the oxidized version of the same element. An inorganic example is quite telling—sulfate (SO_4^{2-}) is a weak ligand ($K_1 = 10^{1.3}$), whereas sulfide (S^{2-}; $K_1 = 10^{52.4}$) is extremely strong.

The distribution of metal-binding functional groups within DOM is broad. Oxygen-containing functional groups are much more abundant than nitrogen- or sulfur-containing groups. In addition, the functional groups of a single element span a range of possible oxidation states. Sulfur functional groups in organic matter range from highly reduced (e.g., thiols, R-SH) to highly oxidized (e.g., sulfonates, $R\text{-}SO_3H$) (Vairavamurthy et al., 1997). Just as the inorganic

example of sulfate versus sulfide suggests, the binding of these organic sites with respect to Hg(II) is substantially different—thiol sites exhibit very strong interactions, whereas oxidized sulfur groups are extremely weak. Further, the structural distribution of binding sites in a ligand significantly affects the ligand's ability to bind a metal (and the subsequent strength of that interaction). For this reason, chelating ligands such as ethylenediaminetetraacetic acid (EDTA) bind metals much more effectively than ligands that interact with a metal at a single site. The heteroatom(s) involved in metal binding, the oxidation state of those heteroatoms, and the steric arrangement of the metal complex are important parameters in determining the binding site orientation and strength in DOM.

While model organic ligands and inorganic examples are illustrative, they do not adequately capture the heterogeneity of DOM and the effect of DOM on mercury behavior in the environment. For instance, Ravichandran et al. demonstrated that the effects of DOM on both the dissolution (1998) and inhibition of precipitation (1999) of HgS(s) were poorly replicated by compounds known to interact strongly with mercury. In another example, some model compounds increase Hg(II) methylation because they bind Hg(II) and make it more bioavailable (Schaefer and Morel, 2009). However, increased methylation rates when mercury speciation is controlled by a model compound are inconsistent with the often observed decrease in methylation rates in the presence of DOM (Miskimmin et al., 1992; Barkay et al., 1997).

We begin the discussion of Hg(II)–DOM interactions by first considering the strength of that interaction. The measurement of metal–organic matter binding constants is most frequently quantified with a conditional stability constant. Comparison of constants can be difficult because the constants are specific to the conditions of the experiment, and are not often defined in

consistent ways, if they are defined at all. For example, Benoit et al. (2001) defined a conditional stability constant for the reaction:

$$Hg^{2+} + RXH^{n-} = HgX^{(n-1)} + H^{+} \qquad \text{(Equation 1.2)}$$

and a corresponding conditional stability constant of log K = 10.6–11.8 depending on the DOM isolate. Alternatively, Haitzer et al. (2002) defined a stability constant for the reaction:

$$Hg + DOM = HgDOM \qquad \text{(Equation 1.3)}$$

and report a corresponding conditional stability constant of log K = 23.2 ± 1.0 L kg^{-1}. The Benoit et al. (2001) example assumes some known stoichiometry, a pKa for the acid functional group, and the ability to calculate a molar concentration of DOM for the calculation of Hg(II) speciation at a given pH. The Haitzer et al. (2002) constant is a mass-based constant (hence the units liters per kilogram), and while free of some assumptions, does not account for pH. When a series of reasonable assumptions are made, and a consistent definition of the constant is used, these conditional stability constants agree, and show very strong binding between Hg(II) and DOM. Only organic thiols exhibit Hg(II) binding strengths comparable in strength to the mercury–DOM interaction observed in these two studies.

The notion that mercury binding to DOM is dominated by thiol-like sites at environmental levels of mercury is well supported in the literature. A number of binding constant studies have measured large conditional stability constants between organic matter and Hg(II) that are consistent with binding by thiols. These studies have used whole water (Hsu and Sedlak,

2003; Lamborg et al., 2003; Han and Gill, 2005; Black et al., 2007), organic matter isolated from natural waters (Benoit et al., 2001; Haitzer et al., 2002, 2003), organic matter extracted from peats (Drexel et al., 2002; Khwaja et al., 2006), and intact peats (Skyllberg et al., 2000; Drexel et al., 2002). In addition to the variety of organic matter sources and types, a variety of methods were employed including equilibrium dialysis–ligand exchange, reducible mercury titration, octanol–water or toluene–water partitioning, competitive ligand exchange–solid phase extraction, and bromide competition. The consistent conclusions between these significantly different approaches argue for the ubiquity of strong thiol-like binding sites in organic matter.

Although it is clear that some conditions give rise to the measurement of strong binding sites, there are also mercury–organic matter studies that measure weaker carboxyl- and phenol-like interactions between Hg(II) and DOM (Cheam and Gamble, 1974; Lovgren and Sjoberg, 1989; Yin et al., 1997; Haitzer et al., 2002). The predominant difference between these observations and the observations of thiol-like binding sites is the amount of mercury in solution relative to the amount of organic matter. Studies with higher ratios of mercury to DOM measure weaker binding constants. The balance between thiol-like and carboxyl-like binding sites in DOM is driven by the relative abundance of these types of sites. Using one DOM isolate, Haitzer et al. (2002) reported a carboxyl content of DOM of 5.45 mmol/g and a reduced sulfur content of DOM of 0.32 mmol/g. Even if all of the reduced sulfur was in the form of thiols that can interact with metals, there would be an abundance of weaker carboxyl sites in the DOM. However, reduced sulfur in organic matter may be in the form of thiols, dithiols, or polysulfides (with thiophenes also observed in soil humic material; Vairavamurthy et al., 1997; Solomon et al., 2003). Without cleaving sulfur–sulfur bonds, dithiols, and polysulfides in DOM are unlikely to bind with Hg(II) as strongly as thiols (Basinger et al., 1981). Thus, even quantification of

reduced sulfur is unlikely to indicate how many strong, thiol-like binding sites may be present in DOM. By measuring the conditional stability constant of Hg(II) with DOM over a wide range of Hg:DOM ratios, Haitzer et al. (2002) was able to quantify the strong binding capacity of a DOM isolate from the Florida Everglades (Figure 1.4). DOM from different environments may have slightly different strengths and capacities (Haitzer et al., 2003), but the measurements by Haitzer et al. (Haitzer et al., 2002) provide an excellent example of thiol-like versus carboxyl-like binding sites. As indicated in Figure 1.4, below 1 μg Hg (mg DOM)$^{-1}$ the stability constant is approximately 10^{23} L kg^{-1}, whereas above 10 μg Hg (mg DOM)$^{-1}$ the stability constant is approximately 10^{10} L kg^{-1}. In this study, the stability constant of 10^{23} L kg^{-1} is consistent with thiol-like binding sites, whereas the constant of 10^{10} L kg^{-1} is consistent with carboxyl-like sites. At approximately 1 μg Hg (mg DOM)$^{-1}$, the conditional stability constant begins to decrease, suggesting some carboxyl-like sites are effectively competing for Hg(II), lowering the observed stability constant, and giving an approximate cutoff for the amount of strong binding sites present in the DOM.

Several studies suggest that Hg(II) strong binding sites in soil organic matter are composed of multiple sulfur atoms (Xia et al., 1999; Khwaja et al., 2006; Skyllberg et al., 2006). If we assume that DOM binding sites are similar to soil organic matter binding sites, and two atoms of reduced sulfur are involved in binding a single Hg(II) atom, the strong binding site capacity of DOM reported by Haitzer et al. (2002) represents only 3.1% of the reduced sulfur (1.8% of the total sulfur) in the DOM isolate. Some of the reduced sulfur is likely to be present as weaker binding dithiols and polysulfides, although Xia et al. (1999) interpreted EXAFS data to indicate that there is evidence for the participation of a dithiol-like moiety in Hg(II) binding in concert with strong-binding thiol-like sites. In addition, the multiple-thiol nature of the strong

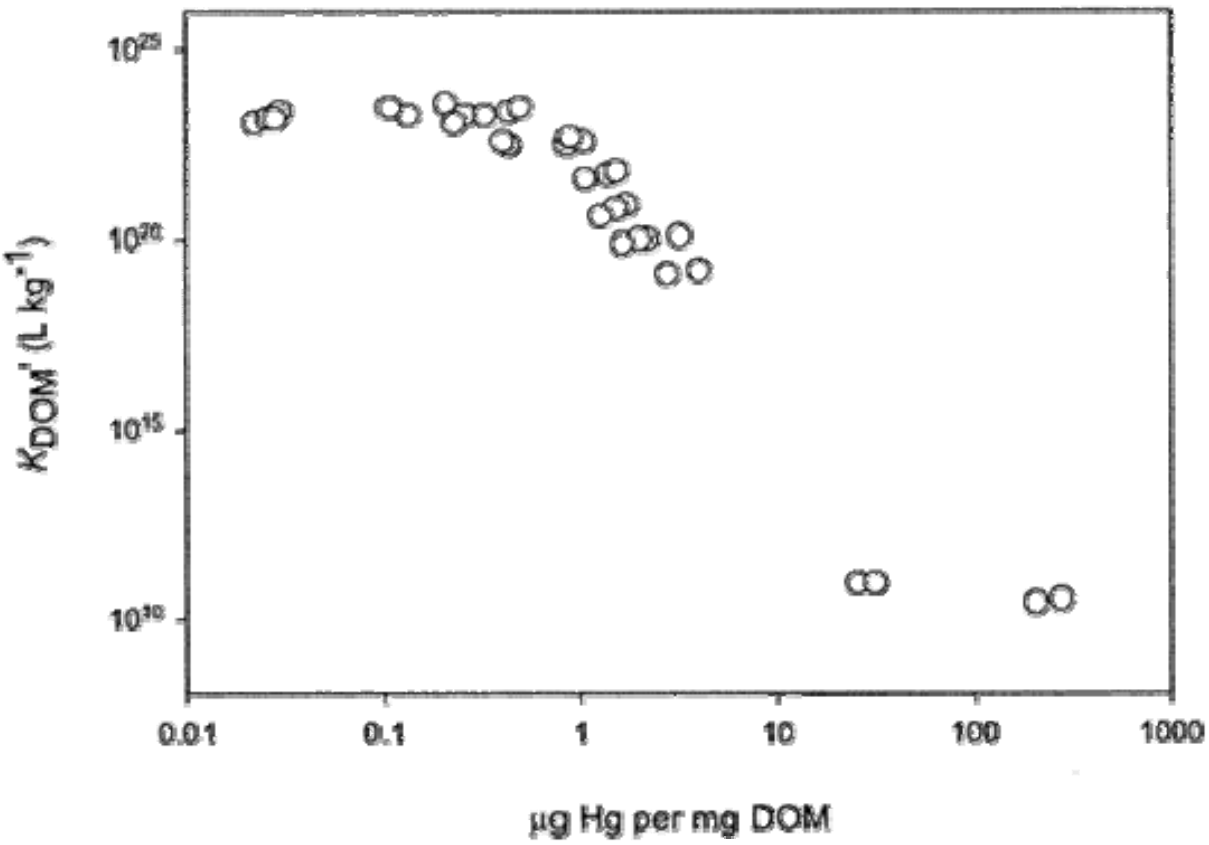

Figure 1.4. Conditional stability constant (K_{DOM}') for the binding between Hg(II) and a DOM isolate from the F1 site in the Florida Everglades versus the ratio of total mercury to DOM. Reproduced from Figure 6 of Haitzer et al. (2002).

binding sites presents the possibility that lone thiols exist in the DOM but do not strongly interact with Hg(II). Finally, a portion of the reduced sulfur pool may be sterically inaccessible to Hg(II), thus accounting for a portion of reduced organic sulfur that does not participate in Hg(II) binding. Whatever the specific stoichiometry of the Hg(II) binding sites, the Hg(II)–DOM bonds are slow to form, despite the rapid water exchange rate of the Hg(II) ion (Stumm and Morgan, 1996). The highest stability constants for Hg(II)–DOM binding are only measured after approximately 24 h of equilibration time (Gasper et al., 2007; Miller et al., 2007), which gives further evidence for strong DOM binding sites that are highly specific and difficult for Hg(II) to access.

Han and Gill (2005) expand the discussion to a broad set of DOM samples by making their own measurements of conditional stability constants and compiling the Hg(II)–DOM conditional stability constants of multiple studies under one consistent definition of a stability constant (reasonable assumptions were required for some studies). The result shows the variation in ligand concentration (DOM binding sites) as a function of the stability constant (Figure 1.5). These data depict a continuous distribution of strong Hg(II) binding sites, with the strongest sites also being the least abundant—a phenomenon that is consistent with conclusions for other metals (Town and Filella, 2000) and presents the most robust method for describing the distribution of strength and abundance of Hg(II) complexing sites in DOM observed across multiple studies.

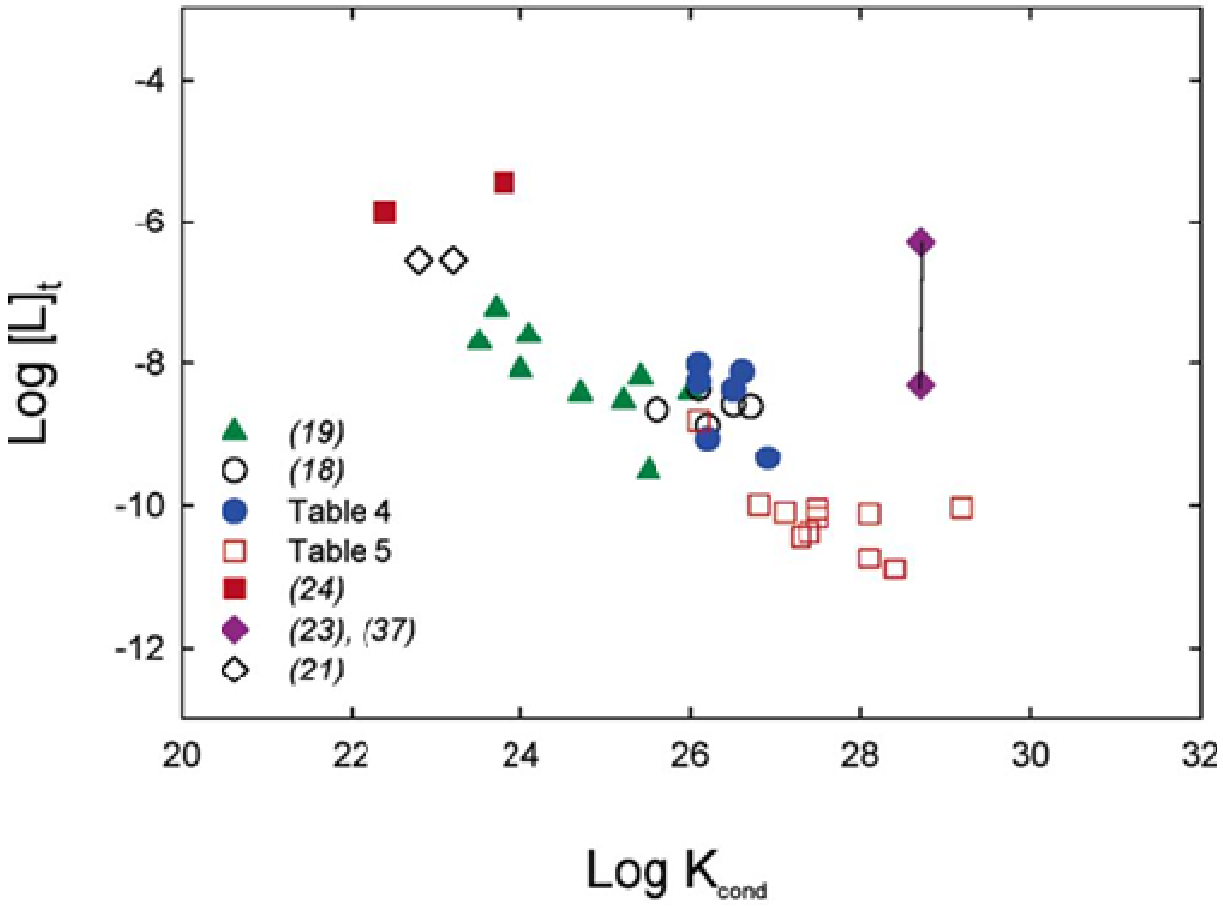

Figure 1.5. The relationship between mercury ligand concentration ($[L]_t$) and the HgL conditional stability constant (K_{cond}) for natural water samples and DOM isolates. Reproduced from Figure 4 of Han and Gill (2005); references are those within Han and Gill (2005).

1.6 MERCURY BINDING ENVIRONMENT

The first known direct observations of Hg(II) binding environments in organic matter were reported by Xia et al. (1999) using EXAFS spectroscopy. Using a humic acid extracted from an organic-rich soil horizon and the soil itself, they observed Hg(II) binding environments at mercury to reduced sulfur (S_{red}) molar ratios of 3.1:1 and 0.56:1, respectively, that are composed of oxygen functional groups as well as sulfur functional groups (Figure 1.6a and 1.6b). Hesterberg et al. (2001) built on this work by using EXAFS to examine Hg(II) binding environments as a function of the Hg:S molar ratio in a different soil humic acid extract (~70% of total sulfur was in a reduced state). In general, as the Hg:S ratio decreased from 1.7 to 0.18, the average number of sulfur atoms coordinating Hg(II) increased, while the average number of oxygen atoms coordinating Hg(II) decreased. At the lowest Hg:S ratio, approximately 90% of the Hg(II) binding by the extracted humic acid was by reduced sulfur functionalities. Further work in soils at Hg:S_{red} ratios as low as 0.01 showed three coordinating sulfur atoms—two sulfur atoms were in a linear S–Hg–S binding arrangement and a third sulfur atom stabilized the complex from a greater distance than the two linear sulfur atoms (Figure 1.6c; Skyllberg et al., 2006). At Hg:S_{red} ratios greater than 0.1, the complex was similar to what Hesterberg et al. (2001) observed with a Hg(II) complex composed of a sulfur atom as well as coordinating oxygen or nitrogen functional groups (Figure 1.6d). Overall, the results of X-ray spectroscopy examinations support the conclusions arrived at through binding constant measurements—namely that reduced sulfur functional groups play a dominant role in Hg(II) binding by organic matter when the Hg:DOM ratio is sufficiently low.

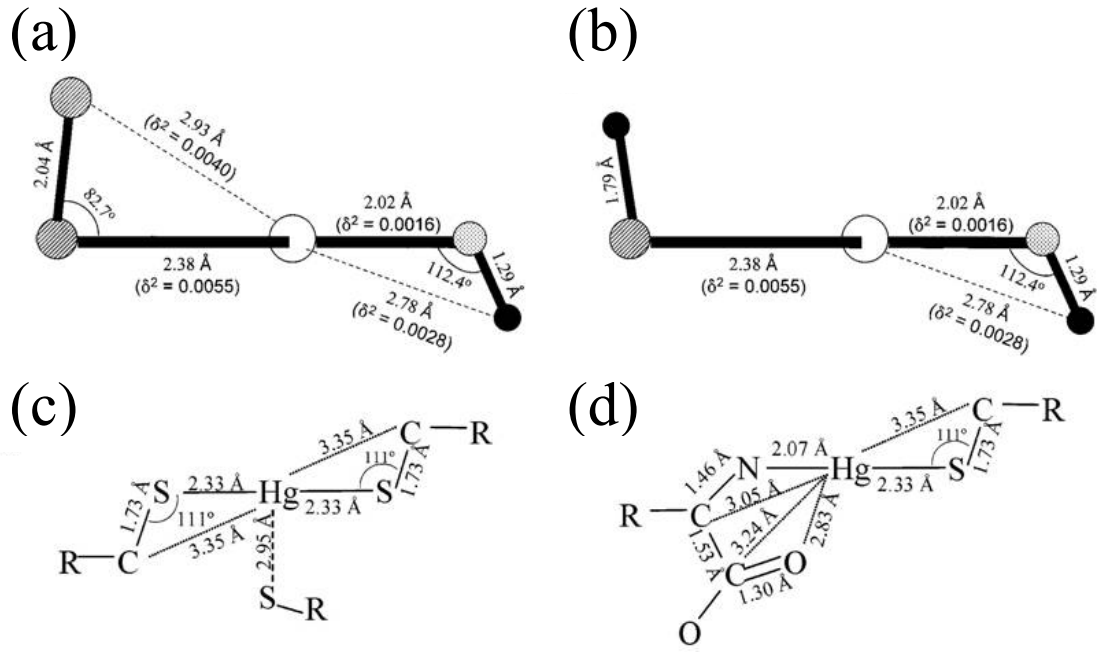

Figure 1.6. Four proposed binding arrangements for Hg(II) in soil organic matter. (a) and (b) are for Hg:S_{red} ratios of 0.56 and 3.1, respectively (open circles represent Hg, hatched represent S, dotted represent O, and closed represent C); each Hg(II) bond is presented with its length in angstroms (Å), and Debye–Waller factor (σ^2), a measure of the dynamic and static disorder of the bond. (c) and (d) represent potential structures from systems with Hg:S_{red} ratios of 0.01–0.05 and 0.10–0.40, respectively. (a) and (b) are from Xia et al. (1999); (c) and (d) are from Skyllberg et al. (2006).

The studies that make direct observations of Hg(II) binding by organic matter either use whole soil or organic matter extracted from soil rather than aquatic DOM. One of the primary differences between studying aquatic DOM and soil organic matter is the concentration. While aquatic DOM concentrations are typically on the order of milligrams per liter, these studies with soil and soil organic matter were done between 2.1 and 50 g L^{-1}, introducing the potential for intermolecular interactions that are far less likely in DOM solutions. Aggregation, in particular, may be problematic because it could shield binding sites from the bulk solution, preventing Hg(II) interactions. However, the processes that contribute sulfur to organic matter (e.g., abiotic incorporation of inorganic sulfide, biological sources) may be similar in aquatic DOM and soil organic matter from organic horizons and probably lead to similar distributions of sulfur functional groups. Aquatic DOM (Haitzer et al., 2002) and soil humic substances (Skyllberg et al., 2006) both exhibit a capacity for strong Hg(II) binding that includes <5% of all reduced organic sulfur, suggesting that reduced sulfur content of organic matter is a poor proxy for the amount of strong binding sites in both aquatic and soil environments.

1.7 METHYLMERCURY BINDING STRENGTH AND ENVIRONMENT

Studies of methylmercury binding by DOM have followed much the same trajectory as Hg(II) binding studies. Through a combination of binding constant studies at varying ratios of methylmercury to organic matter and the application of spectroscopic methods (particularly in the case of methylmercury interactions with soil organic matter), thermodynamic constants have been developed in concert with a detailed understanding of the methylmercury binding environment in organic matter.

The studies that have measured methylmercury binding by organic matter (dissolved and soil or peat derived) have measured conditional binding constants (under varying conditions, including pH) as high as approximately 10^{17} (based on the reaction RS + CH_3Hg^+ = CH_3HgSR; Karlsson and Skyllberg, 2003) and have generally concluded that the strength of the MeHg–organic matter interaction is indicative of methylmercury binding by thiol-like binding sites (Hintelmann et al., 1995; Amirbahman et al., 2002; Khwaja et al., 2010). These studies have noted pH-dependent methylmercury binding by organic matter, particularly at slightly acidic conditions of pH <5. This pH dependence is important because it suggests that thiol groups of varying pKa values and binding affinities are important at different pH values. For example, Amirbahman et al. (2002) effectively modeled methylmercury binding using a three-site model with the sites having p*K*a values of 4, 7, and 10, which are representative p*K*a values for disulfane (RSSH), cysteine, and a general thiol, respectively. Alternatively, models that use thiol sites that only have higher p*K*a values of 8.50 and 9.95 (Karlsson and Skyllberg, 2003) or only have one low p*K*a of 4.0 (Khwaja et al., 2010) have been created. The differences in the conclusions between these studies are more likely the result of experimental parameters, methods, and modeling approaches than structurally different binding environments.

In addition to identifying thiol-like methylmercury binding sites in organic matter, conditional stability constant studies have been used to examine the capacity of organic matter for binding methylmercury. The study with the highest methylmercury concentrations observed the weakest sites, but those weaker sites were still thought to be thiol-like (Amirbahman et al., 2002). The strong binding site content of organic matter for methylmercury has been identified as 0.2–13 ng MeHg $(mg\ DOM)^{-1}$ by equilibrium dialysis (Hintelmann et al., 1997) and 14.3–206 ng MeHg $(mg\ DOM)^{-1}$ by gel permeation chromatography/hydride generation inductively

coupled plasma mass spectrometry (ICP-MS) (O'Driscoll and Evans, 2000)\. The work of Amirbahman et al. (2002) was carried out between approximately 20 and 215 ng MeHg (mg DOM)$^{-1}$, which suggests that the three binding sites they modeled were at least representative of methylmercury binding at more environmentally relevant MeHg:DOM ratios. Studies at lower MeHg:organic matter ratios measure conditional stability constants that are only somewhat higher (Karlsson and Skyllberg, 2003; Khwaja et al., 2010). The range of methylmercury binding constants is much narrower than the range of observed Hg(II) binding constants (e.g., 10^{10}–10^{23} L kg^{-1} as observed by Haitzer et al. (2002) for carboxyl-like and thiol like DOM sites), likely because the range of MeHg concentrations used to study binding has been narrower and focused on the strong sites. The studies that have examined methylmercury binding constants to organic matter are generally consistent in their conclusions that thiol-like sites dominate binding, although binding constants increase as the ratio of methylmercury to organic matter decreases.

X-ray spectroscopy of MeHg bound to organic matter has confirmed the findings of binding constant studies by directly identifying sulfur-containing binding sites for MeHg in organic matter. At sufficiently low MeHg:organic matter ratios, MeHg binding environments consist of a thiol bond (Hg–S distance of 2.30–2.40 A°) and a Hg–C bond from the methyl group (Qian et al., 2002; Yoon et al., 2005). Increasing the MeHg:Sred ratio causes a transition in the average binding environment from sulfur dominated to oxygen dominated (Figure 1.7). Only at MeHg:S_{red} well below 1 does S_{red} dominate MeHg binding. This transition represents the transition from thiol-like sites to carboxyl-like sites, and supports the results of model compound studies where methylmercury is bound by a single ligand site (Schwarzenbach and Schellenberg, 1965). For comparison, a typical environmental ratio of 0.1 ng MeHg (mg DOM)$^{-1}$ is a MeHg:S_{red} ratio of about 0.002 if the DOM is 1% total sulfur and 70% of that sulfur is reduced.

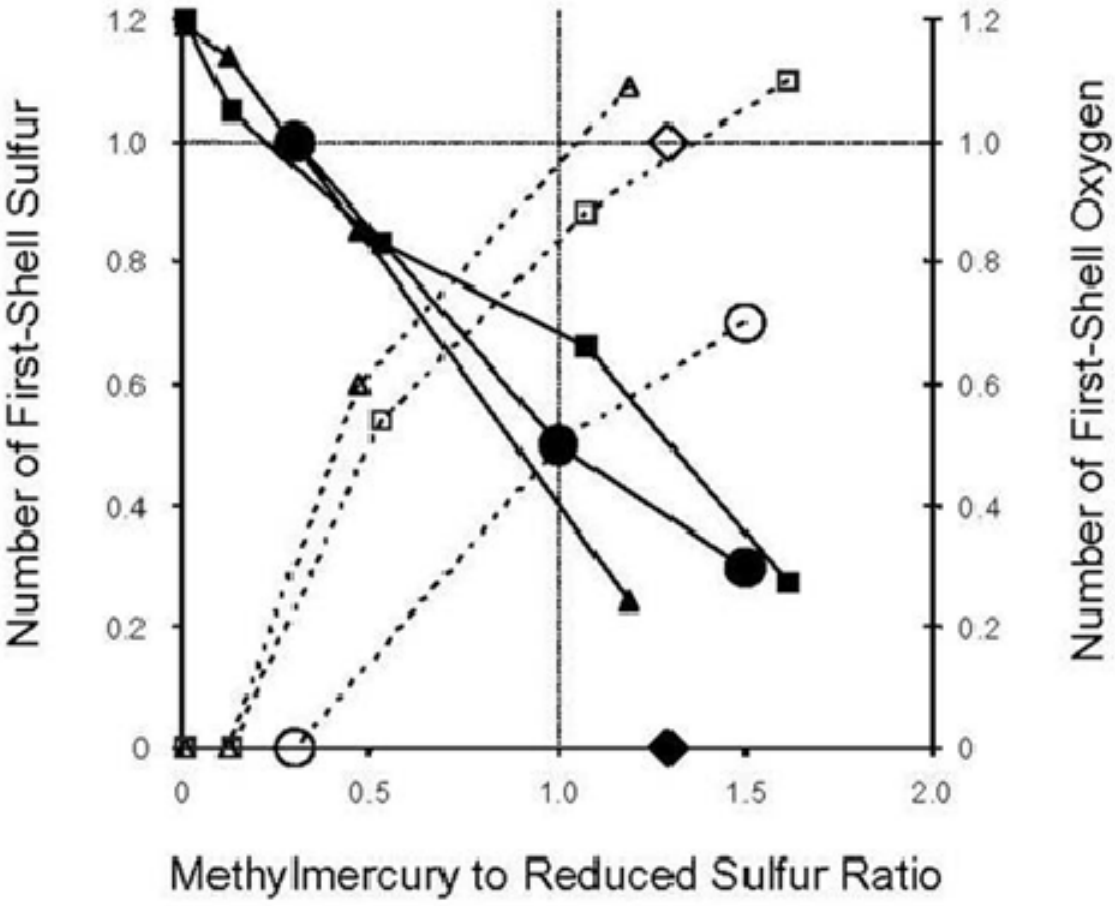

Figure 1.7. The structural variation in methylmercury binding environments with organic matter as a function of the ratio of methylmercury to reduced sulfur. Closed symbols represent the number of sulfur atoms coordinating methylmercury, and open symbols represent the number of oxygen atoms coordinating methylmercury. Reproduced from Figure 7 of Yoon et al. (2005).

Although other reduced sulfur sites exist in DOM, there is no evidence of anything other than a single thiol-like site coordinating methylmercury at environmentally relevant amounts of methylmercury.

1.8 DOM AND MERCURY MINERAL DISSOLUTION

The role of DOM in the dissolution and precipitation reactions of mercury minerals is a critical consideration in some environments. The mercury–sulfide minerals cinnabar (α-HgS) and metacinnabar (β-HgS) make up the majority of mine wastes related to mercury and gold mining (Kim et al., 2000; Lowry et al., 2004), and are also found in environments contaminated by mercury from industrial applications (Barnett et al., 1997; Boszke et al., 2008; Han et al., 2008). Laboratory experiments have demonstrated the potential for metacinnabar to form in natural systems that contain only mercury, sulfide, and DOM (Ravichandran et al., 1999; Deonarine and Hsu-Kim, 2009; Slowey, 2010). Mercury phases other than cinnabar and metacinnabar can be found in the environment (e.g., HgO, $HgCl_2$) and are typically related to mining activities (Kim et al., 2000; Rytuba, 2000), but the sulfide minerals are by far the most thermodynamically stable. It has also been speculated that precipitation of HgS minerals is the dominant mechanism of mercury loss from active mercury pools (Stein et al., 1996). Colloidal forms of HgS minerals may be the dominant transport mechanism for mercury in mining-impacted ecosystems (Slowey et al., 2005b). Mercury methylation requires transport of mercury species across microbial membranes, and that process is generally only possible with dissolved species (Morel et al., 1998). Despite the low solubility and slow dissolution of many mercury minerals, methylation has been observed in environments downstream from mercury-bearing mine deposits (Hines et

al., 2006; Holloway et al., 2009), which suggests that thermodynamic calculations of solubility may not tell the whole story of dissolution, precipitation, bioavailability, and transport.

The dissolution of cinnabar and metacinnabar in the absence of DOM (and other complicating aspects of natural environments) indicates that dissolution at circumneutral pH is thermodynamically unfavorable (i.e., low mineral solubility), kinetically slow, and similar to minerals generally considered stable (Barnett et al., 2001). In systems designed to simulate acid mine drainage (Burkstaller et al., 1975), or with uncontrolled pH (Holley et al., 2007), the dissolution rates are one to two orders of magnitude higher, but are still relatively slow. Even 14 M HNO_3 is insufficient for rapid dissolution of metacinnabar and cinnabar (Mikac et al., 2003); aqua regia is necessary to completely dissolve the minerals (Bloom et al., 2003; Kim et al., 2003).

Several mechanisms for the slow dissolution of HgS(s) in the absence of organic matter have been proposed, and depend strongly on the conditions of the system. Sulfide (Paquette and Helz, 1995), polysulfide (Jay et al., 2000), and elemental sulfur (Paquette and Helz, 1997) promote dissolution of HgS(s) under anoxic conditions. In contrast to ligand-promoted dissolution under anoxic conditions, oxidative dissolution by Fe(III) (Burkstaller et al., 1975), and dissolved oxygen (Barnett et al., 2001; Holley et al., 2007) has also been documented. The oxidized sulfur species released during oxidative dissolution provide a good measurement of mineral dissolution rates, but measurement of the dissolved mercury concentration has been shown to severely underpredict HgS(s) dissolution (Burkstaller et al., 1975; Barnett et al., 2001; He et al., 2007; Holley et al., 2007). Voltammetric evidence shows that Hg(II) is adsorbed to the HgS(s) surface after dissolution (Holley et al., 2007). It has been speculated that adsorbed Hg(II) may reduce HgS(s) dissolution rates (Barnett et al., 2001), although the introduction of chloride

to complex aqueous Hg(II) did not increase HgS(s) dissolution rates in oxygenated systems at neutral pH (Ravichandran et al., 1998; Barnett et al., 2001). Chloride did increase the rate of cinnabar dissolution in acidic Fe(III) solutions (Burkstaller et al., 1975). The general oxidative dissolution reaction proposed by Barnett et al. (2001):

$$HgS(s) + 2 \equiv S - H + 2O_2(aq) \leftrightarrow (\equiv S-)_2 Hg + SO_4^{2-} + 2H^+ \quad \text{(Equation 1.4)}$$

involves the adsorption of released Hg(II) to a sulfhydryl surface site (≡S–H) and is circumstantially supported by evidence of a SO_4^{2-}:H^+ ratio of 1:2 in HgS(s) dissolution experiments.

The introduction of DOM to cinnabar dissolution experiments generally results in increased dissolution of the mineral phase (Ravichandran et al., 1998; Waples et al., 2005; He et al., 2007). The data also suggest that not all DOM has the same degree of reactivity. DOM isolates from a range of environments showed mercury release rates from cinnabar dissolution that differed by a factor of 200 (Waples et al., 2005). Because HgS(s) dissolution is not well represented by mercury release rates, the mineral dissolution rate is difficult to compare to studies that used oxidized sulfur species to more accurately measure dissolution rates. However, both studies that measured mercury release from cinnabar dissolution in the presence of DOM isolates note undetectable mercury concentrations in the aqueous solution in the absence of DOM. Increases in DOM concentration resulted in increased dissolution of mercury from cinnabar (Ravichandran et al., 1998), but only up to a threshold after which mercury release was independent of DOM concentration (Waples et al., 2005)—a common characteristic of ligand-promoted dissolution mechanisms characterized by maximum DOM adsorption to the mineral

surface. The DOM isolates most effective at dissolving cinnabar were the most aromatic and highest molecular weight (Ravichandran et al., 1998; Waples et al., 2005) as shown in Figure 1.8. Because the rate of dissolution depended on the aromaticity of DOM, the rate of dissolution was also correlated with the SUVA of the DOM isolates (aromaticity, molecular weight, and SUVA covary in DOM samples). Despite the relationship between SUVA and cinnabar dissolution rate, SUVA was not a good predictor of the amount of DOM adsorbed to the cinnabar surface, unlike what has been observed for oxide minerals (McKnight et al., 1992; Wang et al., 1997). In addition, total sulfur and reduced sulfur contents of the DOM isolates were poor indicators of mercury release from cinnabar (Ravichandran et al., 1998; Waples et al., 2005), even though sulfur functional groups represent the strongest mercury binding sites.

The relationship between aromaticity (and other covarying properties) of DOM and mercury release during cinnabar dissolution does not itself distinguish a mechanism. It is clear from observed sulfate concentrations in excess of released mercury concentrations that oxidative dissolution is taking place and that Hg(II) adsorption to the cinnabar surface is also taking place in the presence of DOM (Ravichandran et al., 1998; Holley et al., 2007). Mercury release from cinnabar did not change in the absence of oxygen, suggesting that DOM may play a major role in the oxidative process that releases mercury (Ravichandran et al., 1998). Certain portions of the DOM pool, especially quinones, are capable of participating in redox reactions and have been found in wide-ranging environments (Cory and McKnight, 2005). It is unlikely that DOM complexation of mercury plays a major role in increasing mercury release from cinnabar. Dialysis membrane experiments that separated DOM from the cinnabar surface but allowed mercury to pass and complex with the DOM showed mercury release rates that were much lower

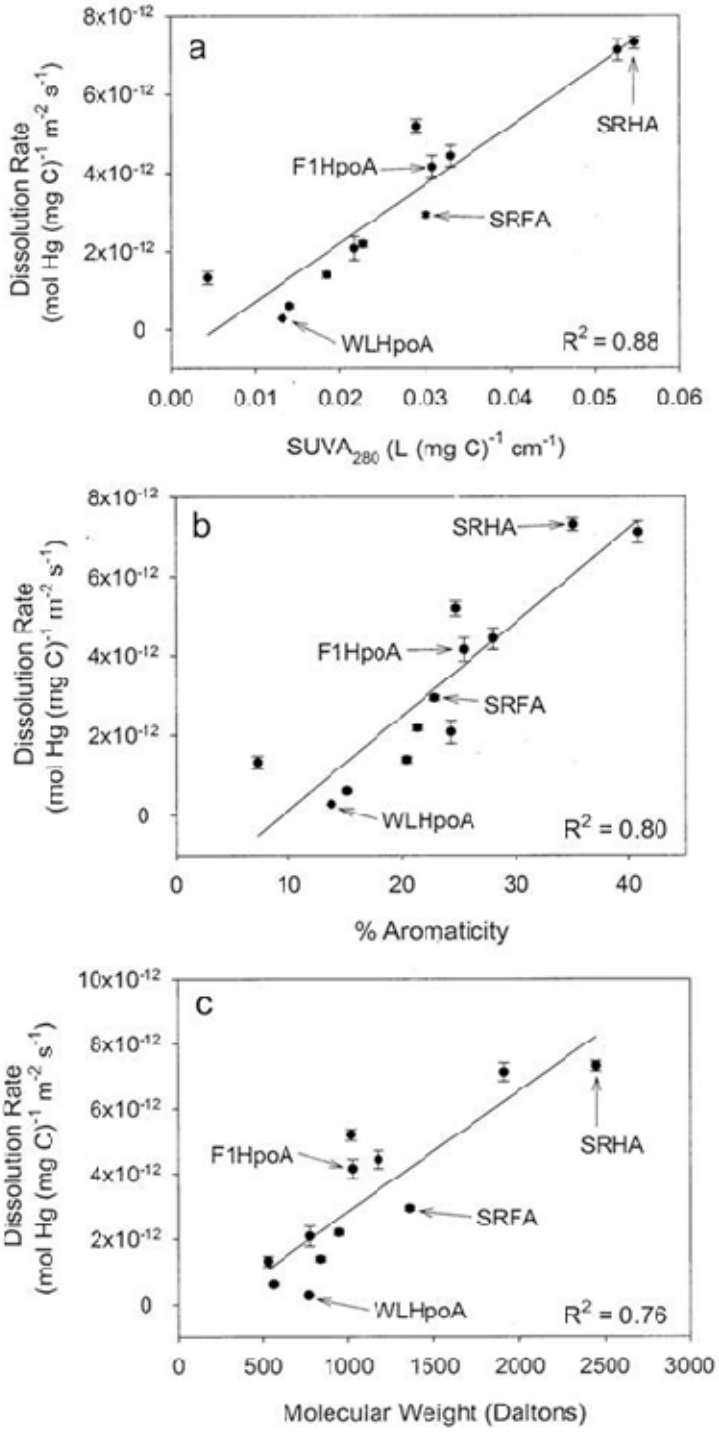

Figure 1.8. The relationship between cinnabar dissolution rate (normalized to DOC exposure and surface area) and three parameters of DOM: specific UV absorbance at 280 nm *(*SUVA280*)*, aromatic carbon, and average molecular weight. WL HPoA is the hydrophobic acid isolate from Williams Lake, MN; F1 HPoA is the hydrophobic acid isolate from the F1 site in the Florida Everglades; Suwannee River fulvic acid (SR FA) and Suwannee River humic acid (SR HA) are the fulvic acid and humic acid isolates, respectively, from the Suwannee River, GA. Reproduced from Figure 2 of Waples et al. (2005).

than when DOM was allowed to contact the cinnabar surface (Waples et al., 2005). Also, the amount of mercury released in solution was well in excess of the strong binding sites of the DOM (Waples et al., 2005). This is not to say that aqueous binding of Hg(II) has no effect on mercury release from cinnabar. Although most ligands proved inadequate for increasing cinnabar dissolution (even strong Hg(II)-chelating agents like EDTA), the thiol ligands cysteine and thioglycolic acid did increase mercury release, just not to the extent of organic matter extracted from natural waters (Ravichandran et al., 1998). It is important to note that the concentration of reduced sulfur functional groups in the experiments with model compounds were typically two orders of magnitude greater than the concentration of reduced sulfur in the DOM experiments, and only a fraction of the reduced sulfur in DOM participates in mercury binding. Although the mechanism for DOM promotion of cinnabar dissolution is uncertain, it is clear that DOM adsorption to the cinnabar surface is a critical component of the dissolution mechanism.

Waples et al. (2005) proposed that the effective rate of DOM-enhanced dissolution of cinnabar is a function of the competitive effects between two distinct pools of DOM—one that promotes dissolution and one that inhibits dissolution. The dissolution-promoting group tends to be more aromatic and readily leaves the cinnabar surface after solubilizing Hg(II) atoms. The dissolution-inhibiting group tends to irreversibly adhere to the surface and block the adsorption of the dissolution-promoting pool to surface sites. When the two pools interact with cinnabar simultaneously, and in equal quantities, dissolution rates were not drastically slower than when only the dissolution-promoting pool had access to the cinnabar. However, when the dissolution-inhibiting pool equilibrated with the cinnabar surface before the dissolution-promoting pool was introduced, the rate of cinnabar dissolution was much slower than when the dissolution-promoting pool alone was allowed access to the cinnabar surface. Organic matter derived from

terrestrial origins tends to have more of the dissolution-promoting components than organic matter derived from microbial sources.

The enhanced dissolution of cinnabar and metacinnabar in the presence of unfractionated, natural waters not only supports the role of DOM but also points to the complexities introduced by other constituents of natural waters. In particular, the presence of multivalent cations (e.g., Ca^{2+} ,Mg^{2+}, and Al^{3+}) has been shown to drastically change the dissolution of cinnabar in the presence of DOM. Surface water shows mercury release from cinnabar dissolution that is as much as two orders of magnitude lower than the same water after it is passed through a cation exchange resin, which removes multivalent cations (Ravichandran et al., 1998). Some studies have not observed increased cinnabar dissolution rates in the presence of natural waters containing divalent cations (Holley et al., 2007), but other studies have. Specifically, metacinnabar dissolution was higher in low DOC creek water compared to a DOC-free, divalent cation-free NaCl system, and high DOC water from the Florida Everglades increased dissolution to a greater extent than the low DOC creek water (Barnett et al., 2001). Both DOC-containing waters had significant Ca(II) concentrations, suggesting the effect of the DOM in these waters (about an order of magnitude increase in HgS(s) dissolution over the NaCl solution) may not have been fully realized.

1.9 DOM AND MERCURY MINERAL PRECIPITATION

In supersaturated solutions consisting of only mercury and sulfide, the precipitation of HgS(s) takes place within seconds, starting as polysulfide-like Hg–S chains, transitioning to clusters, then less crystalline metacinnabar, and finally forming crystalline metacinnabar

particles (Charnock et al., 2003). Cinnabar is the thermodynamically more favorable form of HgS(s) on the earth's surface, but metacinnabar forms first, eventually transforming into cinnabar (Potter and Barnes, 1978). Metacinnabar precipitated *in situ* (as opposed to HgS(s) transported from mining activities) has been observed in relatively few environmental sites, and those sites tend to have higher total mercury concentrations because of local mercury contamination sources (Barnett et al., 1997; Lechler et al., 1997; Beldowski and Pempkowiak, 2003; Han et al., 2008). Transmission electron microscopic images of the metacinnabar formed in the soils near Oak Ridge, TN (a mercury-contaminated site) show particles with diameters of approximately 100 nm. If these particles exist in unimpacted environments, they are likely to go undetected because of their small size (i.e., they will pass 0.2 μm and larger filters and be considered "dissolved") and the difficulty of observing small particles in low abundance in a complex matrix. Thermodynamic speciation of mercury in sulfidic systems focuses on a suite of Hg–S complexes to explain significant amounts of filter-passing mercury (Dyrssen and Wedborg, 1991; Paquette and Helz, 1997; Benoit et al., 1999b; Jay et al., 2000; Tossell, 2001; Charnock et al., 2003; Lennie et al., 2003; Bell et al., 2007), but as the Oak Ridge microscopy data show, insoluble inorganic metacinnabar particles can also pass filters and be "dissolved." Generally speaking, membrane filtration is not done consistently and introduces significant artifacts, especially when the distinction between dissolved and particulate is important (Hedberg et al., 2011). In addition, the speciation models tend to discount the effect of DOM because sulfide strongly out competes even the strongest DOM binding sites. Uncertainties in the Hg–S thermodynamic constants, which suggests metacinnabar may be a stable form of mercury at environmental concentrations (Deonarine and Hsu-Kim, 2009), inconsistent partitioning of mercury–sulfide species to octanol in the presence of DOM (Miller et al., 2007), and the

observation that metacinnabar particles in the presence of DOM partition to octanol (Deonarine and Hsu-Kim, 2009) suggest that DOM is important to mercury speciation in the presence of sulfide and that metacinnabar may be an important form of mercury to consider in natural sulfidic environments.

In the presence of sulfide and DOM, at least some fraction of the mercury takes the form of small metacinnabar particles (Ravichandran et al., 1999; Deonarine and Hsu-Kim, 2009; Slowey, 2010). Stabilization of metal–sulfide particles by organic matter is not a new observation: CuS(s) and ZnS(s) stabilization has been observed in laboratory studies (Horzempa and Helz, 1979), experimental wetlands (Weber et al., 2009), and microbial biofilms (Labrenz et al., 2000; Moreau et al., 2007). The DOM fractions most capable of stabilizing HgS(s) halted nanocolloidal growth at 1–5 nm in diameter (Deonarine and Hsu-Kim, 2009; Slowey, 2010), and stabilized aggregates on the order of 20–200 nm (Ravichandran et al., 1999; Deonarine and Hsu-Kim, 2009; Slowey, 2010). DOC concentrations as low as about 0.5 mg C/L have been shown to effectively slow the aggregation of HgS(s) particles, and increasing DOM concentrations have even stronger negative effects on the growth rate (Deonarine and Hsu-Kim, 2009). Approximately 3 mg C/L has been shown to completely stabilize HgS(s) aggregates <100 nm for at least 24 h (Deonarine and Hsu-Kim, 2009). In sulfidic systems with 10 mg/L DOM and $<10^{-4.3}$ M Hg, all of the mercury passed through a 0.1 − μm filter, but when the mercury concentration was raised to $10^{-2.3}$ M, all of the mercury was retained by the filter (Ravichandran et al., 1999), indicating that size of HgS(s) aggregates depended on total mercury concentration. Considering that environmental concentrations of mercury are on the order of 10^{-10} M, it is not surprising that sampling with 0.2 and 0.45 μm filters have identified an abundance of "dissolved" mercury, even in sulfidic systems. Membrane filtration only provides an operational definition of

dissolved species, can be problematic for other metals (Hedberg et al., 2011), and is probably also problematic in distinguishing between dissolved and colloidal forms of mercury.

Similar to the case of HgS(s) dissolution, DOM samples that are more aromatic tend to be most effective in stabilizing HgS(s) precipitates or aggregates (Ravichandran et al., 1999; Deonarine and Hsu-Kim, 2009; Slowey, 2010). The HgS(s) that precipitates in the presence of more aromatic DOM samples is less crystalline than the HgS(s) that precipitates in the presence of less aromatic DOM (Slowey, 2010). Humic and fulvic acids maintain more mercury in solution (as determined by filtration) than other fractions of the DOM pool (Ravichandran et al., 1999). A decrease in the SUVA of DOM that remains in solution after reaction with mercury and sulfide indicates the preferential loss of aromatic carbon as HgS(s) precipitates and DOM adsorbs to the surface (Ravichandran et al., 1999). The adsorption of DOM to HgS(s) surfaces leads to more negatively charged surfaces, which in turn increases electrostatic repulsion and particle stabilization (Ravichandran et al., 1999; Deonarine and Hsu-Kim, 2009). Decreased HgS(s) particle growth in the presence of DOM was observed at lower ionic strength, proving that electrostatic repulsion, which becomes more powerful at lower ionic strength, is the primary mechanism for DOM-coated HgS(s) particle stabilization (Deonarine and Hsu-Kim, 2009).

The exact mechanism for DOM adsorption to HgS(s) is somewhat unclear. Various thiol-containing model ligands have proven to be at least partially effective in preventing HgS(s) aggregation, whereas weaker inorganic and carboxyl ligands were not effective (Ravichandran et al., 1999; Deonarine and Hsu-Kim, 2009). HgS(s) particles are more negatively charged when the thiol ligands thioglycolic acid or cysteine are adsorbed to the surface, much like when DOM is adsorbed. The sulfur content of DOM was not a good predictor of DOM adsorption to cinnabar and metacinnabar (Ravichandran et al., 1998; Waples et al., 2005), although it is clear

that total sulfur is not a good predictor of Hg(II) binding capacity, and thus may not be a good predictor of surface activity either. If the mechanism of DOM adsorption to HgS(s) is similar to the adsorption on oxide minerals, the process involves ligand exchange with surface sites, and is not entirely reversible (Gu et al., 1994). A complex relationship exists between DOM binding sites, DOM aromaticity, and HgS(s) surface sites, which promotes the stability of small HgS(s) particles, although the precise mechanism is an area of ongoing study.

Including Ca^{2+} in the solutions satisfied negative surface charges of the DOM coated HgS(s) by binding with the DOM or adsorbing to the HgS(s) surface, which decreased the electrostatic charge and promoted aggregation to larger particles (Ravichandran et al., 1999). Whole water has not been shown to be especially effective in stabilizing small HgS(s) aggregates (at a mercury concentration of $10^{-4.3}$ M) until the water was run through a cation exchange resin to remove multivalent cations. Following cation exchange, the whole water was more effective than before the cation exchange at stabilizing colloidal HgS(s), but was still less effective than the hydrophobic DOM isolate from the whole water (Ravichandran et al., 1999). The promotion of HgS(s) aggregation by multivalent cations becomes less pronounced (as defined by the amount of $0.1 - \mu m$ filterable mercury) at lower total mercury concentrations (Ravichandran et al., 1999).

At this point, it is clear that DOM can simultaneously stabilize HgS(s) particles and promote the dissolution of HgS(s). These two mechanisms compete with one another in systems supersaturated with mercury and sulfide. The precipitation and redissolution of significant amounts of HgS(s) in the presence of DOM occurs somewhat cyclically over several hundred hours when the initial sulfide concentration is well in excess of the total mercury concentration (Slowey, 2010). DOM can consume excess sulfide and incorporate the sulfide into the organic

matter structure (Casagrande et al., 1979; Heitmann and Blodau, 2006). Therefore, ecosystems that have continuous input of sulfide from sulfate-reducing microbes may always have the drivers necessary for dissolution and precipitation. Increasing sulfide concentrations increases the redissolution of DOM-coated HgS(s) (Slowey, 2010). The increased redissolution may be due to the formation of mercury–sulfide complexes (Paquette and Helz, 1995; Benoit et al., 1999b; Jay et al., 2000; Lennie et al., 2003; Bell et al., 2007), or it may be due to an interaction with the DOM. At lower sulfide concentrations, more Hg(II) will be bound by the DOM. DOM interacting with Hg(II) may not be available for surface interactions, and thus cannot promote the redissolution of HgS(s). Interacting with all of these processes are multiple pools of DOM that behave differently—some promote dissolution and some inhibit it—and the extent and reversibility of surface adsorption of each pool has not been adequately studied.

The DOM-stabilized HgS(s) observed in laboratory experiments strongly resembles the HgS(s) observed in a mercury-contaminated field site. The HgS(s) formed at the field site was not perfectly crystalline, but resembled metacinnabar, and the size of the HgS(s) particles was on the order of tens of nanometers (Barnett et al., 1997). The fact that the HgS(s) from the field site was more rapidly dissolved than crystalline metacinnabar (Barnett et al., 1997; Han et al., 2008) indicates that special considerations must be made to determine mercury speciation in these environments. The thermodynamic constants for DOM-stabilized metacinnabar-like HgS(s) may not be well represented by the thermodynamic constants of crystalline metacinnabar. The kinetics of dissolution of poorly crystalline, DOM-coated metacinnabar may be significantly different from the kinetics of well-formed metacinnabar. Altered thermodynamic or kinetic properties of naturally formed nanocolloidal sized HgS(s) may also be attributable to their size,

as the interfacial energy of a small particle is likely to destabilize the particle and promote dissolution (Gilbert and Banfield, 2005).

The role that nanocolloidal HgS(s) stabilized by DOM plays in uncontaminated environments is not entirely clear. Direct observation of nanocolloidal metacinnabar-like HgS(s) in the laboratory has been limited to concentrations of total mercury that are orders of magnitude higher than typically found in uncontaminated environments. However, ultracentrifugation shows the removal of nanocolloidal mercury species (that are presumably poorly crystalline HgS(s)) when the total mercury concentration is as low as about 1 nM (Slowey, 2010). The only direct observation of nanocolloidal HgS(s) in the environment has thus far been limited to contaminated sites and sites impacted by mining activity. These studies have identified HgS(s) species as small as a few nanometers in diameter, and the aggregates of these particles only reach 200 nm on the top end. Thus, if HgS(s) is present in natural ecosystems, it has always been defined as dissolved when samples are filtered through membranes with pores sizes of 0.2 μm or greater. Low total mercury concentrations are also likely to make it difficult to find HgS(s) species in natural samples that contain significant amounts of other colloidal species. While direct observation of nanocolloidal HgS(s) has not been observed in uncontaminated natural environments, there is strong circumstantial evidence that it exists.

When considering the biogeochemistry of mercury in natural ecosystems, DOM must be considered in almost all processes from the atomic scale to the field scale. Much is known about the binding of mercury and methylmercury by DOM and the positive correlations between mercury and DOM in natural environments. However, other interactions and processes are not as well understood. Data show interesting and potentially important interactions between DOM and HgS(s) minerals, but many of the molecular scale mechanisms are somewhat unclear. Inherent

difficulties in studying DOM include the spatial and temporal variability of DOM in natural environments, and isolating the effects of a small but important subset of molecules from a large pool of organic molecules. Continued study of mercury–DOM interactions on all relevant scales will expand our ability to predict and understand mercury biogeochemistry, and will potentially help us assess and mitigate the ecological and health effects of mercury.

Chapter 2

Formation of Nanocolloidal Metacinnabar in Mercury-DOM-Sulfide Systems

Chase A. Gerbig[*,‡], Christopher S. Kim[§], John P. Stegemeier[§], Joseph N. Ryan[‡], George R. Aiken[⊥]

[‡]Department of Civil, Environmental, and Architectural Engineering, University of Colorado Boulder, 428 UCB, Boulder, CO 80309, United States

[§]School of Earth and Environmental Sciences, Chapman University, One University Drive, Orange, CA 92866, United States

[⊥]U.S. Geological Survey, 3215 Marine St., Suite E127, Boulder, CO 80303, United States

*Corresponding Author: phone (303) 541-3050, email chase.gerbig@colorado.edu

Chapter published in *Environmental Science and Technology*

Citation:
Gerbig, C.A., Kim, C.S., Stegemeier, J.P., Ryan, J.N., Aiken, G.R., 2011. Formation of nanocolloidal metacinnabar in mercury-DOM-sulfide systems.
Environ. Sci. Technol. **45**, 9180-9187.

2.1 ABSTRACT

Direct determination of mercury (Hg) speciation in sulfide containing environments is confounded by low mercury concentrations and poor analytical sensitivity. Here we report the results of experiments designed to assess mercury speciation at environmentally relevant ratios of mercury to dissolved organic matter (DOM) (i.e., <4 nmol Hg (mg DOM)$^{-1}$) by combining solid phase extraction using C_{18} resin with extended X-ray absorption fine structure (EXAFS) spectroscopy. Aqueous Hg(II) and a DOM isolate were equilibrated in the presence and absence of 100 μM total sulfide. In the absence of sulfide, mercury adsorption to the resin increased as the Hg:DOM ratio decreased and as the strength of Hg-DOM binding increased. EXAFS analysis indicated that in the absence of sulfide, mercury bonds with an average of 2.4 ± 0.2 sulfur atoms with a bond length typical of mercury-organic thiol ligands (2.35 Å). In the presence of sulfide, mercury showed greater affinity for the C_{18} resin, and its chromatographic behavior was independent of Hg:DOM ratio. EXAFS analysis showed mercury–sulfur bonds with a longer interatomic distance (2.51–2.53 Å) similar to the mercury–sulfur bond distance in metacinnabar (2.53 Å) regardless of the Hg:DOM ratio. For all samples containing sulfide, the sulfur coordination number was below the ideal four-coordinate structure of metacinnabar. At a low Hg:DOM ratio where strong-binding DOM sites may control mercury speciation (1.9 nmol mg^{-1}) mercury was coordinated by 2.3±0.2 sulfur atoms, and the coordination number rose with increasing Hg:DOM ratio. The less-than-ideal coordination numbers indicate metacinnabar-like species on the nanometer scale, and the positive correlation between Hg:DOM ratio and sulfur coordination number suggests progressively increasing particle size or crystalline order with increasing abundance of mercury with respect to DOM. In DOM-containing sulfidic systems

nanocolloidal metacinnabar-like species may form, and these species need to be considered when addressing mercury biogeochemistry.

2.2 INTRODUCTION

Predicting the fate and transport of soft, chalcophilic metals in the environment depends in part on metal speciation in the presence of sulfide and dissolved organic matter (DOM). The speciation of mercury (Hg) is of particular concern because of the potential formation of methylmercury (especially in sulfate reducing systems; Compeau and Bartha, 1985) and bioaccumulation in aquatic food chains (Benoit et al., 2003). Studies of other metals have identified nanocolloidal metal-sulfide minerals in sulfide-containing systems, including ZnS(s) in biofilms (Labrenz et al., 2000) and at microbial interfaces (Moreau et al., 2007), and CuS(s) in experimentally flooded wetlands (Weber et al., 2009) and experimental systems containing DOM (Horzempa and Helz, 1979). Colloidal mercury-sulfide minerals, particularly metacinnabar (β-HgS(s)), the low-temperature polymorph of HgS(s), have been observed in experimental systems (Ravichandran et al., 1999; Deonarine and Hsu-Kim, 2009; Slowey, 2010), and at mining (Slowey et al., 2005a) and contaminated field sites (Barnett et al., 1997) but not in natural sulfate-reducing environments with relatively low mercury concentrations and no point-source contamination (Gilmour et al., 1998). Efforts to thermodynamically model the speciation of Hg(II) primarily focus on Hg-DOM complexes in the absence of sulfide and Hg-sulfide complexes in the absence of DOM. Provided the mercury concentration is sufficiently low, DOM exhibits a high affinity for Hg(II), dominating mercury speciation in typical oxic surface waters (Benoit et al., 2001; Haitzer et al., 2002, 2003; Hsu and Sedlak, 2003; Lamborg et al.,

2003; Han and Gill, 2005). The high strength of Hg-DOM interactions at low Hg:DOM ratios, coupled with directly observed mercury soil organic matter binding sites (Skyllberg et al., 2000; Khwaja et al., 2006; Skyllberg et al., 2006), suggests DOM binding sites are thiol-like in nature, although the mercury coordination environment has never been directly observed in aquatic DOM as it has been in soil organic matter. Studies of mercury speciation with sulfide in the absence of DOM show rapid precipitation of metacinnabar (Charnock et al., 2003) and a number of dissolved mercury-sulfide complexes (e.g., $HgHS_2^-$, $Hg(HS)_2^0$, HgS_2^{-2}, HgS^0), of which neutrally charged complexes have been hypothesized to be the most important for methylation (Paquette and Helz, 1997; Benoit et al., 1999a; Benoit et al., 1999b; Tossell, 2001; Lennie et al., 2003; Bell et al., 2007).

Thermodynamic models that suggest mercury-sulfide complexes dominate mercury speciation at low mercury concentrations do not compare well with empirical observations of colloidal HgS(s) stabilized by DOM in experimental systems. In sulfide- and DOM-containing systems with a mercury concentration of 50 μM, metacinnabar particles were observed as particles or aggregates of less than 100 nm in diameter. At 50 nM Hg, the particles or aggregates, if present, were too small to remove via conventional centrifugation (Ravichandran et al., 1999). Similar work using ultracentrifugation has demonstrated removal of mercury particles from solutions with concentrations as low as 1 nM Hg, although the removed mercury was only definitely characterized as metacinnabar-like at 10 μM Hg (Slowey, 2010). The metacinnabar particles formed in the presence of DOM, sulfide, and relatively high concentrations of total mercury (i.e., >10 μM) become coated with DOM, which increases electrostatic repulsion and prevents aggregation and bulk precipitation of metacinnabar (Ravichandran et al., 1999; Deonarine and Hsu-Kim, 2009; Slowey, 2010). The direct observation of DOM-stabilized

metacinnabar particles is limited to studies conducted at mercury concentrations far in excess of most natural systems, where only the weakest DOM binding sites are relevant for mercury speciation (Haitzer et al., 2002). Speciation calculations, however, suggest that DOM-stabilized HgS(s) may also be present at common environmental levels of mercury, DOM, and sulfide (Deonarine and Hsu-Kim, 2009).

The goal of this study was to empirically determine mercury speciation in DOM-containing solutions with and without free aqueous sulfide at Hg:DOM ratios and total mercury concentrations that are lower than previously studied and span a range of Hg-DOM binding strengths. We adopted a solid phase extraction (SPE) method previously used to determine Hg-DOM binding constants to concentrate hydrophobic mercury species (Benner et al., 1997; Hsu and Sedlak, 2003) and applied this method over a wide range of Hg:DOM ratios. The speciation of mercury concentrated by SPE was subsequently examined with extended X-ray absorption fine structure (EXAFS) spectroscopy for samples of selected Hg:DOM ratios. The results presented in this paper provide direct insight into the nature of the Hg-DOM bond and on the role of DOM in mercury speciation in sulfidic environments.

2.3 METHODS

DOM Isolation. Whole water was collected from the F1 site (26º21'35"N, 80º22'14"W) in the Florida Everglades, filtered through a 0.3 µm glass fiber filter, acidified to pH 2 with HCl, and passed through a column of Amberlite XAD-8 resin according to the method of Aiken et al. (1992). The hydrophobic acid fraction (HPoA; comprised of humic and fulvic acids) was retained on the XAD-8 resin and eluted with 0.1 N NaOH. The eluate was hydrogen-saturated,

desalted, freeze-dried, and stored for later use. This DOM isolate has been used in several studies of mercury-organic matter interactions (Ravichandran et al., 1999; Haitzer et al., 2002, 2003; Waples et al., 2005). Information on the DOM source and characterization is available elsewhere (Gilmour et al., 1998; Ravichandran et al., 1998).

Experimental Solutions. Two identical sets of experimental solutions were prepared – a set for experiments only involving SPE, and a set for SPE followed by EXAFS analysis of mercury on the resin. Experimental solutions for both sets were prepared in deionized water (≥18.0 MΩ cm resistivity) and contained 0.01 M NaH_2PO_4, enough $NaClO_4$ to bring the ionic strength to 0.1 M (as calculated by Visual MINTEQ; Gustafsson, 2010) and an appropriate amount of 0.1 M NaOH to bring the pH to 6.5±0.1. DOM stock solution was prepared daily, filtered (0.45 μm Supor membranes), and added to the experimental solutions to yield a DOM concentration of approximately 10 mg L^{-1} for all SPE and most SPE-EXAFS experiments (measured range 8.6–11.3 mg DOM L^{-1}). Some of the SPE-EXAFS experiments were conducted at approximately 50 mg DOM L^{-1}. Appropriate volumes of Hg(II) stock solution ($Hg(NO_3)_2$ in 10% HNO_3) were spiked into the experimental solutions to achieve mercury concentrations ranging from 0.35 nM to 1.4 μM. The range of mercury and DOM concentrations allowed some experiments to be conducted at a Hg:DOM ratio at or below 4 nmol Hg (mg DOM)$^{-1}$, the ratio at which all strong binding DOM sites become saturated and weak-binding sites begin to also bind mercury (Haitzer et al., 2002). Sulfide-containing solutions were prepared in an oxygen-free glovebox. Sodium sulfide ($Na_2S \bullet 9H_2O$; washed before use) stock solution was prepared daily and added to experimental solutions to bring the total sulfide concentration to 100 μM. Solution bottles were wrapped with aluminum foil to prevent photoreactions and allowed to mix at room temperature on a shaker table rotating at 150 rpm. Solutions were equilibrated for 20–24 h,

which has been shown elsewhere to give sufficient time for Hg-DOM equilibration (Gasper et al., 2007; Miller et al., 2009) and Hg-DOM-sulfide equilibration (Miller et al., 2007; Deonarine and Hsu-Kim, 2009). Containers for solution/stock preparation and sampling were glass with Teflon-lined caps cleaned in a solution of 10% HNO_3 and 10% HCl (trace metal-grade) for at least 24 h and baked at 400 ºC for 4 h.

Solid Phase Extraction. The SPE portion of the experiments was carried out on glass columns (10 cm length, 0.9 cm diameter; Spectrum Chromatography) packed with 0.500 g of C_{18} resin (Supelclean ENVI-18, Spectrapor). The column fittings and lines were Teflon, except for the pump tubing, which was polyvinylchloride. Resin-free columns and tubing were cleaned with a mixture of 10% HNO_3 and 10% HCl and rinsed repeatedly with deionized water. Clean resin was prepared in the column by suspending resin in methanol and rinsing (20 min per rinse at 4 mL min^{-1}) with deionized water followed by 5 mM HCl, repeating once, and concluding with deionized water. The loss of mercury to a resin-free column (<5%) and contamination from a resin-filled column (<0.03 nM) were sufficiently small to be ignored in the subsequent SPE experiments, but there was some DOC contamination from resin-filled columns (<5 mg C L^{-1}; presumably methanol).

Cleaned and resin-filled columns were loaded with approximately 1 L of experimental solution for SPE experiments and 2 L of solution for SPE-EXAFS experiments. Experimental solutions were pumped through the cleaned resin-filled columns at a flow rate of 4.0±0.2 mL min^{-1}. After expunging the first 2 mL of solution out of each column, the remaining loaded volume was collected as effluent fractions for chemical analyses. Resin was harvested from the column following solution loading and was stored under an oxygen-free atmosphere for sulfide-containing experiments until EXAFS analysis. Mercury recovery from the SPE experiments,

including mercury in effluent fractions and mercury adsorbed to the resin, was greater than 90% of the total mercury loaded. Error in the SPE of mercury was related to errors in mercury measurements (described in next section) and depended on the amount of mercury passing through the resin. At high retentions (>90%) the error was less than 1% retained mercury, and at lower retentions (~60%) the error was approximately 4% retained mercury.

Sample Analysis. Dissolved organic carbon (DOC) concentrations were determined using a total organic carbon analyzer (OI Analytical Model 700). DOM concentrations were calculated based on DOC measurements and the carbon content of the Everglades F1 HPoA isolate (52.2% C by mass). Measurements of ultraviolet and visible light absorbance at wavelengths ranging from 254 to 412 nm were made using a UV - visible spectrophotometer (Agilent model 8453) with a 1 or 5 cm path length quartz cuvette.

Total aqueous mercury concentrations in initial and effluent samples from the SPE were determined by cold vapor atomic fluorescence spectroscopy using a Millennium Merlin mercury analyzer according to EPA Method 245.7. Analytical mercury stocks were prepared from National Institute of Standards and Technology (NIST) standard reference material 3133. Mercury standards and most samples were oxidized with 1% (v/v) $KBr/KBrO_3$ solution. High DOM and sulfide-containing samples were oxidized with 2% (v/v) $KBr/KBrO_3$ solution to ensure sufficient residual oxidant to preserve mercury after oxidation of organic matter and sulfide species. Acceptable recovery of standards was 80–120% with less than 20% relative difference in duplicate measurements. Typical recovery was 90–110% with less than 10% relative difference. The detection limit for any given run was always below 0.013 nM Hg based on three standard deviations of seven replicates of a sample with a concentration one-half of the lowest standard.

Solid phase mercury concentrations on the harvested chromatography resin were measured on a DMA-80 direct mercury analyzer (Milestone Inc.) by thermal decomposition of the sample, catalytic conversion to elemental mercury, amalgamation, and atomic absorption. Calibration was done with a series of standard reference materials obtained from NIST and Environment Canada. Acceptable recovery of the reference materials was 80–120%.

Extended X-ray Absorption Fine Structure Spectroscopy. Resin samples were prepared for EXAFS by loading 2 L of the experimental solutions outlined in Appendix Table A1 onto C_{18} resin. Two liters of solution were necessary to maximize the amount of mercury loaded onto the resin due to the relatively high concentration threshold (approximately 40 ppm Hg) needed to collect viable EXAFS spectra. The top third of the resin in the column was removed from the column and used for EXAFS analysis because solid phase mercury analysis indicated it was more concentrated than the resin in the bottom two-thirds of the column.

EXAFS data were collected on wiggler beamline 11–2 at the Stanford Synchrotron Radiation Lightsource using a Si(220) monochromator crystal in the $\varphi = 90^{o}$ crystal orientation. Mercury L_{III}-edge EXAFS spectra were collected using an aluminum coldfinger liquid nitrogen cryostat (77 K) to minimize thermal vibration and improve the quality of the spectra from low mercury concentration samples. The resin samples were loaded into aluminum holders in an oxygen-free environment, enclosed in Kapton tape, and quickly transferred to the liquid nitrogen cryostat to minimize exposure to oxygen. Spectra were collected on a 32-element high-throughput germanium detector in fluorescence-yield mode. Gallium filters were used to minimize interference from inelastic scattering. $HgCl_2$ was used as an internal standard for energy calibration of each spectrum collected.

Multiple scans (13 - 22) were collected for each sample, energy-corrected using the calibration standard, deadtime-corrected for potential loss of signal due to finite photon detection times, and averaged together. After background subtraction, the data were converted to *k*-space with a k^3-weighting and Fourier-transformed. The EXAFS spectra were fit over a *k*-range of 2.0–9.5 $Å^{-1}$ using phase and amplitude functions from model single-shell scattering paths generated in SIXPack (Webb, 2005) using Feff6l (Rehr et al., 1991). H–C, Hg–O, and Hg–S models (the only realistic first shell interactions in Hg–DOM-sulfide systems) were created and constrained based on the results of the first shell fitting of the resin samples. Mixed interactions were attempted (i.e., Hg–O and Hg–S), but single atom interactions consistently proved to be better fits. Given the limited energy range over which spectra were resolvable, only first shell fitting was successfully completed for each resin sample. The scale factor (S_0) was fixed at 0.9 for all samples, and the Debye–Waller factor (σ^2), which serves as a measure of thermal vibration and static disorder around mercury in the sample, was first allowed to float for all fits; the average Debye–Waller factor for all samples (0.007 $Å^2$) was selected and final fits fixed at this value in order to directly compare fitting results between samples.

2.4 RESULTS

DOM Solid Phase Extraction. The absorption of ultraviolet and visible (U–vis) light was used to track DOM adsorption to the C_{18} resin because small amounts of methanol contamination in effluent fractions led to erratic DOC measurements. DOM retention by the resin was consistent regardless of mercury concentration (0.35 nM–1.4 μM) or the presence or absence of sulfide (Figure 2.1a). DOM retention decreased as the volume of loaded solution increased

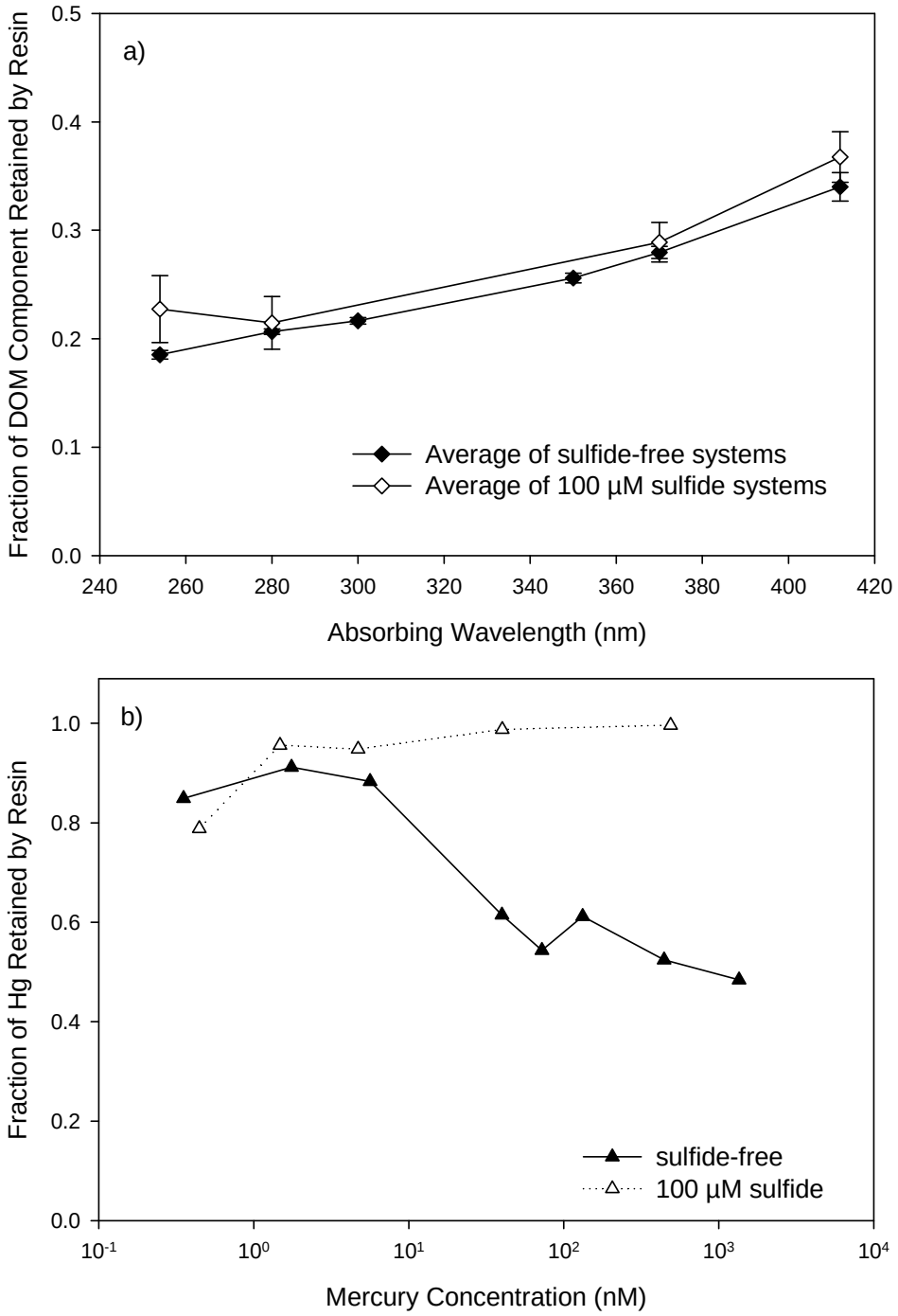

Figure 2.1. (a) The average fraction of ultraviolet and visible light-absorbing DOM components retained by the C_{18} resin as a function of absorbing wavelength for approximately 1 L of eight sulfide-free and five sulfide-containing solutions. Error bars represent 95% confidence intervals for all mercury concentrations. (b) The fraction of total mercury retained on C_{18} resin for all experiments with DOM (8.6-11.3 mg DOM L^{-1}) and with and without sulfide as a function of total mercury concentration.

(Appendix Figure A1). The fraction of UV–vis-absorbing components retained by the resin increased with increasing wavelength but was generally low – less than 35%. The UV–vis absorbance of DOM at 254 nm correlates well with the aromaticity of the organic matter (Weishaar et al., 2003), although more conjugated molecules are expected to absorb at 412 nm. These data indicate that the more conjugated organic molecules are also somewhat more hydrophobic and preferentially adsorb to the resin.

Mercury Solid Phase Extraction. Retention of mercury by C_{18} resin was a function of mercury concentration and the presence or absence of sulfide (Figure 2.1b), unlike the retention of DOM. Mercury adsorption to the column did not change substantially through the course of loading up to 1 L of sulfide-free solution (Appendix Figure A2). The overall efficiency of mercury adsorption from sulfide-free solutions was dependent on the mercury concentration in the loading solution (Figure 2.1b). At 5.6 nM Hg and below, the retention of mercury was 85–91%. At 39 nM Hg and above, retention dropped to 48–61%.

Retention curves for mercury in systems containing 100 μM total sulfide were distinctly different from those without sulfide (Appendix Figure A2). The retention of mercury from a sulfide-containing solution with 0.45 nM Hg increased as the total volume loaded increased. In contrast, at mercury concentrations from 1.5 to 490 nM, the mercury adsorption was consistently high (Figure 2.1b, Appendix Figure A2). Based on these chromatography results, the mercury species formed in the presence of sulfide at higher mercury concentrations are slightly more hydrophobic (>99% retention at 490 nM) than those formed at lower mercury concentrations (95% retention at 1.5 nM) and substantially more hydrophobic than those formed in the absence of sulfide. For all cases, greater than 60% of the mercury retained by the resin was present in the top one-third of the column based on solid phase analysis.

The 0.45 nM Hg and sulfide solution resulted in uncommon chromatographic behavior – the retention of mercury increased as the volume of solution loaded onto the resin increased. Such behavior indicates that the sorbent phase becomes more favorable for the sorption of the compound in solution as the amount of the sorbed compound increases. In the mercury-DOM-sulfide systems in this study, two components are accumulating on the resin—mercury and DOM—and either could be responsible for the increased retention of mercury with loaded volume. Either the adsorption of mercury from solution could promote the sorption of more mercury, which could potentially lead to the formation of mercury species on the resin which are not present in solution, or the adsorption of DOM from solution could promote the adsorption of more DOM along with the bound mercury species.

To determine which mechanism was responsible for the increasing mercury retention with increased loading, we compared the retention of mercury from the 0.45 nM Hg, 100 μM sulfide, 10.6 mg DOM L^{-1} solution with the retention of mercury after the resin was preloaded with DOM (Figure 2.2). A mercury-free preloading solution (9.8 mg DOM L^{-1}, 100 μM sulfide, 428 mL) was loaded onto C_{18} resin and followed with an identical solution that also contained 0.40 nM Hg. The DOM retention was identical in both systems as indicated by the retention of UV_{254} absorbing components (Figure 2.2). After preloading the resin with DOM, mercury retention was initially very high (>97%), and the retention did not increase with increased loading volume as observed in the system without preloading. We interpret the difference in mercury retention to mean that mercury-mercury interactions were not driving mercury retention because the DOM-preloaded system showed high mercury retention at the beginning of mercury loading. Had mercury retention increased with volume after DOM preloading, there would have been evidence for mercury-mercury interactions, which would have brought into question

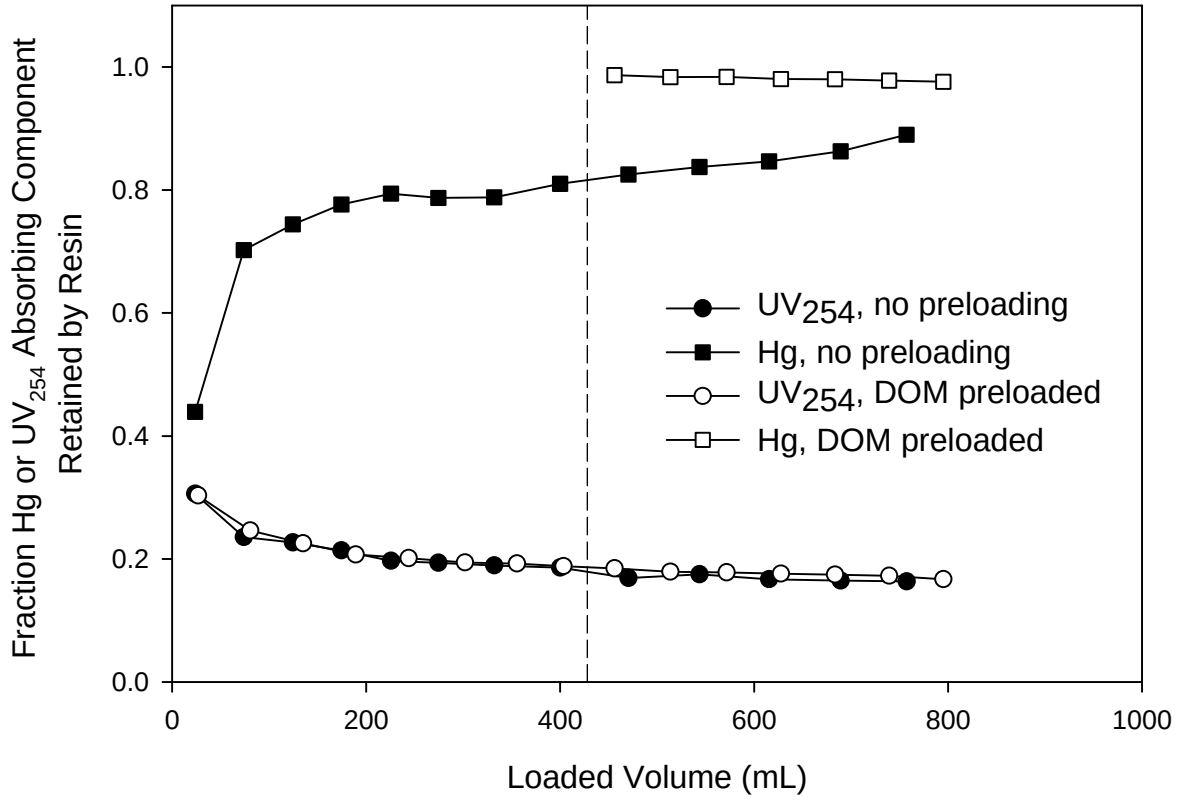

Figure 2.2. Mercury retention and DOM retention (as measured by the UV absorbance of DOM components that absorb at 254 nm) for a system without DOM preloading of the resin and a system with DOM preloading of the resin. The system without preloading (0.45 nM Hg, 10.6 mg DOM L^{-1}, 100 μM sulfide) was run as a standard chromatography experiment with the mercury-containing solution started at a loaded volume of 0 mL. The preloaded system consisted of DOM preloading (9.8 mg DOM L^{-1}, 100 μM sulfide) up to a volume of 428 mL (dashed vertical line) at which time an identical solution equilibrated with mercury (0.40 nM) was loaded on to the resin.

whether the mercury species on the resin are present in solution. Instead, we surmise that DOM served as a bridge between the mercury species in solution and the resin, and an abundance of DOM on the resin increased mercury affinity for the sorbent phase.

Extended X-ray Absorption Fine Structure Spectroscopy. Experimental and fitted mercury L_{III}-edge EXAFS spectra and the Fourier transforms corresponding to the conditions outlined in Appendix Table A1 are shown in Figure 2.3. The EXAFS spectra of the three sulfide-containing systems (Figure 2.3b, 2.3c, and 2.3d) are in phase with one another and out of phase with the sulfide-free sample (Figure 2.3a). This corresponds with the alignment of the primary Fourier transform features of the sulfide-containing samples (indicated in Figure 2.3 by a vertical line) and the misalignment of the sulfide-containing samples with the sulfide-free sample. The spectra for samples with added sulfide (2.3b, 2.3c, and 2.3d) were best modeled by a mercury–sulfur bond in the first shell with a Hg–S interatomic distance of 2.51–2.53 Å (±0.01–0.02 Å, depending on the sample; Figure 2.3). The mean sulfur coordination number for the sulfide-containing samples increased with increasing Hg:DOM ratio from 2.3±0.2 sulfur atoms at 1.6 nmol Hg (mg DOM)$^{-1}$ to 3.3±0.2 sulfur atoms at 34 nmol Hg (mg DOM)$^{-1}$. The spectra for the sample without added sulfide (2.3a) was also best modeled by mercury–sulfur bonds in the first shell, despite the absence of added sulfide in the sulfide-free system. The Hg-DOM interaction was fit with a significantly shorter Hg–S distance of 2.35±0.01 Å and a coordination number of 2.4±0.2 sulfur atoms.

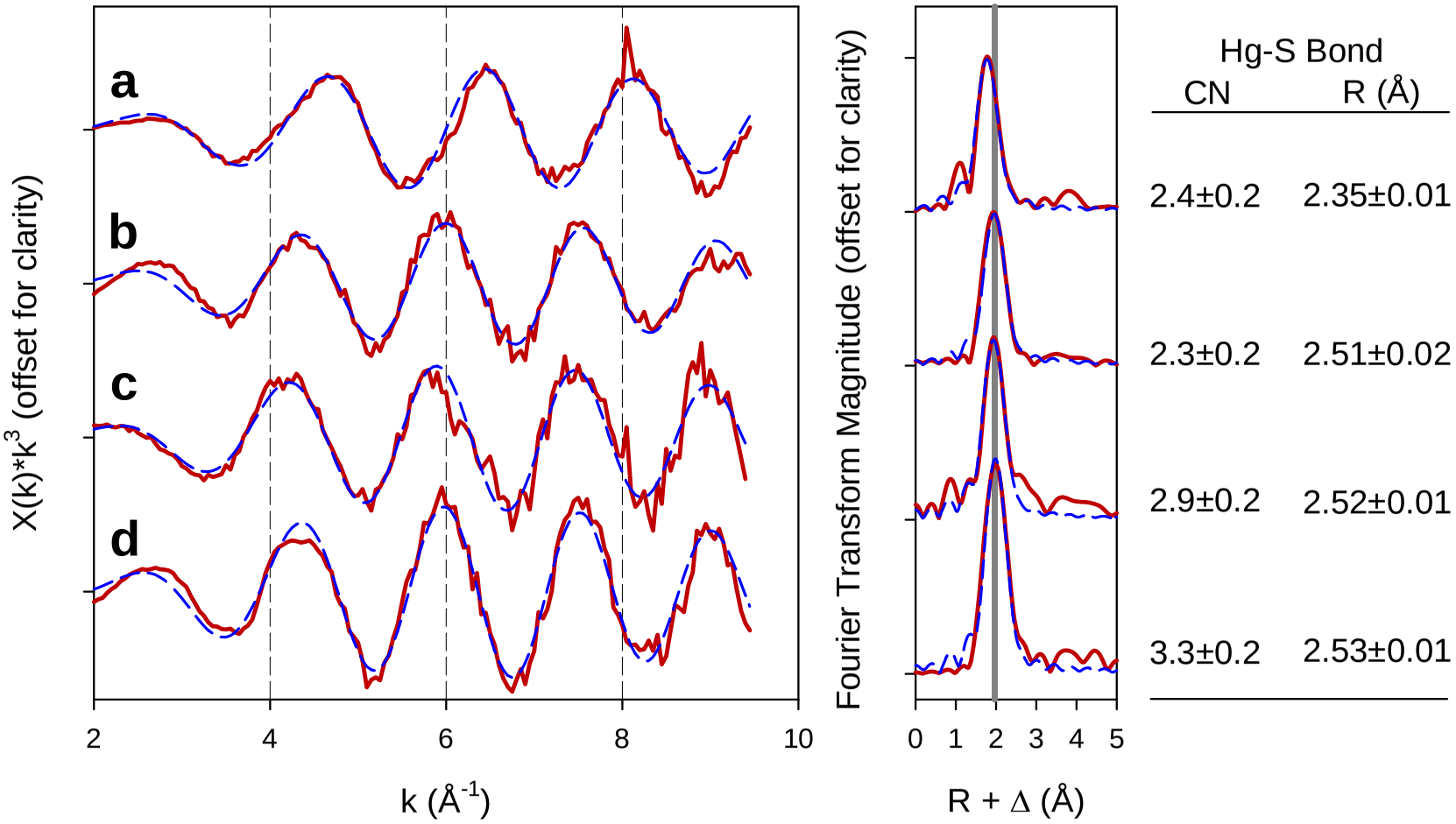

Figure 2.3. k^3-weighted mercury L_{III}-edge EXAFS, Fourier transforms, and fitting results for collected spectra (solid) and fits (dashed) for the four SPE-EXAFS samples: (a) sulfide-free at a Hg:DOM ratio of 4.0 nmol Hg (mg DOM)$^{-1}$; (b, c, and d) 100 µM total sulfide and Hg:DOM ratios of 1.9, 4.9, and 34 nmol Hg (mg DOM)$^{-1}$, respectively. Solution chemistries are summarized in Appendix Table A1. All spectra are best fit by a Hg-S interaction. The sulfur coordination number (CN) and average bond distance (R) are noted for each sample with the 95% confidence interval (2σ). The Debye-Waller factor (σ^2) was fixed at 0.007 Å^2 for all four fits.

2.5 DISCUSSION

Mercury-Dissolved Organic Matter Interactions. In the absence of sulfide and at sufficiently low Hg:DOM ratios, we hypothesized that Hg-DOM binding would be dominated by mercury – sulfur interactions because (1) Hg-DOM binding studies have measured large stability constants consistent with thiol-like sites (Haitzer et al., 2002; Lamborg et al., 2003) and (2) Hg-soil organic matter (SOM) studies using EXAFS spectroscopy have detected Hg–S bonds at low Hg: SOM ratios (Skyllberg et al., 2000; Nagy et al., 2011). We observed 2.4 coordinating sulfur atoms at 2.35 Å, which is consistent with observations of a 2–3 sulfur coordination environment in soil organic matter and soil humic acid as detected by X-ray spectroscopy (Skyllberg et al., 2006; Nagy et al., 2011) and pH titrations (Khwaja et al., 2006). The Hg–S interatomic distance is in good agreement with two-coordinate mercury binding environments observed for model thiolates (Manceau and Nagy, 2008) and represents the first known direct observation of mercury binding environments in aquatic DOM. Sulfur is a relatively minor element in DOM (1.7 wt % in the isolate used in this study), and the proportion of sulfur that is actually involved in metal binding is low (<2% of the total sulfur in this isolate based on 2.4 atoms/site and a binding capacity of 4 nmol (mg DOM)$^{-1}$). We also expect that these types of sites are ubiquitous in organic matter. Similar sites been directly observed in peats and organic matter extracted from peat (Skyllberg et al., 2000; Nagy et al, 2011). Additionally, DOM from a wide range of environments has a similar mercury binding strength at a fixed Hg:DOM ratio, which suggests that sites with similar functional groups are present in all DOM sources (Haitzer et al., 2003). The observation of multiple sulfur atoms per site suggests the possibility that these sites may be (1) of biological origin (e.g., dithiols in protein residues), (2) the result of abiotic sulfide

incorporation into DOM, or (3) the result of multiple DOM molecules coordinating a mercury atom.

The concentration requirement, or detection limit, of EXAFS restricted identification of the Hg-DOM binding environment to a Hg:DOM ratio of 4.0 nmol Hg (mg DOM)$^{-1}$, which is the strong binding capacity of the DOM isolate (Haitzer et al., 2002). Hg:DOM ratios in most environmental settings are typically a few orders of magnitude lower than this strong binding capacity. The chromatographic data suggest we can extrapolate information gained at the Hg:DOM ratio of 4.0 nmol Hg (mg DOM)$^{-1}$ to lower and more environmentally relevant Hg:DOM ratios. The sulfide-free data in Figure 2.1b show high retention of mercury (>85%) at mercury concentrations below 5.6 nM Hg and lower retention of mercury (<62%) at mercury concentrations above 39 nM Hg.

When normalized to the DOM content of each system (all had approximately 10 mg DOM L^{-1}), the transition observed between 5.6 and 39 nM Hg corresponds to a transition between 0.67 and 4.6 nmol Hg (mg DOM)$^{-1}$. Below the 4 nmol Hg (mg DOM)$^{-1}$ strong binding capacity of the DOM, the Hg-DOM complexes are significantly more hydrophobic with respect to the C_{18} resin than they are above the strong binding capacity. The transition from more to less hydrophobic complexes as the Hg:DOM ratio increases past 4 nmol Hg (mg DOM)$^{-1}$ corresponds to the transition from thiol-like Hg-DOM binding strengths to carboxyl-like Hg-DOM binding strengths (Haitzer et al., 2002). Both types of complexes are significantly more hydrophobic than the mercury-free DOM, which is only retained at about 20% as measured by the retention of UV_{254} absorbing components (Figure 2.1a). The sulfur dominated binding environment observed with EXAFS at 4 nmol Hg (mg DOM)$^{-1}$ is likely only present in a small subset of DOM molecules and that subset is more hydrophobic than other portions of the DOM

pool. The chromatography data shown in Figure 2.1b, coupled with our understanding of DOM binding strengths, suggests that the small number of DOM molecules involved in the directly observed sulfur dominated mercury binding at 4 nmol (mg DOM)$^{-1}$ persist at lower, more environmentally significant Hg:DOM ratios where EXAFS was not possible.

Mercury-Dissolved Organic Matter-Sulfide Interactions. The EXAFS spectra from all three sulfide-containing samples were best fit with a Hg–S scattering interaction at an interatomic distance of 2.51–2.53 Å (Figure 2.3). The Hg–S interatomic distance from all three samples agrees, within uncertainty, with the 2.53 Å Hg–S distance in crystalline metacinnabar (Charnock et al., 2003). The observed EXAFS spectra are not consistent with cinnabar (which has six coordinating sulfur atoms at three distinct distances; Charnock et al., 2003), polymeric HgS species that exhibit two sulfur atoms at a shorter distance of 2.30 Å (Bell et al., 2007), neutrally charged complexes (i.e., HgS(aq) and HgHSOH(aq)) with a single Hg–S interaction at less than 2.40 Å (Tossell, 2001), nor the Hg-DOM interaction described previously. In addition, simultaneous fits of a Hg–S scattering path at 2.53 Å indicative of metacinnabar and a Hg–S scattering path at 2.35 Å indicative of Hg-DOM complexes showed no significant DOM binding in systems that contained sulfide.

The Hg–S bond distance is independent of Hg:DOM ratio for the three sulfide-containing samples and matches well with metacinnabar, but the sulfur coordination numbers are all lower than the four-coordinate structure of crystalline metacinnabar. The modeled coordination numbers may be explained by imperfectly ordered crystal structures or nanosized HgS(s) particles where under-coordinated mercury atoms on the particle surface comprise a large percentage of all mercury atoms in the phase. The disorder in the particles may even be greater than the coordination number implies because the Debye–Waller factor was fixed in the EXAFS

modeling, which implicitly assumes that changes in the spectra were related to changes in coordination number and not the degree of disorder. The modeled coordination number increases with increasing Hg:DOM ratio (Figure 2.3, samples b, c, and d), which suggests that the Hg:DOM ratio is an important factor in dictating the size or crystalline order of the metacinnabar-like species. Metacinnabar-like species formed at the lowest Hg:DOM ratio resemble the initial phases of metacinnabar crystallization characterized by under-coordinated mercury atoms, whereas the metacinnabar-like species formed at the highest Hg:DOM ratio resembles a structure approaching that of bulk crystalline metacinnabar (Charnock et al., 2003). The interaction of DOM with particle surfaces and subsequent control of particle aggregation has been documented for HgS(s) (Ravichandran et al., 1999; Deonarine and Hsu-Kim, 2009; Slowey, 2010) and other metal sulfides and metal oxides (e.g., Kodama and Schnitzer, 1977; Horzempa and Helz, 1979), although the formation of HgS(s) has never been directly observed at the mercury concentrations and Hg:DOM ratios at which mercury is interacting with the strongest DOM binding sites. The strong DOM binding sites are not strong enough to prevent the formation of metacinnabar, but the metacinnabar that forms when mercury speciation is dominated by thiol sites is smaller or less ordered than metacinnabar formed at higher Hg:DOM ratios.

Our results show that the portion of DOM interacting with the surface of HgS(s) and preventing growth is more hydrophobic with respect to fractionation on C_{18} resin than the DOM that remains in solution. The majority of the DOM in our SPE experiments passed through the column, although the portions of the DOM that absorb light at higher wavelengths, which presumably represents greater conjugation, are retained on the resin to a greater degree than the bulk DOM (Figure 2.1). Additionally, the hydrophobic fraction retained by the resin favors

adsorption of metacinnabar-like mercury species (Figure 2.2). These results are supported by previously observed preferential adsorption of aromatic DOM molecules to colloidal metacinnabar particles (Ravichandran et al., 1999).

EXAFS-derived coordination numbers can be used to estimate particle sizes when they are significantly lower than the coordination number of the bulk phase and the particles are well ordered (Calvin et al., 2003; Frenkel, 2007). The less-than-ideal sulfur coordination numbers for the three metacinnabar-like samples observed in this study indicate the particles are on the nanometer scale. Referred to as the termination effect, this phenomenon arises when under-coordinated atoms on a particle surface make up a significant fraction of the atoms in the particle. The abundance of under-coordinated atoms drives down the average coordination number for particles in the diameter range of tens of nanometers or less. If we assume that the HgS(s) is perfectly crystalline, the less-than-ideal coordination numbers of the mercury–sulfur bonding observed in this study point to particles that are less than 20 nm in diameter, with the smallest (and most under-coordinated) particles as small as just a few nanometers in diameter. In a previous study designed to assess the importance of DOM in inhibiting the precipitation of metacinnabar (Ravichandran et al., 1999), metacinnabar colloids decreased in sized with decreasing mercury concentration. The minimum mercury concentration for direct characterization, 50 μM, led to metacinnabar particles or aggregates less than 100 nm as determined by centrifugation. We have now identified evidence for smaller metacinnabar-like nanoparticles at 50 nM Hg. Our results are also consistent with observations at 10 μM Hg of poorly crystalline and under-coordinated HgS(s) particles that are on the nanometer scale (Slowey, 2010).

The results presented here contrast with the conclusions of octanol–water partitioning studies which suggest neutrally charged species (e.g., HgS^0 and $Hg(SH)_2$) dominate mercury speciation in the presence of sulfide in natural environments (Benoit et al., 1999b). DOM significantly alters the octanol partitioning of Hg–S species when mercury concentrations are as low as 0.1 nM (Miller et al., 2007), and the partitioning of amorphous metacinnabar-like nanoparticles to octanol has been demonstrated at a mercury concentration of 3 μM (Deonarine and Hsu-Kim, 2009). Our study bridges the concentration divide by empirically observing a metacinnabar-like species at an intermediate mercury concentration, which chromatography suggests is present at even lower mercury concentrations than could be directly observed with EXAFS. Mercury-sulfide speciation modeling predicts metacinnabar will form at the intermediate and high mercury concentrations used in this study. However, the speciation modeling is ambiguous at the low concentrations in this study below about 4 nM Hg because on the uncertainty in thermodynamic constants (constants for the modeling reproduced in Appendix Table A2). If metacinnabar is not formed below 4 nM, then speciation modeling predicts hydrophilic complexes (primarily $HgHS_2^-$) will dominate in these systems (quantitative speciation presented in Appendix Figure A3). Hydrophilic complexes will not be retained by the C_{18} resin. Our data show the mercury species in sulfidic systems are consistently retained at high levels by the resin, which indicates that the HgS(s) observed at higher mercury concentrations also dominates at lower, more environmentally relevant concentrations. Modeling efforts elsewhere have shown that uncertainty in thermodynamic constants, particularly the metacinnabar solubility product, makes mercury speciation difficult to predict at environmentally relevant concentrations (Deonarine and Hsu-Kim, 2009). Our results provide empirical evidence

that a discrete inorganic metacinnabar-like phase is stabilized by dissolved organic matter at mercury concentrations and Hg:DOM ratios that are more representative of natural systems.

Environmental Implications. Conventional filtration methods are insufficient to diagnose the presence or absence of nanosized particles in the environment; however, the potential exists to use a chromatographic approach to detect the presence of mercury-containing nanoparticles. Hsu-Kim and Sedlak (2005) noted the adsorption of mercury species to C_{18} resin when a wastewater effluent sample was exposed to sulfide. As that study and another (Deonarine and Hsu-Kim, 2009) have noted, some of those mercury species are not labile to a strong competing ligand, such as glutathione, whereas dissolved complexes with organic matter are labile. Now that direct observation of mercury speciation has identified metacinnabar (or at least, a metacinnabar-like phase) as a potential source of that nonlabile portion at lower mercury concentrations approaching environmentally relevant concentrations, the potential exists to identify similar species in natural anoxic waters with a chromatographic approach.

Knowledge of the speciation of mercury is paramount in assessing the extent and kinetics of the biologically driven conversion of mercury into methylmercury. While this study does not attempt to determine the role of speciation in methylation, it provides evidence that sulfate-reducing microbes, which typically reside in sulfide- and organic matter-rich environments, are likely to be exposed to disordered, nanoparticulate metacinnabar stabilized by dissolved organic matter. Our results are consistent with the observation of poorly crystalline, nanometer-scale HgS(s) particles in a mercury contaminated site (Barnett et al., 1997) and illuminate the role of DOM in HgS(s) formation and stabilization. The mechanism of that stabilization, the rate of nanoparticle growth and aggregation, and the role DOM-coated nanoparticulate metacinnabar plays in methylation are critical areas for further research. In addition, the thermodynamics of a

nanoparticulate phase are not necessarily well represented by thermodynamic constants of the bulk phase (Gilbert and Banfield, 2005), and thus mercury speciation models may need to account for disordered nanoparticulate HgS(s).

Chapter 3

Effects of Kinetics, Sulfide Concentration, and Dissolved Organic Matter Characteristics on the Size and Structure of Metacinnabar-like Nanoparticles in Mercury-Dissolved Organic Matter-Sulfide Systems

Chase A. Gerbig[*,‡], Christopher S. Kim[§], John P. Stegemeier[§], Joseph N. Ryan[‡], George R. Aiken[⊥]

[‡]Department of Civil, Environmental, and Architectural Engineering, University of Colorado Boulder, 428 UCB, Boulder, CO 80309, United States

[§]School of Earth and Environmental Sciences, Chapman University, One University Drive, Orange, CA 92866, United States

[⊥]U.S. Geological Survey, 3215 Marine St., Suite E127, Boulder, CO 80303, United States

*Corresponding Author: phone (585) 704-8167, email chase.gerbig@colorado.edu

Manuscript to be submitted to *Environmental Science and Technology*

3.1 ABSTRACT

Understanding mercury (Hg) speciation in systems containing dissolved organic matter (DOM) and sulfide is necessary for predicting the fate and transport of mercury in the environment. We have characterized metacinnabar-like nanoparticles in Hg-DOM-sulfide systems by concentrating mercury from aqueous solutions containing a suite of DOM isolates on a chromatography resin, and examining the mercury binding environment with extended X-ray absorption fine structure (EXAFS) spectroscopy. The amount of time that mercury equilibrated with DOM before sulfide exposure (12-142 h) and the amount of time that the Hg-DOM-sulfide system was allowed to equilibrate (4-121 h) did not significantly change the structure of the metacinnabar-like species. In all cases with variable equilibration times, metacinnabar-like nanoparticles were under-coordinated with respect to sulfur, although the mercury-sulfur bond distances were consistent with metacinnabar. Significant changes in the sulfur coordination number were observed with variable sulfide concentrations (1-100 μM). The changes in sulfur coordination number suggest that the metacinnabar-like nanoparticles were significantly smaller or more disordered at lower sulfide concentrations. The size or disorder of metacinnabar nanoparticles was also correlated with the specific ultraviolet absorbance (SUVA) of the DOM isolate in the system. DOM isolates of higher SUVA stabilized metacinnabar-like nanoparticles that were smaller or more disordered than those stabilized by DOM isolates of low SUVA. Sulfide concentration and DOM composition are important factors for predicting the structural order of metacinnabar-like nanoparticles formed in Hg-DOM-sulfide systems.

3.2 INTRODUCTION

Mercury is an excellent example of the difficulties associated with understanding metal behavior in natural systems and the importance of resolving those difficulties so that we can address the serious environmental and human health effects of certain metals. Mercury contamination is widespread, and microbes in many natural systems methylate mercury, which creates a potent neurotoxin that has negative implications for human health (Mason et al., 1995; Morel et al., 1998). One of the key steps in the methylation process is microbial uptake of mercury from solution, but there is an incomplete understanding of the uptake process (is it active or passive?) and the forms of mercury that are present in solution and available for methylation (Schaefer et al., 2011).

The speciation of mercury in aquatic environments with low mercury concentrations depends on several factors, including the impact of dissolved organic matter (DOM), and the presence of sulfide. DOM is ubiquitous in environmental systems and it controls mercury speciation in the absence of sulfide by strongly binding aqueous mercury (Haitzer et al., 2002, 2003; Hsu and Sedlak, 2003; Lamborg et al., 2003; Black et al., 2007). Mercury speciation in the presence of sulfide is more complex. The uncertainty in thermodynamic constants for mercury-sulfide species leads to ambiguous conclusions about the presence of metacinnabar (β-HgS(s)), the low temperature polymorph of HgS(s) (Benoit et al., 1999b; Miller et al., 2007; Deonarine and Hsu-Kim, 2009). Laboratory experiments have demonstrated that metacinnabar precipitation is likely, even at low mercury concentrations (Ravichandran et al., 1999; Deonarine and Hsu-Kim, 2009; Slowey, 2010; Gerbig et al., 2011) although precipitated metacinnabar has only been definitively identified in contaminated sites with high mercury concentrations (Barnett et al.,

1997). One explanation for the discrepancy between field and laboratory observations of metacinnabar is that DOM complicates identification of metacinnabar particles in natural systems.

DOM generally slows or halts particle aggregation by adsorbing to the surface of particles, which increases electrostatic repulsion and steric hindrance between particles, and slows aggregation (Horzempa and Helz, 1979; Liang and Morgan, 1990; Tiller and O'Melia, 1993). Preferential adsorption of the hydrophobic portion of organic matter to mineral surfaces has been demonstrated in the field (McKnight et al., 1992) and in the laboratory (Wang et al., 1997). Aggregates of metal sulfides precipitated in the presence of hydrophobic organic matter can be stabilized at 100 nm or less in diameter, and the primary particles that comprise the aggregates are significantly smaller than 100 nm (Ravichandran et al., 1999; Lau and Hsu-Kim, 2008; Deonarine and Hsu-Kim, 2009; Deonarine et al., 2011). Some evidence exists to suggest that the primary particles are not well-crystallized (Slowey, 2010; Gerbig et al., 2011). Furthermore, particles that form at high metal-to-DOM ratios are more crystalline than those that form at low ratios (Gerbig et al., 2011). Most environmental systems where mercury is a concern have very low Hg:DOM ratios (Grigal, 2002), but techniques to identify and characterize nanoparticles in environmental systems are generally lacking (Howard, 2010). We know that organic matter has significant effects on particle behavior at high metal-to-DOM ratios, but relatively little is known about the effects of DOM at lower Hg:DOM ratios.

In this paper, we used a solid-phase extraction/extended X-ray absorption fine structure (EXAFS) spectroscopy technique (Gerbig et al., 2011) to examine four variables that are potentially important to the size and crystallinity of HgS(s) formed in the presence of DOM: (1) reaction time between mercury and DOM before sulfide addition, (2) reaction time between

mercury, DOM, and sulfide after sulfide addition, (3) sulfide concentration at fixed Hg:DOM ratios, and (4) the properties of the DOM present during HgS(s) formation. The solid phase extraction concentrates mercury from aqueous solutions, and EXAFS examines the local binding environment of mercury atoms within the HgS(s). All solutions had Hg:DOM ratios well below those used in other studies of metal-sulfide precipitation in the presence of organic matter. We quantified the changes in HgS(s) size and crystallinity as a function of kinetics, sulfide concentration, and DOM characteristics at conditions that more closely resemble natural systems.

3.3 METHODS

Solution composition. Aqueous solutions of mercury, DOM, and sulfide were prepared in deionized water (≥18 MΩ cm) which contained a phosphate buffer (10 mM) for a final pH of 6.5±0.1 and enough sodium perchlorate to bring the ionic strength to 0.1 M as calculated by Visual MINTEQ (Gustafsson, 2010). Sodium phosphate and sodium perchlorate stocks were filtered through 0.45 μm polyethersulfone membranes (Pall Corporation, Supor) before addition to the deionized water. DOM stock solutions (200 mg L^{-1}) were prepared gravimetrically, 0.45 μm-filtered, and diluted into the buffered water. Following DOM addition, Hg(II) stock solution ($Hg(NO_3)_2$ in 10% HNO_3) was added to bring the total mercury concentration to the desired level. After mercury and DOM were allowed to equilibrate for a period of time (t_1), sulfide was added to the sample from a stock solution ($Na_2S{\cdot}9H_20$, washed with deionized water before use). The sulfide-amended solution was allowed to equilibrate for another period of time (t_2) before it was run through a solid phase extraction column to extract the mercury species. Sulfide and

DOM stock solutions were prepared daily and mercury stock solutions were prepared monthly. All samples were prepared in an oxygen-free glove box (95% N_2, 5% H_2) to prevent exposure to oxygen. One liter of sample was prepared for each condition. The sample bottles were covered in aluminum foil to prevent photoreactions and mixed at room temperature on a shaker table (Thermo Scientific, Max Q 2000) rotating at 150 rpm. Containers for all solutions, stocks, and samples were glass with Teflon®-lined caps. The containers were cleaned in a solution of 10% HNO_3 and 10% HCl for 24 h and baked at 400°C for 4 h.

Solid phase extraction. Details for the solid phase extraction of mercury from aqueous solution to prepare samples for EXAFS were described by Gerbig et al. (2011). In brief, the aqueous solution was passed through a glass chromatography column filled with 0.500 g of cleaned C_{18} resin (Supelclean ENVI-18, Spectrapor) at a flow rate of 4.0 mL min^{-1} in a glove box filled with 95% N_2 and 5% H_2. Most of the mercury was retained in the upper one-third of the loaded resin, which was removed from the column and kept under a N_2/H_2 atmosphere until EXAFS analysis. The retention of mercury by the resin in the solid phase extraction was greater than 98% of the total mercury in solution for all samples.

Experimental conditions. A variety of conditions were manipulated in this study, including the origin of the DOM, sulfide concentration, and equilibrium times (t_1 and t_2). The solution composition and kinetics for each sample is outlined in Table 3.1. Most experiments were conducted with the hydrophobic acid (HPoA) isolate from the F1 site in the Florida Everglades (Gilmour et al., 1998). This DOM isolate has been used extensively in mercury studies (Ravichandran et al., 1998; Haitzer et al., 2002, 2003; Waples et al., 2005; Gerbig et al., 2011). The most common sulfide concentration used in this study was 100 μM, and the most common equilibrium times were t_1=24 h and t_2=24 h.

Table 3.1. Solution composition and corresponding mercury L_{III}-edge EXAFS fitting results.

	Solution Composition and Kinetics						Fitting Results[a]			
Figure	Reference Material or DOM Isolate	DOM Concentration (mg L^{-1})	Hg Concentration (nM)	Sulfide Concentration (μM)	Hg-DOM equilibration, t_1 (h)	Hg-DOM-sulfide equilibration, t_2 (h)	Number of Coordinating Sulfur Atoms, N_{eff}	Hg-S Distance (Å)	Debye-Waller factor, σ^2 ($Å^2$)	$X_{red}^{2,b}$
1a	Cinnabar	Comercially available HgS(s) diluted in boron nitride to approximately 300 ppm Hg for EXAFS.					2.1±0.8	2.38±0.02[c]	0.0049±0.0032	130
1b	Cinnabar						3.1±0.5	2.38±0.03[c]	0.0090[d]	148
1c	Metacinnabar						3.8±1.1	2.51±0.02[c]	0.0070±0.0027	167
1d	Metacinnabar						4.6±0.5	2.52±0.02[c]	0.0090[d]	172
1e	none	--	157	100	--	24	3.9±0.3	2.51±0.02	0.0090[d]	13.7
2a	Everglades F1 hydrophobic acid (F1 HPoA)	44.1	161	100	24	121	3.8±0.3	2.52±0.01	0.0083[d]	23.0
2b	Everglades F1 hydrophobic acid (F1 HPoA)	43.7	158	100	24	12	3.8±0.4	2.50±0.02	0.0083[d]	44.8
2c	Everglades F1 hydrophobic acid (F1 HPoA)	44.3	142	100	24	4	3.6±0.3	2.51±0.01	0.0083[d]	38.0
2d	Everglades F1 hydrophobic acid (F1 HPoA)	47.7	169	100	142	23	3.5±0.4	2.50±0.02	0.0083[d]	17.7
2e	Everglades F1 hydrophobic acid (F1 HPoA)	46.4	171	100	24	23	3.4±0.4	2.50±0.03	0.0083[d]	12.9
2f	Everglades F1 hydrophobic acid (F1 HPoA)	47.7	169	100	12	23	3.4±0.4	2.50±0.02	0.0083[d]	25.8
4a	Everglades F1 hydrophobic acid (F1 HPoA)	44.2	399	100	24	24	4.3±0.3	2.53±0.01	0.0098[d]	14.5
4b	Everglades F1 hydrophobic acid (F1 HPoA)	43.1	424	10	24	24	3.7±0.3	2.52±0.02	0.0098[d]	19.8
4c	Everglades F1 hydrophobic acid (F1 HPoA)	46.7	748	1	24	24	2.9±0.2	2.53±0.01	0.0098[d]	16.2
4d	Everglades F1 hydrophobic acid (F1 HPoA)	45.0	95	100	24	24	3.0±0.2	2.52±0.02	0.0098[d]	28.1
4e	Everglades F1 hydrophobic acid (F1 HPoA)	46.5	115	10	23	24	2.4±0.2	2.51±0.02	0.0098[d]	21.2
4f	Everglades F1 hydrophobic acid (F1 HPoA)	46.0	110	1	23	24	2.1±0.2	2.46±0.02	0.0098[d]	24.5
6a	Pacific Ocean fulvic acid (PO FA)	44.0	142	100	23	24	4.2±0.4	2.49±0.02	0.0091[d]	94.9
6b	Williams Lake hydrophobic acid (WL HPoA)	46.9	158	100	23	24	3.6±0.3	2.51±0.02	0.0091[d]	46.3
6c	Everglades 2BS hydrophobic acid (2BS HPoA)	47.8	163	100	24	23	3.7±0.3	2.51±0.02	0.0091[d]	87.5
6d	Everglades F1 hydrophobic acid (F1 HPoA)	46.4	171	100	24	23	3.4±0.4	2.50±0.02	0.0091[d]	7.7
6e	Suwannee River fulvic acid (SR FA)	47.4	154	100	24	23	3.2±0.2	2.51±0.01	0.0091[d]	14.6

[a]All mercury interactions were best fit by sulfur bonds. [b]Reduced chi-squred. A goodness-of-fit parameter that accounts for variations in the degrees of freedom between fits. [c]Fit for the shortest Hg-S interaction only. [d]Fixed.

The DOM isolates were prepared by acidifying filtered water to a pH of 2, passing it through XAD-8 resin (Amberlite), eluting the DOM from the resin with 0.1 N NaOH, hydrogen-saturating the eluate, desalting, and freeze-drying the isolate. The other four DOM isolates used in this study, in addition to the F1 HPoA, were Florida Everglades site 2BS hydrophobic acid (2BS HPoA), Suwannee River fulvic acid (SR FA), Williams Lake hydrophobic acid (WL HPoA), and Pacific Ocean fulvic acid (PO FA). The field locations where the DOM samples were collected from are described in Appendix Table A3. The only difference between the hydrophobic acid and fulvic acid isolates is that the hydrophobic acid isolates also contain the humic acid component of the DOM, which has been removed from the fulvic acid samples by precipitation at a pH of 1. The structural and chemical characteristics of the DOM samples are listed in Appendix Table A4.

Chemical analyses. Dissolved organic carbon concentrations were measured with an OI 700 Analytical Model 700 total organic carbon analyzer. The method involves acidification of aqueous samples to remove inorganic carbon, persulfate oxidation of organic carbon, and subsequent infrared detection of evolved carbon dioxide. Acceptable recoveries were defined as 90-110% recovery of a sodium benzoate standard and >80% recovery of a caffeine standard. Dissolved organic carbon concentrations were converted to dissolved organic matter concentrations based on the carbon content of the DOM isolates presented in Appendix Table A4. Measurements of ultraviolet (UV) light absorbance of DOM samples at 254 nm were made on an ultraviolet-visible spectrophotometer (Agilent, model 8453) with a 1 cm quartz cuvette.

Total mercury concentrations were measured with a mercury analyzer (Millennium Merlin) according to EPA Method 245.7. Mercury stocks were prepared from National Institute of Standards and Technology standard reference material 3133. Samples were oxidized with 2%

(v/v) $KBr/KBrO_3$ for at least 24 h. Sufficient residual oxidant was verified with starch iodide paper. Acceptable recovery of standards was 80-120% with less than 20% relative difference in duplicate measurements. Typical recovery was 90-100% with 10% relative difference. Precision and recovery were verified by analyzing U.S. Geological Survey standard reference mercury samples. The detection limit for any given run was always below 0.013 nM Hg as defined by three times that standard deviation of seven replicates of a sample with a concentration one-half of the lowest standard.

EXAFS spectroscopy. Mercury L_{III}-edge EXAFS spectra were collected on beam line 11-2 at the Stanford Synchrotron Radiation Lightsource using a Si(220) monochromator crystal in the $\varphi=90°$ orientation. Resin samples were loaded into 2 mm-thick aluminum holders and sealed into the holders with Kapton® tape, all in an oxygen-free atmosphere. A liquid nitrogen cryostat was used to keep the sample temperature at 77 K during spectra collection to minimize noise from thermal vibrations and to minimize beam damage of the sample. Spectra were collected on a 32-element germanium detector in fluorescence yield mode. Gallium filters were used to minimize inelastic scattering and $HgCl_2$ was used as an internal standard for energy calibration of each spectra.

Two solid reference materials were examined along with the resins from solid phase extraction. Cinnabar and metacinnabar (Alfa Aesar; mercury(II) sulfide red and mercury(II) sulfide black, respectively) powders were diluted into boron nitride for a total mercury concentration of approximately 300 ppm Hg. The relatively low concentration was necessary to ensure the spectra could be collected in fluorescence yield mode without saturating the detector in a setup identical to that used for the resin samples.

The number of EXAFS scans varied depending on the concentration of mercury in the sample and the data quality. With the exception of the reference materials (which only required three scans), 9-32 scans were done. The lowest concentration resin sample was approximately 35 ppm Hg, while the highest concentration resin sample was approximately 250 ppm Hg (based on the mass balance of eluted mercury from the solid phase extraction). The scans for each sample were energy-corrected based on the calibration standard, dead time-corrected for the potential loss of signal due to finite photon detection times, and averaged together. Background subtracted spectra were converted to *k*-space with k^3-weighting, and Fourier-transformed.

The EXAFS spectra were fit over a *k*-range of 2.0-9.5 $Å^{-1}$. This is a fairly narrow energy range, but spectra quality degraded substantially beyond k=9.5 A^{-1}. The only possible atoms bound to mercury in these systems are sulfur (from the sulfide or from organic sulfur), carbon (from the organic matter), and oxygen (as a hydroxide species or from the organic matter). Phase and amplitude functions were created for Hg-S, Hg-O, and Hg-C interactions at various bond distances and with various geometries with SixPACK (Webb, 2005) using Feff6l (Rehr et al., 1991).

The initial fits were done by fitting the coordination number, bond distance, Debye-Waller factor (σ^2; a measure of static disorder and thermal vibration), and initial energy correction, while only the scale factor was held constant at 0.9. Improved goodness-of-fit was determined by a decrease in the reduced chi-squared of the fit (X_{red}^2), a parameter the accounts for variations in the degrees of freedome between fits. The initial fits showed that mercury-sulfur interactions were the only viable fits for all samples and that only a single mercury-sulfur interaction was necessary to fit samples with DOM. No significant carbon or oxygen bonding was observed in any fit. We were primarily concerned with changes in nanoparticle size and

crystalline disorder, and three of the fit parameters – the bond distance, the coordination number, and the Debye-Waller factor – can be used to evaluate size and disorder of small particles (Combes et al., 1989; Frenkel et al., 2001; Calvin et al., 2003; Calvin et al., 2005b; Frenkel, 2007). In general, when the coordination number decreases below the coordination number for the bulk phase, the Debye-Waller factor increases above the disorder of the bulk phase, or the bond distance decreases below the distance of the bulk phase, then particle size and/or crystalline order has decreased. The coordination number and Debye-Waller factor are correlated fitting parameters, so fitting both simultaneously makes comparisons between samples ambiguous. We held the Debye-Waller factor constant in comparisons to facilitate the use of coordination number as a measure of particle size or disorder. The constant Debye-Waller factor for each data set (i.e., variable kinetics, variable sulfide and mercury concentrations, variable DOM, Table 3.1) is the average of the Debye-Waller factors from the initial fits where the Debye-Waller factor was allowed to vary. Final fits were determined with this constant Debye-Waller factor (Table 3.1). The Debye-Waller factor is not the same between sets, but averaging it over a smaller number of samples ensures the average more accurately represents the Debye-Waller factor of the data in each set. Thus, comparisons within sets are more robust and in comparisons between sets we account for differences in Debye-Waller factor. Additionally, two fits were generated for the reference materials: one with a varying Debye-Waller factor and one with the average Debye-Waller factor of all of the samples in the study.

3.4 RESULTS

Reference and DOM-free samples. The EXAFS spectra and corresponding Fourier transforms for the cinnabar and metacinnabar reference materials are significantly different from each other (Figure 3.1). The frequency of the oscillations is out of phase because the coordination environment is significantly different between the two samples. The model fit for cinnabar shows 2.1±0.8 sulfur atoms coordinating mercury at 2.38±0.02 Å when the Debye-Waller factor is a fitting parameter (see Table 3.1 for fitting results). This fit agrees with the primary mercury-sulfur interaction in cinnabar of two sulfur atoms at a distance of 2.39 Å from the mercury atom (Charnock et al., 2003). Similarly, the four-coordinate, 2.53 Å sulfur-binding environment in metacinnabar (Charnock et al., 2003) is reproduced accurately (3.8±1.1 sulfur atoms at 2.51±0.02 Å) in the metacinnabar reference material when the Debye-Waller factor is a fitting parameter.

Cinnabar and metacinnabar were also fit with a fixed Debye-Waller factor of 0.0090 $Å^2$, the average value for all of the other samples in this study. When this average Debye-Waller factor is used, the number of coordinating sulfur atoms in the primary mercury-sulfur interaction increases significantly, although the mercury-sulfur bond distance remains the same (Table 3.1). This result is expected because the Debye-Waller factor and the coordination number are correlated parameters in the fitting model. The features of the fit spectra do not change significantly when the Debye-Waller factor is varied (Figure 3.1); there are simply larger amplitudes in the k^3-weighted data and corresponding higher magnitudes in the Fourier transforms. The features in the Fourier transform beyond the primary mercury-sulfur interaction in cinnabar and metacinnabar suggest that these materials have significant long-range order,.

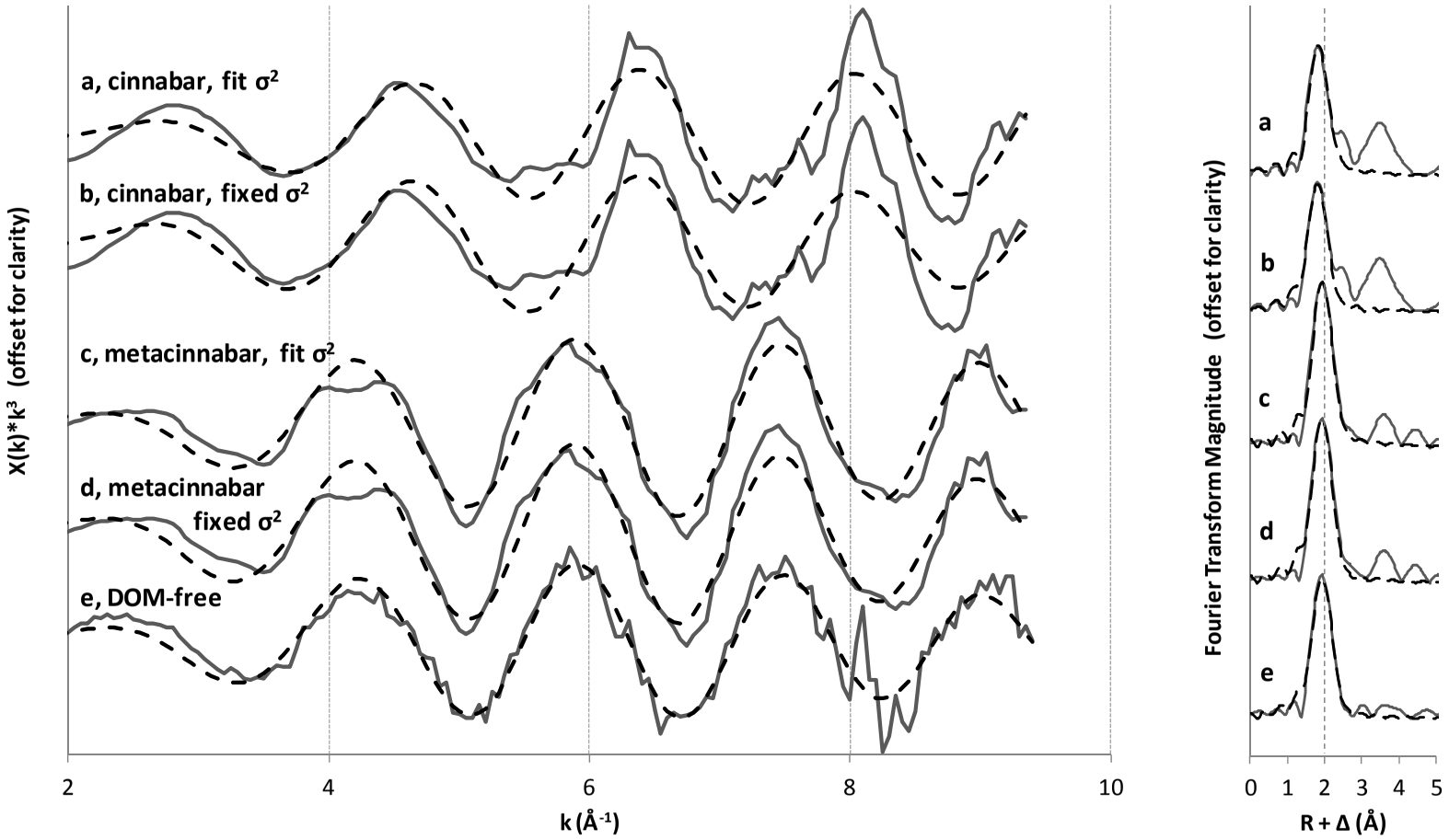

Figure 3.1. k^3-weighted mercury L_{III}–edge EXAFS spectra and Fourier transforms for collected spectra (solid) and fits (dashed) of (a) cinnabar when the Debye-Waller factor was fit (σ^2=0.0049), (b) cinnabar when the Debye-Waller factor was fixed (σ^2=0.0090), (c) metacinnabar when the Debye-Waller factor was fit (σ^2=0.0070), (d) metacinnabar when the Debye-Waller factor was fixed (σ^2=0.0090), and (e) the DOM-free sample with a fixed Debye-Waller factor (σ^2=0.0090). Only the primary peak was fit for cinnabar and metacinnabar. The vertical dashed line in the Fourier transform corresponds to a Hg-S distance of 2.53 Å after accounting for the phase shift (Δ). The fitting results for each sample are summarized in Table 3.1.

which is indicative of well-crystallized materials. The average Debye-Waller factor for the precipitated samples is probably not an accurate representation of the disorder in the reference materials because the reference materials were presumably prepared in highly controlled systems without impurities like DOM to complicated precipitation.

The DOM-free sample shown in Figure 3.1 lacks the clear long-range order that the reference materials have, so its spectrum was fit with the average Debye-Waller factor of the samples in this study (0.0090 $Å^2$). The potential longer-range order that is present in the Fourier transform could not be fit with sufficient certainty to include it in the structural model. The fit of the primary peak (3.9±0.3 sulfur atoms at 2.51±0.2 Å) accurately matches the theoretical coordination environment of metacinnabar and the coordination environment of the metacinnabar reference material examined in this study. Visual MINTEQ (Gustafsson, 2010) predicts that metacinnabar is supersaturated in a solution of 157 nM Hg_T and 100 μM H_2S_T at pH 6.5 based on the equilibrium constants used by Gerbig et al. (2011). The EXAFS data confirm that metacinnabar precipitates in the absence of dissolved organic matter and that the primary mercury-sulfur bonds have the expected metacinnabar structure, although the higher Debye-Waller factor suggests a higher degree of disorder relative to the metacinnabar reference material.

Variable kinetics of equilibrium times. There are no statistically meaningful differences in coordination numbers or bond distances with variation in either Hg-DOM (t_1) or Hg-DOM-sulfide (t_2) equilibration time. The k^3-weighted data (Figure 3.2) shows that all six samples have the same oscillation frequency, although the spectra for some samples (2d, 2e, and 2f) is somewhat noisier than for other samples (2a, 2b, 2c, and 2e). All six samples also show similar mercury-sulfur bond distances (2.50-2.52 Å), and the range of average coordination numbers,

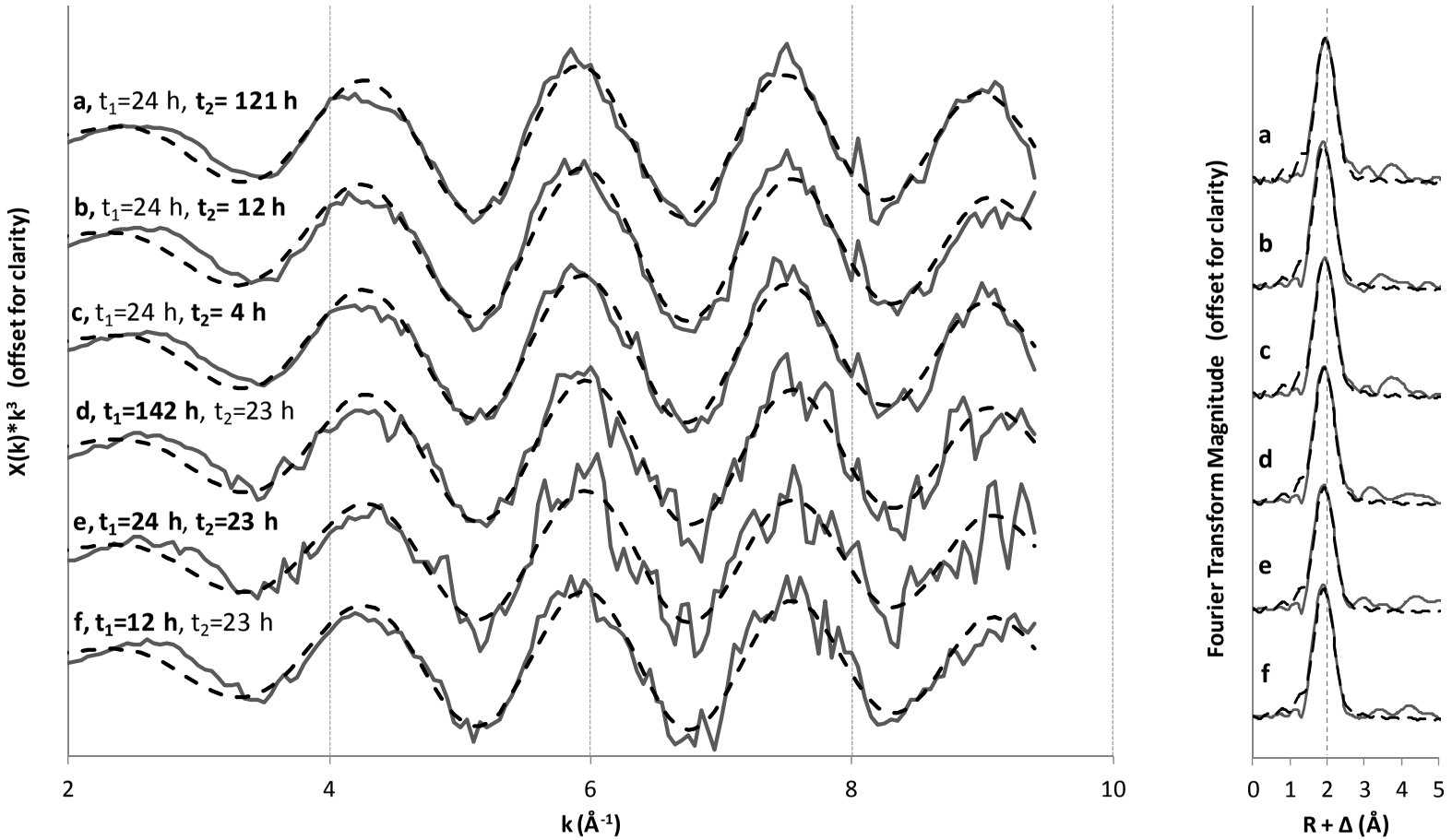

Figure 3.2. k^3-weighted mercury L_{III}–edge EXAFS and Fourier transforms for collected spectra (solid) and fits (dashed) of mercury-DOM-sulfide systems with varied Hg-DOM equilibration times (t_1) and Hg-DOM-sulfide equilibration times (t_2). The Debye-Waller factor was fixed at 0.0083 Å^2 for all fits. The vertical dashed line in the Fourier transform corresponds to a Hg-S distance of 2.53 Å after accounting for the phase shift (Δ). The solution chemistry and fitting results for each sample are summarized in Table 3.1.

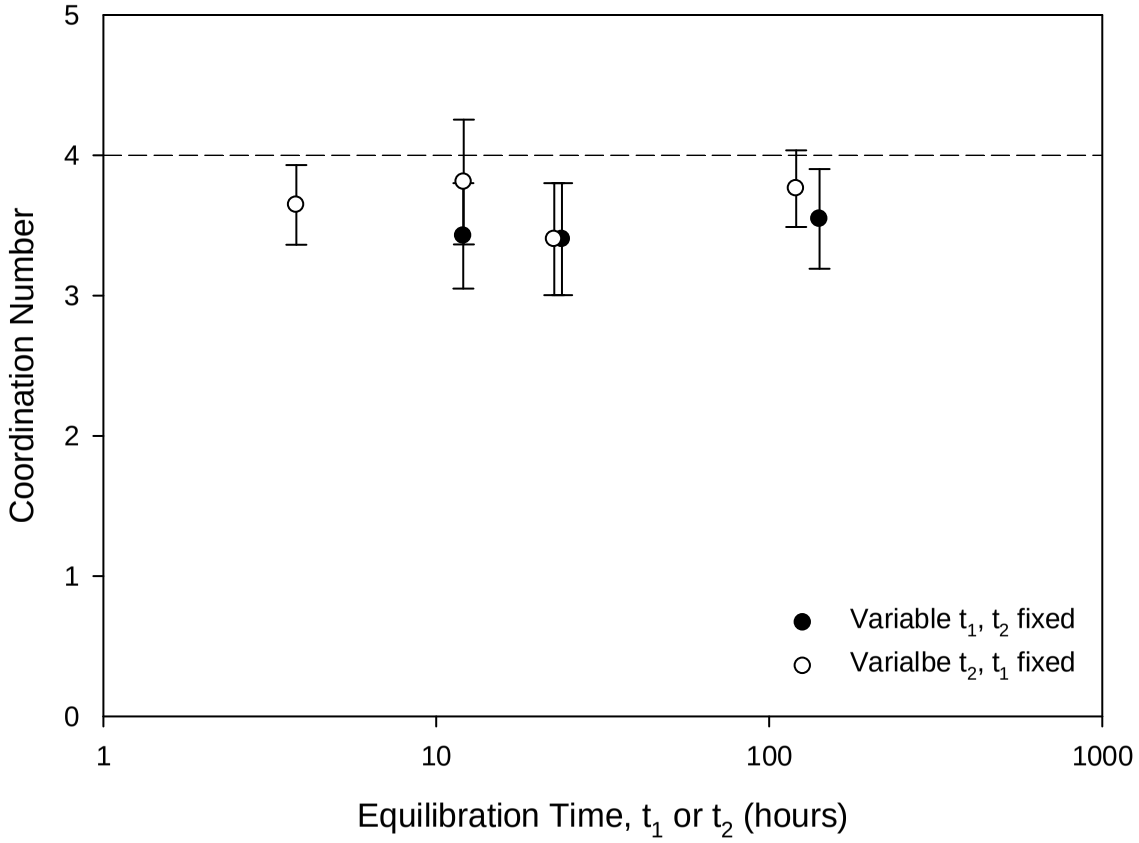

Figure 3.3. The relationship between Hg-DOM equilibration time (t_1) or Hg-DOM-sulfide equilibration time (t_2) and the number of sulfur atoms coordinated to a mercury atom. Equilibration time t_1 is approximately constant (23-24 h) for variable t_2 and equilibration time t_2 is constant (23 h) for variable t_1. Error bars represent 95% confidence intervals. The solution chemistry and Hg L_{III}-edge EXAFS fits are summarized in Table 3.1.

3.4-3.8, is not significantly different among all six samples (Figure 3.3). The Hg-S bond distances are slightly shorter than the distance in ideal metacinnabar, and the uncertainty in four of the samples does not overlap the 2.53 Å distance of metacinnabar, although the range is only 0.01 Å short. The Hg-S distance is not short enough for the mercury species to be interpreted as any known inorganic complexes (Tossell, 2001; Bell et al., 2007), organic complexes (Skyllberg et al., 2006; Gerbig et al., 2011; Nagy et al., 2011), or cinnabar (Charnock et al., 2003), which all have primary Hg-S interactions between 2.30 Å and 2.40 Å. We conclude that the mercury-sulfide species in these systems is imperfectly-ordered metacinnabar-like nanoparticles. The metacinnabar-like nanoparticles form quickly (<4 h) and display the same coordination numbers and bond distances for long periods of time after formation (>121 h). Their structure is not affected by the amount of time that mercury is equilibrated with DOM before sulfide addition.

As expected for small or disordered metacinnabar-like nanoparticles, the number of sulfur atoms coordinating mercury is less than the ideal four-coordinate structure of metacinnabar. The number of coordinating sulfur atoms reported in this study is slightly higher than those reported previously for metacinnabar-like nanoparticles formed at similar Hg:DOM ratios (Gerbig et al., 2011). The slightly higher coordination numbers for these samples may be the result of fitting the EXAFS spectra with a slightly higher Debye-Waller factor, which will give rise to higher coordination numbers, because the two parameters are correlated in the fitting method.

Variable sulfide and mercury concentrations. The variation of sulfide concentration at two mercury concentration ranges – a low range (95-114 nM) and a high range(399-748 nM) (Table 3.1) – gives rise to significant variations in EXAFS spectra (Figure 3.4) and fitting results (Figure 3.5). The k^3-weighted data for five samples (labeled 4a-4e) display similar oscillation

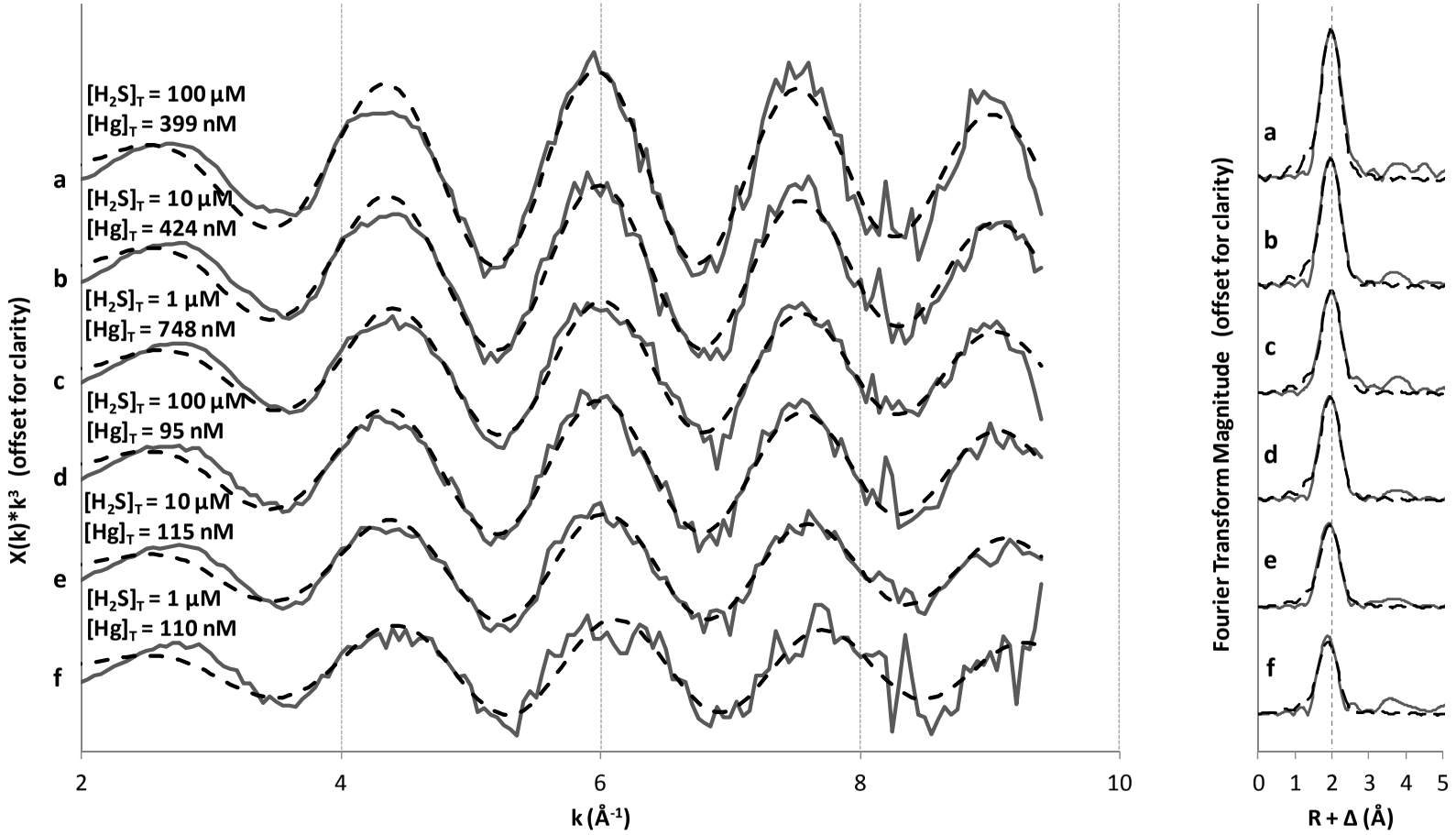

Figure 3.4. k^3-weighted mercury L_{III}–edge EXAFS and Fourier transforms for collected spectra (solid) and fits (dashed) of mercury-DOM-sulfide systems with varied total sulfide and total mercury concentrations. The Debye-Waller factor was fixed at 0.0098 $Å^2$ for all fits. The vertical dashed line in the Fourier transform corresponds to a Hg-S distance of 2.53 Å after accounting for the phase shift (Δ). The solution chemistry and fitting results for each sample are summarized in Table 3.1.

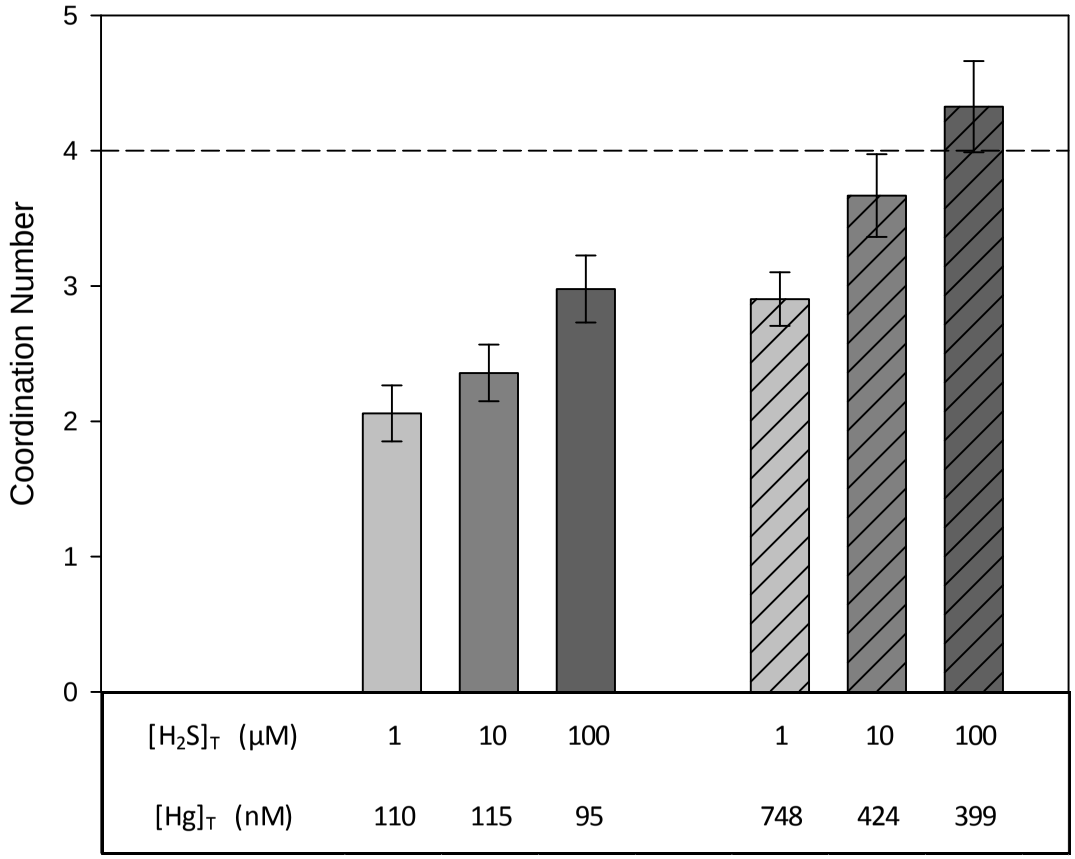

Figure 3.5. The relationship between the number of sulfur atoms coordinating a mercury atom and the amount of mercury and sulfide in solution. The samples correspond to the EXAFS data in Figure 3.4, error bars represent 95% confidence intervals, and the fitting parameters and results are in Table 3.1.

frequencies (Figure 3.4), but the amplitudes differ substantially among samples. These five samples all have Hg-S bond distances that are consistent with metacinnabar (Table .3.1). The 1 μM H_2S_T, 110 nM Hg_T sample (4f) has a Hg-S bond distance (2.46±0.02 Å) that is significantly shorter than the bond distance in metacinnabar, but is longer than other potential mercury-sulfur species (Tossell, 2001; Charnock et al., 2003; Skyllberg et al., 2006; Bell et al., 2007; Gerbig et al., 2011; Nagy et al., 2011). This likely indicates substantial disorder in the HgS(s) that is formed in the system, although it could also suggest a transition to a mercury species with shorter Hg-S bond distances as sulfide and mercury concentrations decrease. All six samples are supersaturated with respect to metacinnabar by several orders of magnitude, as predicted by Visual MINTEQ (Appendix Figure A4; Gustafsson, 2010). In this range of sulfide concentrations (1-100 μM), metacinnabar solubility is most exceeded at the lowest sulfide concentrations because higher sulfide concentrations result in higher concentrations of aqueous mercury-sulfide complexes (Appendix Figure A4).

The five samples that have Hg-S bond distances that are metacinnabar-like still show substantial variations in coordination number, which suggests variations in particle size or crystalline order. As mercury concentration decreases while the sulfide concentration is held constant, or the sulfide concentration decreases while the mercury concentration is held approximately constant, the average number of sulfur atoms coordinating a mercury atom decreases (Figure 3.5). The highest concentrations of mercury and sulfide generate a HgS(s) particle that most closely resembles crystalline metacinnabar (4a; 4.3±0.3 sulfur atoms at 2.53±0.01 Å). The least ordered system (4f; 2.1±0.2 sulfur atoms at 2.46±0.02 Å) was prepared at the lowest concentrations of mercury and sulfide.

The samples with variable mercury and sulfide concentrations had the highest average Debye-Waller factor (0.0098 $Å^2$) of all of the data sets examined. As a result, the coordination numbers tend to be somewhat higher than samples with lower Debye-Waller factors. However, the comparison among samples with the same Debye-Waller factor doesn't change substantially if they are all re-analyzed with a different Debye-Waller factor. The precise coordination number changes slightly (the magnitude of change depends on the magnitude of change in the Debye-Waller factor), and the fits are less precise, but the relative difference between the highest and lowest coordination number remains approximately constant. Regardless of the precise coordination number/Debye-Waller factor pair, the variation in particle size or crystalline order of HgS(s) is a function of the mercury and sulfide concentrations.

Variable dissolved organic matter type. The EXAFS spectra for the five different DOM isolates all had similar k^3-weighted data quality and all showed similar Fourier transformations (Figure 3.6). The number of sulfur atoms coordinating mercury was slightly below the ideal metacinnabar structure for all five samples, and the difference between two of the samples (PO HPoA and F1 HPoA) and metacinnabar was statistically significant (Table 3.1). As with the variable kinetics samples, we interpret these small coordination number differences to be a representation of the changes in nanoparticle size or disorder and not a substantial difference in the mercury species present in the system.

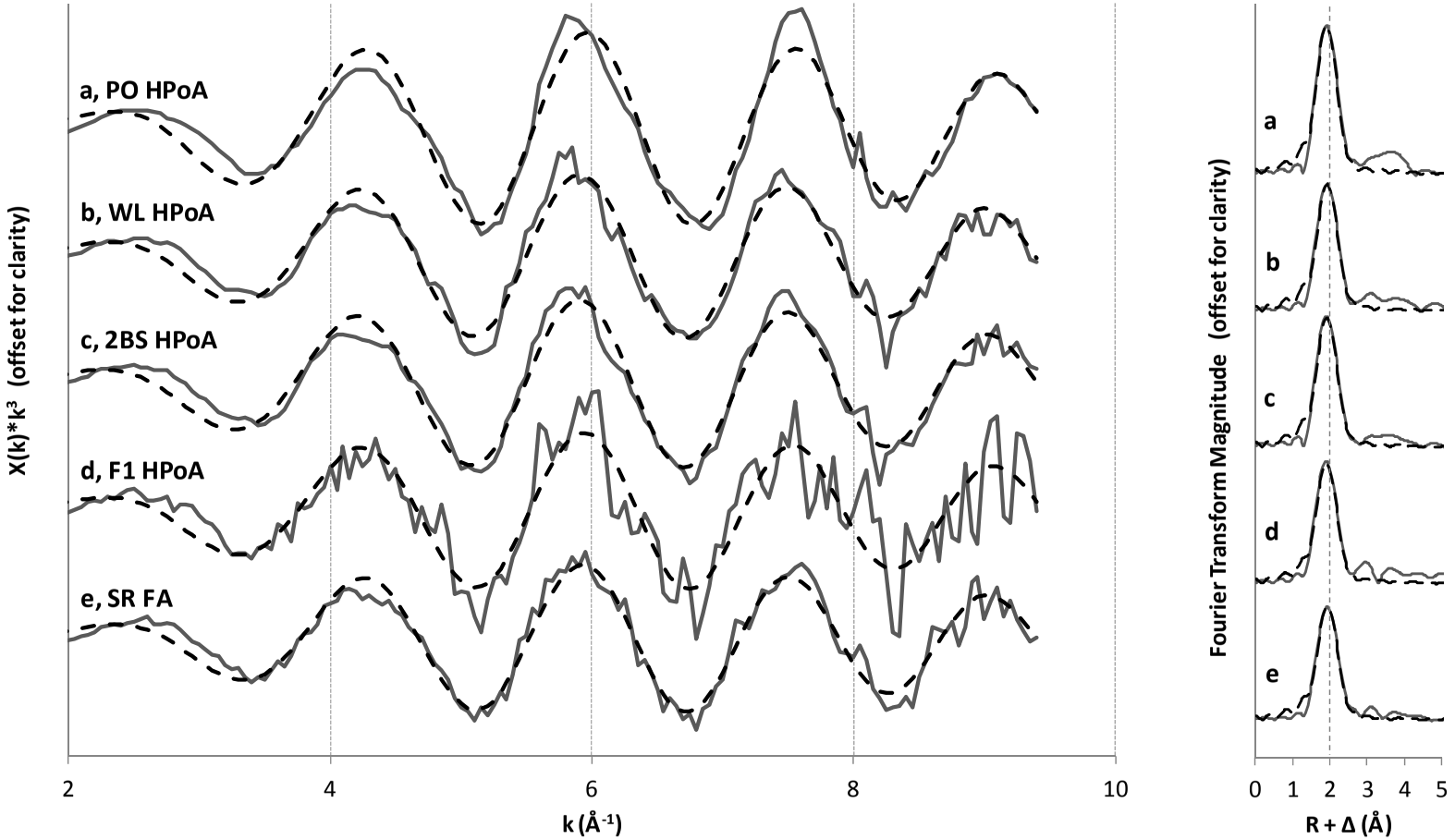

Figure 3.6. k^3-weighted mercury L_{III}–edge EXAFS and Fourier transforms for collected spectra (solid) and fits (dashed) of mercury-DOM-sulfide systems with different DOM isolates. The sulfide concentration is 100 μM for all samples. The range of DOM concentrations is 44.0-47.8 mg L^{-1}. The range of mercury concentrations is 142-171 nM. The Debye-Waller factor was fixed at 0.0091 $Å^2$ for all fits. The vertical dashed line in the Fourier transform corresponds to a Hg-S distance of 2.53 Å after accounting for the phase shift (Δ). The solution chemistry and fitting results for each sample are summarized in Table 3.1.

3.5 DISCUSSION

Nanoparticle size and disorder. In theory, there is a robust relationship between the average number of sulfur atoms coordinating mercury in a metacinnabar particle and the size of that particle (Frenkel, 2007). The relationship between the effective coordination number (N_{eff}) and the diameter of a well-ordered and spherical particle (d) is defined by the equation (Calvin et al., 2003):

$$N_{eff} = \left(1 - \frac{3}{2}\frac{r}{d} + \frac{1}{2}\left(\frac{r}{d}\right)^3\right) N_{bulk} \qquad \text{(Equation 3.1)}$$

where r is the atomic radius (the mercury-sulfur bond distance of 2.53 Å) and N_{bulk} is the number of sulfur atoms (four) coordinating mercury in a large, perfectly crystalline metacinnabar particle. Based on Eqn. 3.1, the coordination number is highly sensitive to the particle diameter for d of less than about 2 nm (Figure 3.7). Above about 6 nm, the change in coordination number is relatively small compared to the change in diameter, and the effective and bulk coordination numbers begin to converge. For values of N_{eff} determined for the metacinnabar-like particles formed in this study, particle diameters of less than 1 nm are predicted by Eqn. 3.1 (Figure 3.7). Eqn. 3.1 assumes well-ordered and spherical particles, which is probably not to be expected for the metacinnabar-like particles formed in this study. Eqn. 3.1 tends to underestimate particle size for disordered or non-spherical particles (Calvin et al., 2005a; Calvin et al., 2005b), but it is still clear that the deviations from the bulk metacinnabar coordination number we observe in this study are at least partially due to particle sizes on the nanometer scale.

If we instead assume that the metacinnabar-like particles are all the same size, we can also interpret the EXAFS results as indicative of changes in the disorder of the crystal structure. For many of the systems the low coordination numbers (e.g., the 1 μM H_2S_T and 110 nM Hg_T

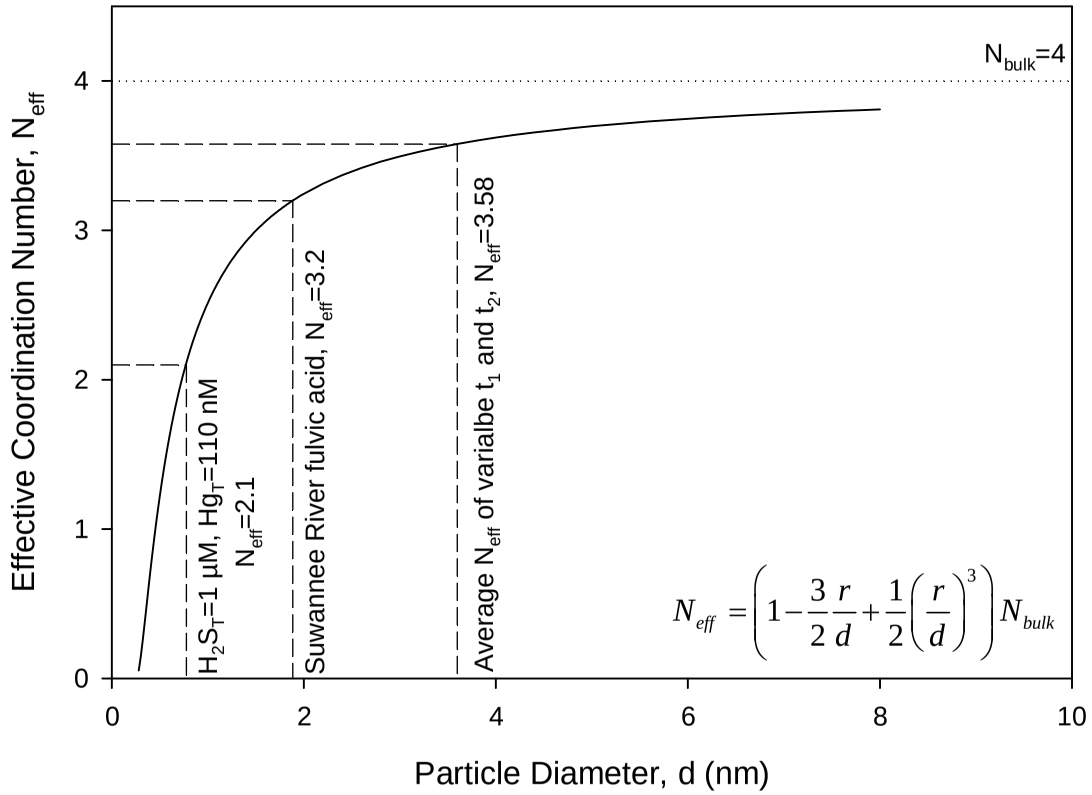

Figure 3.7. The theoretical relationship between effective coordination number (N_{eff}) and the diameter (d) of a particle (Eqn. 3.1). For metacinnabar, N_{bulk}, the coordination number of the bulk phase, is 4; r, the bond distance between the mercury and sulfur atom, is 0.253 nm. The model assumes a spherical geometry and a perfectly-ordered crystal structure. Dashed lines representing three of the modeled systems in this study are plotted for comparison: a sample from the variable sulfide series, H_2S_T=1 µM, Hg_T=110 nM (spectra 4f); a sample from the variable DOM series, Suwannee River fulvic acid (spectra 6e); and the average of all samples in the variable equilibration time series.

sample has a coordination number of 2.1±0.2) suggest substantial disorder. Additionally, all of the samples lack the longer-range order (R>3) observed in the cinnabar and metacinnabar reference materials (Figure 3.1). The Debye-Waller factors for all of the precipitated samples were significantly higher than the fit Debye-Waller factor for the two reference materials (Table 3.1). The Debye-Waller factors observed in this study are significantly higher than the Debye-Waller factors for metacinnabar precipitation in the absence of organic matter at high mercury concentration observed by others (Charnock et al., 2003; Lennie et al., 2003) although the Debye-Waller factors in this study are comparable to studies that have examined metacinnabar precipitation in the presence of organic matter (Slowey, 2010).

Equilibration time. In the absence of dissolved organic matter, and at high mercury and sulfide concentrations, metacinnabar precipitation is rapid – Charnock et al. (2003) reported that the basic metacinnabar crystal structure is apparent in 5 s and the static disorder in the mercury bonds drops to the level of crystalline metacinnabar within 20 min. However, the ideal four-coordinate metacinnabar structure fails to form in the presence of the F1 HPoA organic matter isolate even after several days of exposure to sulfide (Figure 3.3). Other studies have noted slow or halted particle aggregation in the presence of organic matter (Horzempa and Helz, 1979; Ravichandran et al., 1999; Lau and Hsu-Kim, 2008; Deonarine and Hsu-Kim, 2009; Deonarine et al., 2011), but DOM halts the growth of the primary particles as well. These primary particles are exceedingly small (<10 nm), poorly crystalline, or both.

Our data contrasts with the observations of Slowey (2010) who noted cyclical increases and decreases in the amount of dissolved mercury in DOM- and sulfide-containing systems. The cyclical changes in dissolved mercury were attributed to the precipitation, dissolution, and re-precipitation of HgS(s) particles. Organic matter is capable of promoting the dissolution of

HgS(s) (Ravichandran et al., 1998; Waples et al., 2005), but no other studies that have observed HgS(s) stabilization at higher mercury concentrations have noted significant re-dissolution of precipitated HgS(s) (Ravichandran et al., 1999; Deonarine and Hsu-Kim, 2009). Our data indicate that the Hg-DOM-sulfide system rapidly comes to equilibrium after sulfide addition and that no net change in the metacinnabar-like crystal structure occurs over time.

Similarly, the amount of time for which mercury is equilibrated with DOM does not have an effect on the crystal structure of the metacinnabar-like nanoparticles. Hg(II) takes approximately 24 h to come to equilibrium with the strongest DOM binding sites (Lamborg et al., 2003; Gasper et al., 2007; Miller et al., 2009), and the Hg:DOM ratio used in this study is below the 4 nmol mg^{-1} strong binding capacity that has been identified for the F1 HPoA organic matter isolate (Haitzer et al., 2002). Release of mercury from the strong binding sites is either rapid or slow, but inconsequential to the equilibrium form of the metacinnabar-like nanoparticles.

Mercury and sulfide concentration. The significant differences in metacinnabar-like nanoparticle characteristics with varied sulfide and mercury concentration (Figure 3.5) have important implications for our understanding of the forms of mercury that microbes are exposed to in natural systems. All of the samples in Figure 3.5 were super-saturated with respect to metacinnabar, and the systems that were most super-saturated were the ones with the lowest sulfide concentrations. The size or crystallinity of the metacinnabar-like nanoparticles is not a function of the degree of super-saturation.

We see the same relationship between coordination number and Hg:DOM ratio that we observed previously (Gerbig et al., 2011). That is, metacinnabar-like nanoparticles are larger or more ordered when they are formed in systems with a greater abundance of mercury with respect

to DOM. This study shows that at a fixed Hg:DOM ratio (all of the samples in Figure 3.5 have approximately the same DOM concentration, so similar mercury concentrations are also similar Hg:DOM ratios) higher sulfide concentrations also yield larger or more-ordered metacinnabar-like nanoparticles. We conclude that the relative abundance of mercury, DOM, *and* sulfide is important to the size or crystallinity of the metacinnabar-like precipitates. This suggests that, depending on the aqueous chemistry of a sulfidic environment, microbes may be exposed to mercury as (1) aqueous sulfide complexes (Benoit et al., 1999a; Miller et al., 2007), (2) small and poorly ordered metacinnabar-like nanoparticles like those observed in this study at lower mercury and sulfide concentrations, or (3) larger and more-ordered metacinnabar-like nanoparticles like those observed at higher mercury and sulfide concentrations.

DOM characteristics. Although the role of DOM in particle growth and aggregation has long been recognized (e.g., Horzempa and Helz, 1979), relatively few studies have used a suite of DOM isolates to characterize the variability in growth as a function of DOM characteristics. Those studies that do use a variety of DOM isolates have primarily focused on particle aggregation behavior at high metal and particle concentrations. Deonarine et al. (2011) clearly showed that the initial aggregation rate of ZnS(s) particles was correlated with the molecular weight and specific UV absorbance of the DOM isolate in solution. This is consistent with our understanding that more hydrophobic DOM isolates (humic acid, fulvic acid, and hydrophobic acid) are more effective at inhibiting the bulk precipitation of HgS(s) particles (Ravichandran et al., 1999) because these DOM fractions also tend to be the most aromatic, have the highest SUVA, and have the highest molecular weight (Chin et al., 1994; Weishaar et al., 2003). Studies of kinetics of precipitation and aggregation of other metal sulfides have failed to find a

relationship between the organic matter reduced sulfur content (and a suite of other properties) and metal-sulfide growth rates (Deonarine et al., 2011).

There have been some attempts to characterize HgS(s) disorder when it is formed in the presence of different DOM isolates (Slowey, 2010), but the Hg:DOM ratios were significantly higher than what was used in this study (approximately 500 nmol mg^{-1} compared to <4 nmol mg^{-1}), which complicates comparisons. Generally, the HgS(s) was less ordered when it was formed in the presence of Suwannee River humic and fulvic acids than it was when it was formed in the presence of Pony Lake fulvic acid, a DOM isolate with much lower SUVA and aromaticity. In this study there is a statistically significant ($p = 0.05$) negative relationship between the specific ultraviolet absorbance of the DOM isolates at 254 nm ($SUVA_{254nm}$) and the number of sulfur atoms coordinating mercury in the metacinnabar-like precipitates in each system (Figure 3.8). SUVA, the amount of aromatic carbon in DOM, and the molecular weight of DOM are all positively correlated (Chin et al., 1994; Weishaar et al., 2003), which suggests that the relationship between SUVA and coordination number is a function of physical properties of the organic matter structure.

The mechanism of DOM interaction with metal-sulfide particles and the explanation for the role of DOM in slowing or preventing particle growth and aggregation is somewhat unclear. Studies of model compounds have shown that organic thiols, which bind metals strongly, are more effective at preventing aggregation than oxygen- and nitrogen-containing organic compounds, which bind metals less strongly (Gondikas et al.; Lau and Hsu-Kim, 2008; Deonarine and Hsu-Kim, 2009). The only model compounds without thiol groups that effectively slow aggregation are large chelators, such as ethylenediaminetetraacetic acid (EDTA) (Helz and Horzempa, 1983). This would seem to suggest that surface complexation between the ligands

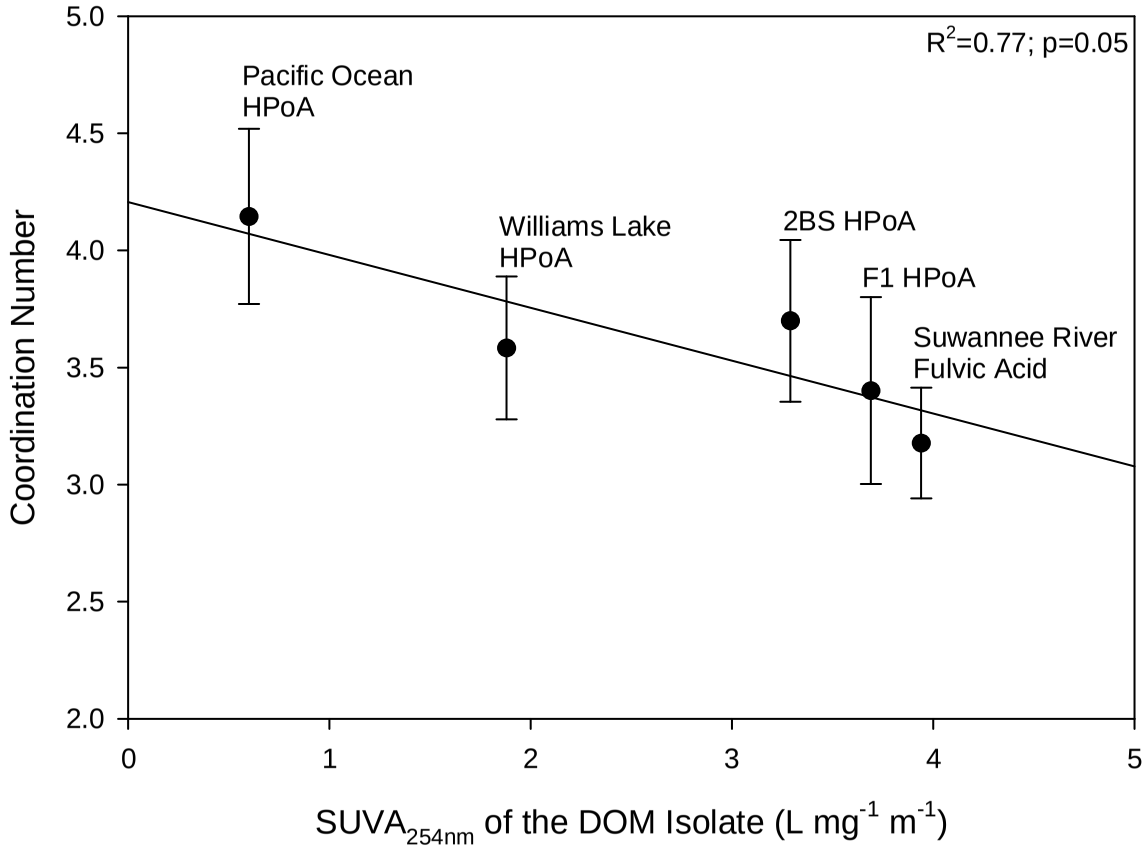

Figure 3.8. The relationship between the specific ultraviolet absorbance at 254 nm ($SUVA_{254nm}$) of the DOM in mercury-DOM-sulfide systems and the number of sulfur atoms coordinating a mercury atom in the metacinnabar-like nanoparticles that form in those systems. The samples correspond to the EXAFS data in Figure 3.6. Error bars represent 95% confidence intervals. The fitting parameters and results are in Table 3.1.

and metals on the particle surface is a critical step in preventing particle aggregation and growth. However, studies that have shown organic matter to be even more effective at preventing particle growth and aggregation than model thiols use metal concentrations grossly in excess of the strong binding capacity of the organic matter (Ravichandran et al., 1999; Lau and Hsu-Kim, 2008; Deonarine and Hsu-Kim, 2009; Deonarine et al., 2011). Furthermore, the reduced sulfur content of organic matter is not a good predictor of particle aggregation rates (Deonarine et al., 2011) or the efficacy of DOM in promoting HgS(s) dissolution, which should be related to surface reactions (Ravichandran et al., 1998; Waples et al., 2005). DOM-induced inhibition of metal-sulfide particle aggregation is a result of the adsorption of DOM to the particle surface. DOM adsorption imparts a negative surface charge which repels other DOM-coated particles, and introduces steric effects which physically prevent particle interaction and aggregation (Horzempa and Helz, 1979; Ravichandran et al., 1999; Deonarine et al., 2011). Multiple properties of DOM are important in particle aggregation. The Hg:DOM ratio suggests that specific ligand-metal interactions are important (Chapter 2), and the relationship between DOM SUVA and coordination number (Figure 3.8) suggests that aromaticity or molecular weight is also an important component of DOM in metal-sulfide precipitation.

Environmental Implications. This study is the first to examine the role of DOM composition in nanoparticle growth at low Hg:DOM ratios where the strong binding sites of the organic matter are relevant for mercury speciation. The $SUVA_{254nm}$ of the DOM isolates is negatively correlated with number of sulfur atoms coordinating mercury in metacinnabar-like nanoparticles (Figure 3.8). This suggests that bulk properties of the DOM isolates, namely aromaticity or molecular weight, are important for nanoparticle growth and aggregation at low Hg:DOM ratios. We can expect the form of mercury in sulfide-containing aquatic environments

to be significantly different depending on the nature of the organic matter present. In waters containing DOM of low $SUVA_{254nm}$, mercury will precipitate as larger and more crystalline HgS(s) nanoparticles, and these particles will aggregate more readily into bulk HgS(s). Conversely, in waters containing DOM of high $SUVA_{254nm}$, mercury-sulfide nanoparticles will be smaller and less crystalline and the particles will be less likely to aggregate into bulk HgS(s).

Microbial uptake and eventual methylation of mercury in aquatic environments, particularly those containing sulfate reducing bacteria which are largely responsible for mercury methylation, depends on the geochemistry of mercury, sulfide, and DOM. It is currently unclear how inorganic mercury enters microbial cells, though several studies suggest that only small, neutrally charged complexes passively traverse microbial membranes (Barkay et al., 1997; Schaefer and Morel, 2009). Some active pathways have also been suggested (Schaefer et al., 2011). However, these studies fail to consider the potential existence of nanocolloidal metacinnabar-like particles, relying instead on speciation calculations that are ambiguous and treat metacinnabar precipitation as the removal of reactive mercury from the environment (Skyllberg, 2008; Deonarine and Hsu-Kim, 2009).

The results of this study have broad implications for nanoparticles in the environment. Organic matter may play a substantial role in stabilizing the nanoparticles and multinuclear clusters that natively form in many natural systems (Rozan et al., 2000; Moreau et al., 2007). The nature of organic matter may be an important factor when considering the stabilization, transport, and bioavialability of metal colloids from contaminated sites (Weber et al., 2009; Pédrot et al., 2011). Non-native nanocolloids introduced for engineering purposes (Liu et al., 2005) or as contaminants (Hyung et al., 2006) are also likely to be affected by organic matter. It is reasonable to expect that DOM will not act uniformly with respect to these nanocolloids, much

as DOM did not act uniformly with respect to the size and crystallinity of the metacinnabar-like nanoparticles observed in this study.

The data in this study are consistent with the suggestion that a continuum of metal complexes, clusters, and particles of different size and order are present in the environment (Rickard and Luther III, 2006; Aiken et al., 2011). Considerations must be made in speciation calculations and models for the size and morphology of the metacinnabar-like nanoparticles we observed. For example, it has long been recognized that amorphous ferric (oxy)hydroxides have different thermodynamic properties than well-crystallized ferric oxides. Poorly crystalline CuS(s) is three orders of magnitude more soluble than covelite, and the dissolution of poorly crystalline CuS(s) is not kinetically hindered like the dissolution of covelite (Shea and Helz, 1989). It has also been shown that natively formed HgS(s) is more easily dissolved than crystalline cinnabar or metacinnabar in natural systems (Barnett et al., 1997; Han et al., 2008). Even well-crystallized particles will exhibit significantly different thermodynamic properties when the particles are nanometers in size due to the destabilizing forces of interfacial energy (Gilbert and Banfield, 2005; Liu et al., 2009). It is reasonable to expect that the metacinnabar-like nanoparticles exhibited in this study have thermodynamic and kinetic properties that are substantially different from the thermodynamic properties of bulk metacinnabar. The role these nanoparticles play in mercury geochemistry needs further research, with an emphasis on how methylating microbes interact with the nanoparticles.

Chapter 4

The Effects of Dissolved Organic Matter, Mercury-to-Dissolved Organic Matter Ratio, Kinetics, and Sulfide Concentration on Mercury Speciation in Aquatic Environments

Chase A. Gerbig[*,‡], Le H. Kieu[§], Mark Marvin-DiPasquale[§], George R. Aiken[⊥], Joseph N. Ryan[‡]

[‡]Department of Civil, Environmental, and Architectural Engineering, University of Colorado Boulder, 428 UCB, Boulder, CO 80309, United States

[§]U.S. Geological Survey, 345 Middlefield Rd., Menlo Park, CA 94025, United States

[⊥]U.S. Geological Survey, 3215 Marine St., Suite E127, Boulder, CO 80303, United States

*Corresponding Author: phone (585) 704-8167, email chase.gerbig@colorado.edu

Manuscript to be submitted to *Environmental Science and Technology*

4.1 ABSTRACT

Methylation of mercury in natural systems depends on the forms of mercury available to methylating microbes. In this study we used a tin-reducible mercury assay to examine the reactivity of mercury under a variety of conditions that may be important to mercury speciation in aquatic environments. Mercury bound to strong thiol binding sites in dissolved organic matter (DOM) was less reducible than mercury bound by several organic ligands, including thiol ligands, and was also less reducible than mercury bound to carboxyl groups in DOM. Mercury precipitated with sulfide in the presence of DOM was less reducible than Hg-DOM complexes, but was more reducible than HgS(s) precipitated without DOM present. The reducibility of poorly crystalline metacinnabar-like HgS nanoparticles coated with DOM increased as the specific ultraviolet light absorbance (SUVA) of the DOM decreased. These results suggest that DOM is an important parameter in assessing the potential for methylation of nanocolloidal metacinnabar-like particles in aquatic environments. The amount of reducible mercury decreased as the time of equilibration with sulfide increased, especially over the first 2 h of equilibration. The time that mercury equilibrated with DOM before sulfide addition affected the reducible mercury fraction but the amount of sulfide in solution had a nominal effect. The tin-reducible assay for mercury is a useful tool for assessing the reactivity of mercury species. The reducible mercury results in this study suggest that nanocolloidal metacinnabar-like particles may need to be considered in methylating systems.

4.2 INTRODUCTION

Mercury contamination presents a significant ecological and human health concern. Most contamination is deposited via atmospheric deposition (Wang et al., 2004); consequently, the contamination is widespread. Sulfate- and iron-reducing microbes convert mercury to methylmercury (Morel et al., 1998; Fleming et al., 2006), which is a potent neurotoxin that accumulates in biota (Mason et al., 1995). Although microbes are known to be the primary pathway for methylmercury production, the forms of inorganic mercury that pass from solution into the cells are unclear. Several important inorganic and organic forms of mercury have been proposed in conjunction with active and passive pathways for the entrance of mercury into microbial cells (Benoit et al., 1999a; Schaefer and Morel, 2009; Schaefer et al., 2011).

Determination of mercury speciation in sulfide-containing environments, where a significant portion of methylation takes place, often relies on speciation models because the speciation of mercury at such low concentrations is difficult to measure empirically. With current thermodynamic data, the models suggest that mercury speciation is dominated by sulfide complexes and that systems are close to the solubility of metacinnabar (β-HgS(s)), the low-temperature polymorph of mercuric sulfide (Skyllberg, 2008). Dissolved organic matter (DOM) is able to strongly bind mercury(II) in the absence of sulfide (Haitzer et al., 2003; Han and Gill, 2005), but even strong-binding thiol groups in DOM cannot out-compete inorganic sulfide for mercury(II). However, DOM significantly complicates mercury speciation in sulfidic systems when the precipitation of metacinnabar is possible (Ravichandran et al., 1999; Miller et al., 2007; Deonarine and Hsu-Kim, 2009; Slowey, 2010; Gerbig et al., 2011). DOM interacts with the surface of precipitating metacinnabar particles, slowing or halting growth of the particles

(Slowey, 2010; Gerbig et al., 2011) and the aggregates that form from the individual particles (Deonarine and Hsu-Kim, 2009; Slowey, 2010). The stabilized metacinnabar-like nanoparticles are small (nanometers in diameter) and poorly crystallized compared to bulk metacinnabar (Chapter 3; Gerbig et al., 2011).

Particles that are nanometers in size are expected to have significantly different thermodynamic properties than bulk materials (Gilbert and Banfield, 2005)(Gilbert and Banfield, 2005). Additionally, poorly-crystallized precipitates typically have different thermodynamic properties than well-crystallized materials. For example, ferric (oxy)hydroxides are more soluble than well-crystallized ferric oxides such as goethite (α-FeOOH) or hematite (Fe_2O_3). Recently precipitated CuS(s) has a solubility product three orders of magnitude greater than the CuS(s) mineral covelite (Shea and Helz, 1989). HgS(s) formed in mercury-contaminated systems is more soluble than metacinnabar (Barnett et al., 1997; Han et al., 2008). Several factors have been shown to impact the size and crystallinity of nanocolloidal metacinnabar-like particles, including the DOM in the system when they precipitated (Chapter 3). Methylating microbes are likely to be exposed to nanocolloidal metacinnabar-like particles coated in DOM, but little is known about the reactivity of these particles and how their reactivity depends on the nature of the DOM interacting with the particle surfaces.

To assess the effect of the nature of DOM and the kinetics of mercury interaction with DOM and sulfide, we examined the reactivity of mercury species in the presence of DOM isolates from eleven sources with and without sulfide using a tin-reducible mercury assay. For this assay, reducible mercury (Hg_R) is defined as the amount of mercury that is quickly converted to elemental mercury (Hg^0) by $SnCl_2$ in an otherwise chemically unaltered sample. A variety of studies utilize reducible mercury measurements to assess the amount of labile mercury in

sediment or water samples (Krabbenhoft et al., 1998; Lindström, 2001; Lamborg et al., 2003; Lamborg et al., 2004; Miller et al., 2007; Marvin-DiPasquale et al., 2009). Most importantly, the fraction of reducible mercury (Hg_R/Hg_T) in soil columns has been shown to positively correlate with the methylation rate of mercury in the natural systems (Marvin-DiPasquale et al., 2009). By examining the fraction of Hg_R in a variety of laboratory systems, we were able to characterize the stability of nanocolloidal metacinnabar particles as a function of important environmental variables and speculate on the significance of nanocolloidal metacinnabar for methylation.

4.3 METHODS

Dissolved organic matter samples. Eleven different organic matter (DOM) samples were used in this study. Freeze-dried isolates were prepared according to the method of Aiken et al. (1992), which utilizes Amberlite XAD-8 and XAD-4 resins to separate dissolved organic matter based on the polarity of the DOM molecules. To prepare hydrophobic acid (HPoA) samples, whole water was filtered through a 0.3 μm glass-fiber filter, acidified to pH 2, and passed through a column of XAD-8 resin, which absorbed the hydrophobic acid portion of the DOM. The sorbed DOM was eluted with 0.1 N NaOH, de-salted, proton-saturated, and freeze-dried. Humic and fulvic acids, which together comprise HPoA, were separated by acidifying the XAD-8 eluate to pH < 1 to precipitate the humic acids (Thurman and Malcolm, 1981), which were removed via centrifugation. The transphilic acid (TPiA) used in this study is the fraction of DOM that passes through the XAD-8 resin and absorbs to the XAD-4 resin at pH 2. TPiA from XAD-4 was eluted and prepared in the same manner as the HPoA.

Most experiments were conducted with the hydrophobic acid isolate (HPoA) from the F1 site in the Florida Everglades. This DOM sample has been used extensively for other mercury studies (Ravichandran et al., 1998; Ravichandran et al., 1999; Drexel et al., 2002; Haitzer et al., 2002, 2003; Waples et al., 2005; Miller et al., 2007; Gerbig et al., 2011). The other ten DOM samples (Table 4.1) represent a range of chemical characteristics and environments. Elemental composition (including reduced sulfur content) and ^{13}C-NMR characterization for most of the organic matter samples is compiled elsewhere (Waples et al., 2005; Deonarine et al., 2011) and is reproduced in Appendix Table A3.

Solution composition. Solutions containing DOM, mercury, and sulfide (where necessary) were prepared in deionized water (≥ 18 MΩ cm). Two different buffers were used to maintain pH 6.5±0.2. Solutions prepared with a phosphate buffer contained 5 mM NaH_2PO_4 and the pH was adjusted with 1 N NaOH. Solutions prepared with a carbonate buffer contained 3 mM $NaHCO_3$ and the pH was adjusted with 0.3 N HNO_3. The ionic strength of all samples was adjusted to 0.1 M with $NaClO_4$ based on calculations done in Visual MINTEQ (Gustafsson, 2010). DOM was added to buffered solutions from stock solutions that were prepared by dissolving the organic matter isolates in deionized water and filtering the stock through 0.45 μm polyethersulfone membranes (Supor, Pall Corporation). Some experiments contained 10 μM of an organic ligand instead of dissolved organic matter (Table 4.2). These compounds were prepared as stocks and added before mercury was added to the solution. Mercury was added after the DOM as a small-volume spike from a stock solution ($Hg(NO_3)_2$ in 10% HNO_3). Sulfide was added after mercury. The sulfide stock was prepared by washing $Na_2S{\cdot}9H_2O$ with deionized water before use. All solutions were prepared in glass flasks with glass stoppers that were cleaned in 10% HCl and 10% HNO_3 and baked at 400°C for 4 h to remove mercury and organic

Table 4.1. Specific ultraviolet absorbance (SUVA) comparison for the DOM isolates used in this study.[a]

DOM Isolate	Measured $SUVA_{254nm}$ ($L\ mg^{-1}\ m^{-1}$)	Measured $SUVA_{280nm}$ ($L\ mg^{-1}\ m^{-1}$)	Reported $SUVA_{280nm}$ ($L\ mg^{-1}\ m^{-1}$)[a]	$SUVA_{280nm}$ agreement (measured/reported)
Pacific Ocean fulvic acid (PO FA)	0.70	0.41	0.44	93%
Williams Lake hydrophobic acid (WL HPoA)	2.10	1.36	1.32	103%
Ohio River hydrophobic acid (OhR HPoA)	2.84	2.01	2.17	93%
Everglades F1 transphilic acid (F1 TPiA)	2.87	1.90	n.a.[b]	--
Ohio River fulvic acid (OhR FA)	3.18	2.20	2.17	102%
Ogeechee River fulvic acid (OgR FA)	4.01	2.96	2.89	102%
Everglades F1 hydrophobic acid (F1 HPoA)	4.18	2.91	3.09	94%
Suwannee River hydrophobic acid (SR HPoA)	5.12	4.01	n.a.[b]	--
Ogeechee River humic acid (OgR HA)	5.64	4.52	5.28	86%
Ohio River humic acid (OhR HA)	6.45	5.06	4.9[c]	103%
Suwannee River humic acid (SR HA)	6.90	5.55	5.47	101%

[a]As reported by Waples et al. (2005) unless noted otherwise. [b]DOM sample was not used by Waples et al. (2005). [c]As reported by Deonarine et al. (2011).

Table 4.2. The reducibility of various mercury complexes with simple organic ligands.[a]

Organic Ligand[b]	Molecular Weight (g mol^{-1})[c]	Hg_R (% Hg_T)
glycolic acid	76.1	91
glycine	75.1	101
EDTA	292.2	85
thioglycolic acid	92.1	105
cysteine	121.2	63
glutathione	307.3	66

[a]Conditions: carbonate buffer, pH 6.5-6.7, model compound concentration 10 µM, Hg_T=0.25-0.27 nM, equilibration time approximately 2 h. [b]Structural models for the organic ligands are available in Appenix Figure A5. [c]Listed molecular weight is for the acidic, mercury-free molecule.

carbon contamination. Sulfide-containing solutions, solutions with an organic thiol ligand, and the stocks used to make those solutions were prepared in a glove box (95% N_2(g), 5% H_2(g)) and were kept anoxic until analysis by sealing the stopper with electrical tape. Flasks were covered with aluminum foil to prevent photoreactions and were allowed to equilibrate quiescently.

Experimental conditions. The parameters varied in this study include DOM source, mercury concentration, sulfide concentration, mercury-DOM equilibration time (t_1), and mercury-DOM-sulfide equilibration time (t_2). The standard sulfide-free system contained about 10 mg L^{-1} of the Everglades F1 HPoA isolate, and 0.25 nM Hg_T, and was equilibrated for about 24 h (t_1). The standard sulfide-containing system contained about 10 mg L^{-1} of the F1 HPoA isolate, 2.5 nM Hg_T, and 100 μM H_2S_T and the equilibration times were about t_1 = 24 h and t_2 = 24 h. More total mercury was used in sulfide-containing systems because reducible mercury was not detectable in the sulfide-containing systems containing Hg_T = 0.25 nM.

Reducible mercury measurement. Reducible mercury (Hg_R) was measured by adding tin chloride reductant to the experimental solutions and measuring the amount of evolved elemental mercury. The reductant stock solution was prepared by dissolving 100.0 g $SnCl_2$ (Certified ACS grade, Fisher Scientific) in 50 mL trace metal-grade HCl to which 400 mL of deionized water was added after the $SnCl_2$ dissolved. The reductant solution was continuously purged with a high-purity He or N_2 gas stream that contained an in-line gold trap to scrub elemental mercury from the gas. The reductant stock solution was added to samples at a ratio of 1.0 mL of reductant solution to 100 mL of sample. Samples with high concentrations of Hg_R were diluted with deionized water before adding the stock solution. The reduced samples were purged with ultrahigh-purity He or N_2 gas flowing at 250-300 mL min^{-1} for 15 min while mixing on a shaker table. The evaded vapor was passed sequentially through a soda lime trap and a gold trap to

remove acid vapors and elemental mercury, respectively. The amount of elemental mercury on the gold trap was analyzed by thermally desorbing the mercury from the gold trap on to a second gold trap, thermally desorbing from the second trap into a high purity Ar gas stream, and utilizing cold vapor atomic fluorescence spectrometry (CVAFS; Tekran Model 2500 mercury analyzer) to detect elemental mercury in the Ar gas stream.

Standards for Hg_R measurements were made from a National Institute of Standards and Technology (NIST) reference material. Standards were spiked into 0.5% (v/v) trace metal-grade HCl immediately before Hg_R measurement. The relative standard deviation of the ratio of standard mercury mass to analytical peak area for all standards was less than 10%. Due to the nature of the analysis, matrix tests were not possible. However, recovery of known mercury spikes into 0.5% (v/v) HCl was 90-100%. Blanks (0.5% HCl) were repeatedly analyzed. The daily detection limit of the method, based on three times the standard deviation of the blank measurements ($n \geq 4$), was always below 0.25 ng Hg and was typically below 0.10 ng Hg. Duplicate measurements were made on approximately 10% of Hg_R samples. The relative difference between duplicates was always less than 10%. Experimental replicates (2-4) were also performed for a subset of experimental systems. Estimates of error presented in this study are for experimental replicates. Reactive mercury was measured on an absolute mass basis, and converted to a concentration based on the volume of analyzed sample. The reactive mercury fraction (Hg_R/Hg_T) is the ratio of the amount of mercury reduced by tin to the total mercury concentration (HgT) in the sample.

Chemical analyses. Total mercury measurements were made according to EPA method 245.7 by oxidizing the sample to destroy mercury-DOM and mercury-sulfide species, followed by reduction with $SnCl_2$, and mercury detection with CVAFS (Millennium Merlin, PS

Analytical). Mercury stocks were prepared from NIST standard reference material 3133. Samples were oxidized with 2% (v/v) $KBr/KBrO_3$ for at least 24 h. Sufficient residual oxidant was verified with starch iodide paper. Acceptable recovery of standards was 80-120% with less than 20% relative difference in duplicate measurements. Typical recovery was 90-100% with 10% relative difference. Precision and recovery were verified by analyzing U.S. Geological Survey standard reference mercury samples. The detection limit for any given run was always below 0.011 nM Hg as defined by three times that standard deviation of seven replicates of a sample with a concentration one-half of the lowest standard.

Dissolved organic carbon concentrations were measured with an OI 700 Analytical Model 700 total organic carbon analyzer. The method involves acidification of aqueous samples to remove inorganic carbon, persulfate oxidation of organic carbon, and subsequent infrared detection of evolved carbon dioxide. Acceptable recoveries were defined as 90-110% recovery of a sodium benzoate standard and >80% recovery of a caffeine standard. Dissolved organic carbon concentrations were converted to dissolved organic matter concentrations based on the carbon content of the DOM isolates (Appendix Table A3). The amount of DOM in experimental systems was calculated based on the dilution of measured DOM stock solutions. Measurements of ultraviolet (UV) light absorbance of DOM samples were made on an ultraviolet-visible spectrophotometer (Agilent, model 8453) with a 1 cm quartz cuvette. The specific UV absorbance (SUVA) was calculated according to the formula (Weishaar et al., 2003):

$$SUVA_{\lambda} = \left(\frac{UV\ absorbance\ at\ \lambda\ (cm^{-1})}{DOC\ (mgC\ L^{-1})}\right) x100 \qquad \text{(Equation 4.1)}$$

at wavelengths of λ = 254 nm and 280 nm. The SUVA values for the DOM samples used in this study compare well with reported SUVA values, as shown in Table 4.1

4.4 RESULTS

The comparison between the amount of reducible mercury in three different systems – standard Hg-DOM, standard Hg-DOM-sulfide, and DOM-free mercury and sulfide – in both buffers is presented in Figure 4.1. The amount of reducible mercury in the phosphate buffer is consistently lower than the amount of reducible mercury in the carbonate system because some of the tin precipitated with the phosphate in the phosphate-buffered solution. No tin precipitation was observed in the carbonate-buffered solution.

Hg-DOM complexes that are formed in the sulfide-free system are more reducible than the mercury species formed in the systems that contain 100 μM sulfide (Figure 4.1). Reducible mercury in sulfide-containing systems is higher when DOM is present. The amount of reducible mercury in sulfide-containing systems without DOM is only slightly above the detection limit for the reducible mercury measurement.

The amount of reducible mercury in sulfide-free systems with DOM is substantially lower than the amount of reducible mercury in systems that contain a suite of organic ligands (Table 4.2). The organic ligands all have reducible mercury fractions greater than 60%, while the reducible mercury fraction in the standard DOM system is less than 15% (Figure 4.1). The organic ligands were equilibrated with mercury for only 2 h, compared to 24 h of DOM equilibration with mercury, but a 24 h equilibration with ethylenediaminetetraacetic acid (EDTA) showed that the reducible mercury fraction did not substantially change from 2 h to 24 h (85% versus 82%, respectively). The Hg-organic ligand binding constant is not a good predictor of the amount of reducible mercury. For example, the binding constants for the dominant glycolic acid, glycine, and thioglycolic acid complexes vary over 36 orders of magnitude

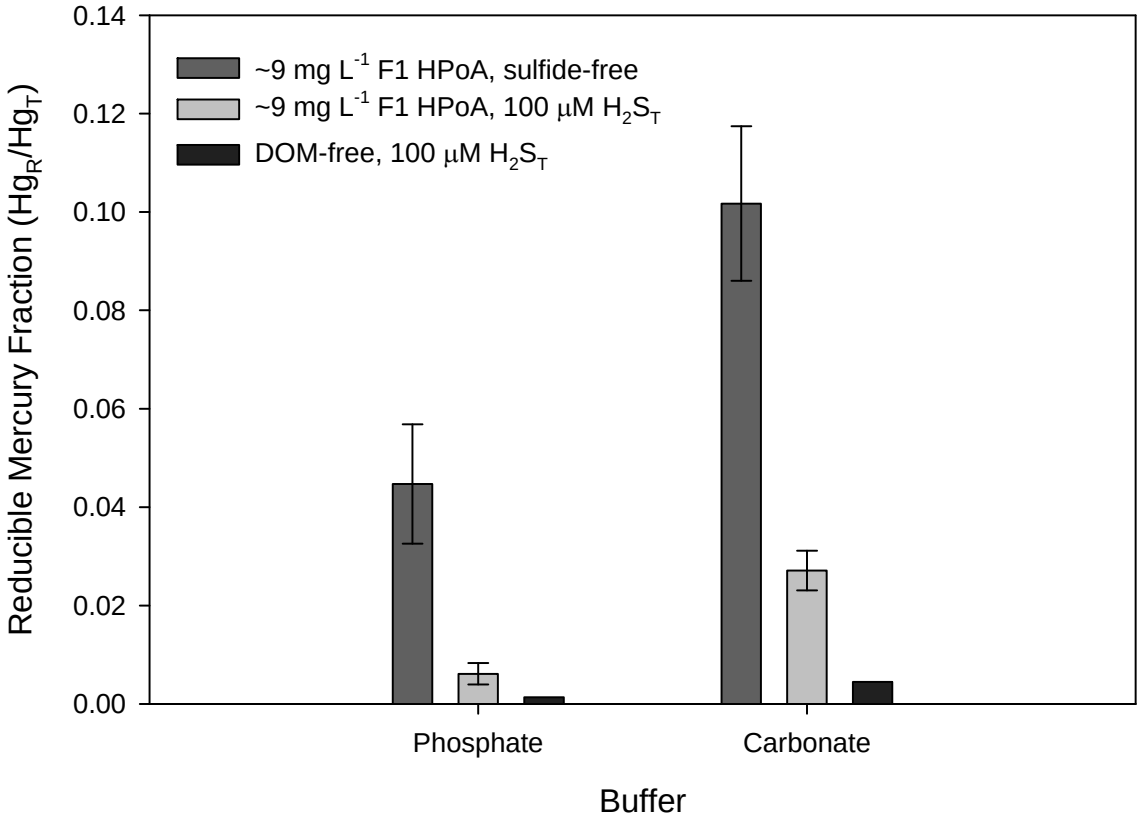

Figure 4.1. Comparison of the reducible mercury fraction under three different conditions in two different buffers. Constant conditions: t_1 = 23.1-23.9 h (for samples with DOM), t_2 = 23.3-25.9 h (for samples with sulfide), Hg_T = 0.26-0.28 nM for sulfide-free systems, Hg_T = 2.3-2.4 nM for sulfide-containing systems. Error bars represent one standard deviation for 2-4 replicates, depending on sample).

(log β_2 = 7.05, 9.3, and 43.8, respectively; Rossotti and Whewell, 1977; NIST, 2004), but the differences in the reducible mercury fraction are small between the samples. The reducible mercury fraction is also generally unrelated to the molecular weight of the complexing ligand. Both thioglycolic acid and cysteine are thiol-containing ligands that bind mercury very strongly (NIST, 2004), and both have similar molecular weights, but the fraction of reducible mercury varies substantially between them.

The amount of mercury relative to the amount of DOM has an important impact on the reducible mercury fraction. At low Hg:DOM ratios, the Hg_R fraction in the phosphate-buffered system is less than 10%, but as the Hg:DOM ratio rises past about 1 nmol mg^{-1}, the amount of reducible mercury increases substantially (Figure 4.2). The same general relationship is observed in the carbonate-buffered system. The Hg:DOM ratio for most sulfide-containing and sulfide-free systems in this study was about 0.03 and 0.3 nmol mg^{-1}, respectively. Both systems are below the Hg:DOM ratio where significant changes are expected in the Hg_R fraction due to a high Hg:DOM ratio.

At a fixed Hg:DOM ratio (~0.03 nmol mg^{-1}), the effect of the mercury-DOM equilibration time (t_1) on the Hg_R fraction in sulfide-free systems is important, especially for short Hg-DOM equilibration times (Figure 4.3). The phosphate-buffered system shows a large decrease in the Hg_R fraction with t_1 between 0.12 and 6 h, at which point there is no major change in the Hg_R fraction up to 70 h. The carbonate-buffered system has a higher Hg_R fraction at high t_1, as we would expect because the carbonate buffer generally shows higher Hg_R fractions than the phosphate buffer (Figure 4.1). The sample from the carbonate-buffered system at low t_1 (< 1 min) showed that Hg_R is initially very high and decreases rapidly to the levels seen in the phosphate-buffered system, in which more gradual changes occur.

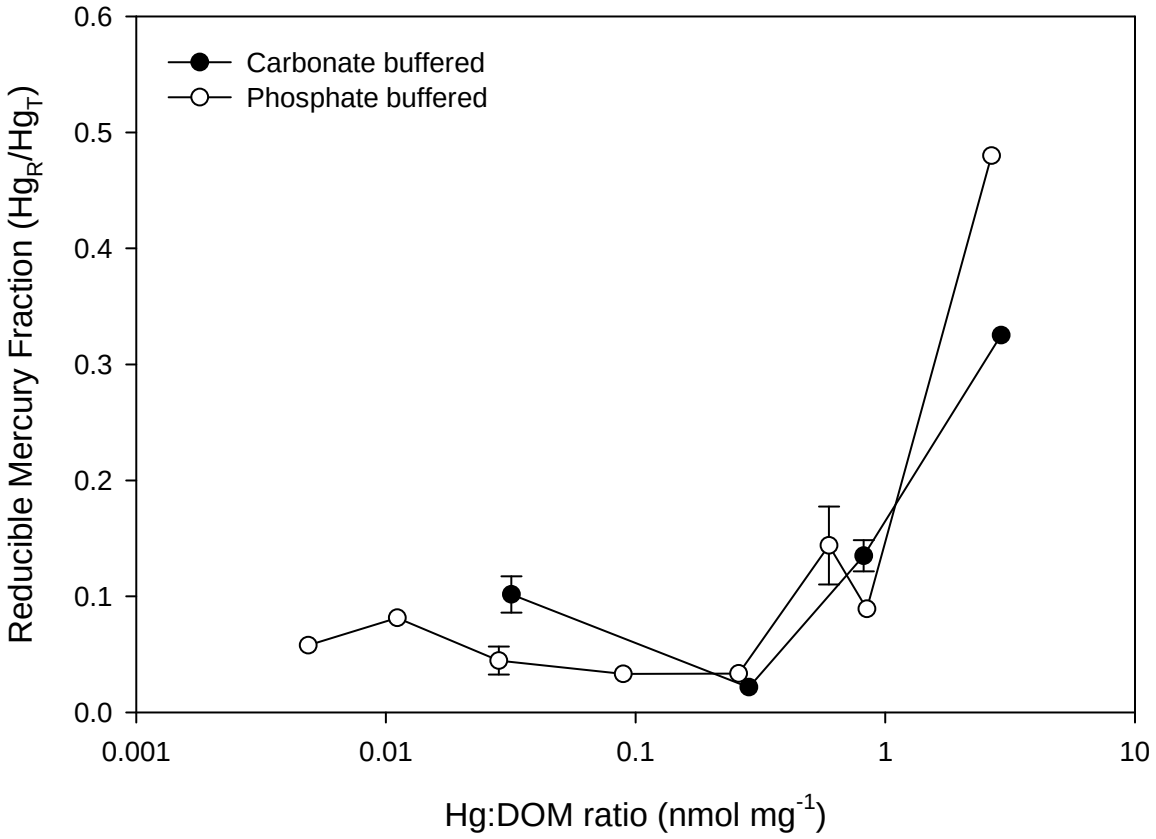

Figure 4.2. The relationship between the reducible mercury fraction and the Hg:DOM ratio for sulfide-free systems with two different buffers. Constant conditions: DOM = 8.8-9.4 mg L^{-1} Everglades F1 HPoA, t_1 = 23.5-24.5 h. Error bars represent one standard deviation for 2-4 replicates, depending on sample.

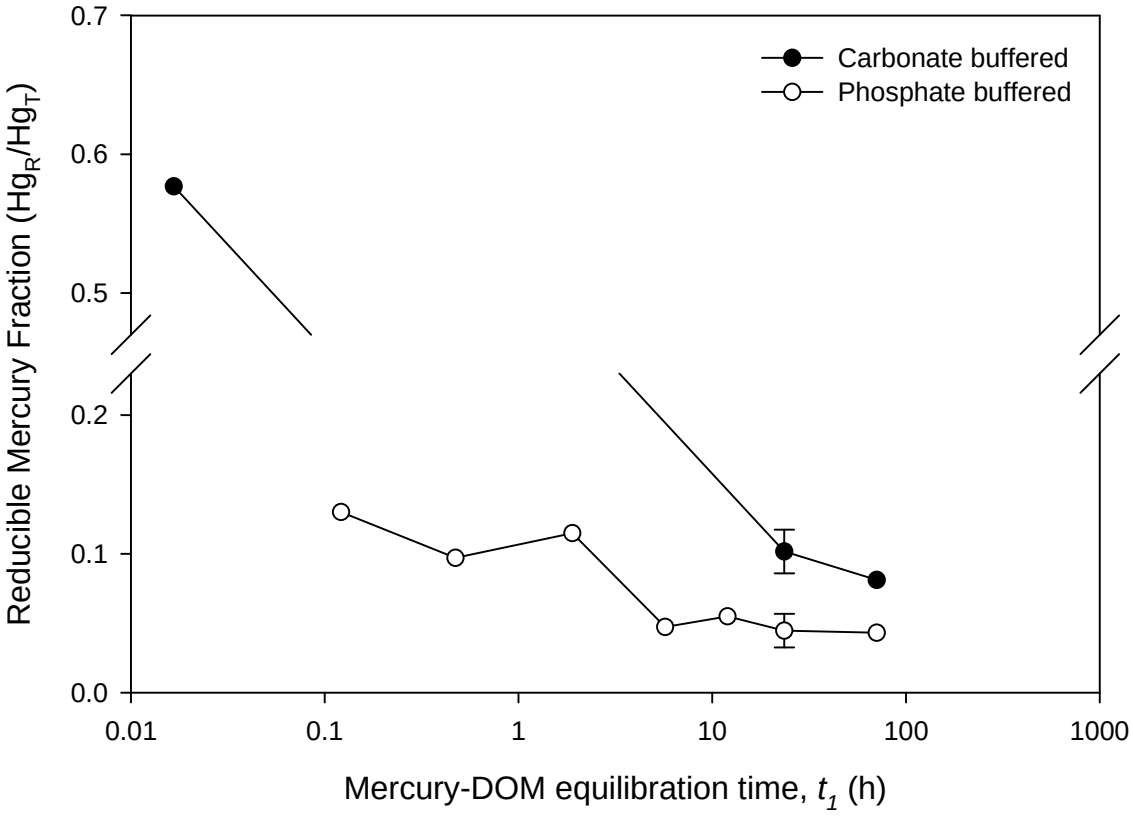

Figure 4.3. The reducible mercury fraction as a function of the mercury-DOM equilibration time (t_1) in sulfide-free systems with two different buffers. Hg_T for the sample at 0.02 h was 0.13 nM; all others were 0.23-0.29 nM. DOM = 8.8-9.4 mg L^{-1} Everglades F1 HPoA for all samples. Error bars represent one standard deviation for three replicates.

$SUVA_{254}$ of the DOM is not good predictors of the Hg_R fraction in sulfide-free systems after we account for mercury contamination in select DOM samples (Figure 4.4a). Three of the DOM samples used in this study – the Ogeechee River HA and FA and the Suwannee River HA – had high background levels of mercury in the isolate. The three contaminated isolates (indicated with asterisks in Figure 4.4) had background mercury contamination of 0.01-0.02 nmol mg^{-1}, which nearly doubled the amount of total mercury in those sulfide-free systems (the other isolates had mercury concentrations that ranged between below the detection limit, 0.1 pmol mg^{-1}, and 0.2 pmol mg^{-1}). The reducibility of the mercury contamination may not be the same as the reducibility of the mercury equilibrated with the other DOM samples. When we exclude the three contaminated DOM isolates from the data presented in Figure 4.4a, there is no relationship between DOM $SUVA_{254}$ and the Hg_R fraction.

DOM in sulfide-containing systems, however, does have a variable impact on the Hg_R fraction depending on the $SUVA_{254}$. The effect of mercury contamination in the three contaminated isolates was less significant in the sulfide-containing systems because the amount of mercury spiked into the system was ten times greater than the amount of mercury spiked into the sulfide-free systems. The four samples with $SUVA_{254}$ values below about 3.5 L mg^{-1} m^{-1} all show reducible mercury levels that are significantly lower than those DOM isolates with higher $SUVA_{254}$ values. Three of the four DOM isolates with the highest SUVA values have Hg_R fractions above 5%. The DOM isolate with the highest $SUVA_{254}$ value, the Suwannee River HA, is somewhat anomalous. The Hg_R fraction for the Suwannee River HA is lower than that for the other DOM isolates with high $SUVA_{254}$ values, but it is still greater than the fraction of Hg_R for the DOM isolates with low $SUVA_{254}$ values.

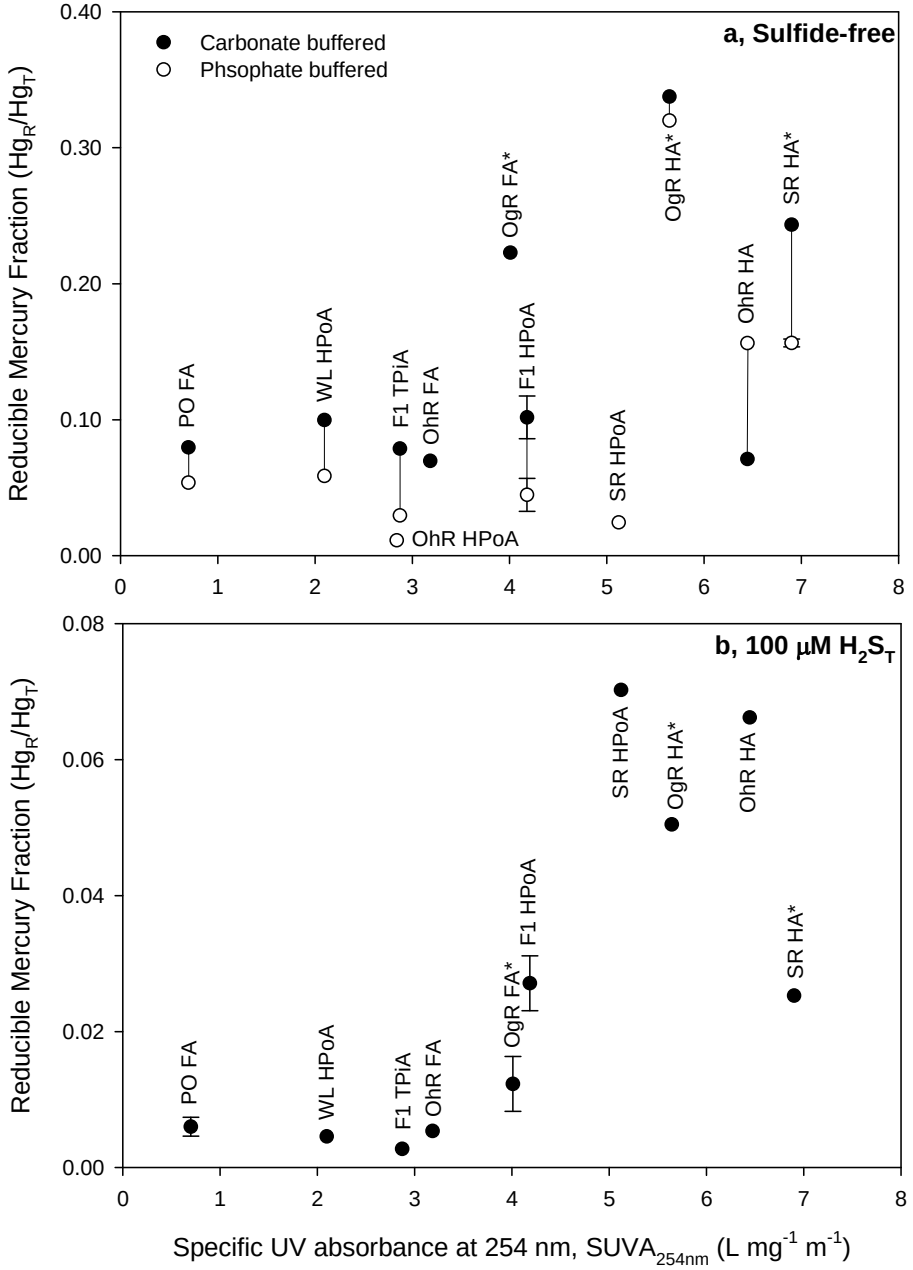

Figure 4.4. The reducible mercury fraction as a function of the specific ultraviolet absorbance of the DOM in the system for (a) sulfide-free systems in two different buffers, and (b) sulfide-containing systems in carbonate buffer. Each sample is labeled with the DOM isolate. Abbreviations correspond to Table 4.2. Samples with an asterisks had high background levels of mercury. DOM = 6.9-10.5 mg L^{-1}; Hg_T = 0.23-0.37 nM in sulfide-free systems, except for DOM samples with high background mercury concentrations (*); Hg_T = 2.1-2.8 nM in sulfide-containing systems; t_1 = 22.1-24.0 h for all samples; t_2 = 23.5-24.5 h for all sulfide-containing samples. Error bars represent one standard deviation for 2-4 replicates, depending on sample.

Equilibration times in sulfide-containing systems had mixed effects on the Hg_R fraction. An increase in the time for mercury to equilibrate with Everglades F1 HPoA (t_1) had little effect on the Hg_R fraction when t_2 was fixed at about 24 h (Figure 4.5a). The increase in the Hg_R fraction with increasing t_1 was small on an absolute scale, and the only potentially meaningful difference in the Hg_R fraction is between t_1 = 0.17 h and 70.2 h (0.19% and 0.95% Hg_R, respectively). An increase in the time for the Hg-DOM (Everglades F1 HPoA as the DOM isolate) solution to equilibrate with sulfide (t_2) decreased the Hg_R fraction (Figure 4.5b). The Hg_R fraction dropped from about 5.9% at t_2 = 0.17 h to 0.3% at t_2 = 2.0 h. There was a slight increase in the Hg_R fraction beyond about 10 h, but the increase was small compared to the decrease in Hg_R over the first 2 h.

The amount of sulfide added to the system also had a small effect on the reducible mercury fraction (Figure 4.6). The Hg_R fraction increased as the total sulfide concentration was increased from 0.3 to 3 μM. From 3 to 100 μM, the Hg_R fraction decreased with increasing total sulfide concentration. Most of the changes in Hg_R with variable sulfide concentration are too small to be significant. The 95% confidence interval of the replicated system at 100 μM H_2S_T is ±0.6%. If we apply that interval to all of the other samples, the only significant difference is between the sample with the low Hg_R fraction at 0.3 μM H_2S_T and sample with the high HgR fraction at 3 μM H_2S_T. The variable sulfide system is also complicated by likely changes in sulfide concentration over time. The amount of sulfide in the system is reported as the initial concentration based on dilution of the stock solution used to prepare the sample. The sulfide concentration is expected to decrease over time as it reacts with organic matter (Heitmann and Blodau, 2006; Einsiedl et al., 2008). The half-life for sulfide incorporation into DOM, in systems similar to those used in this study, has been reported as 3.9 h (Heitmann and Blodau, 2006). The

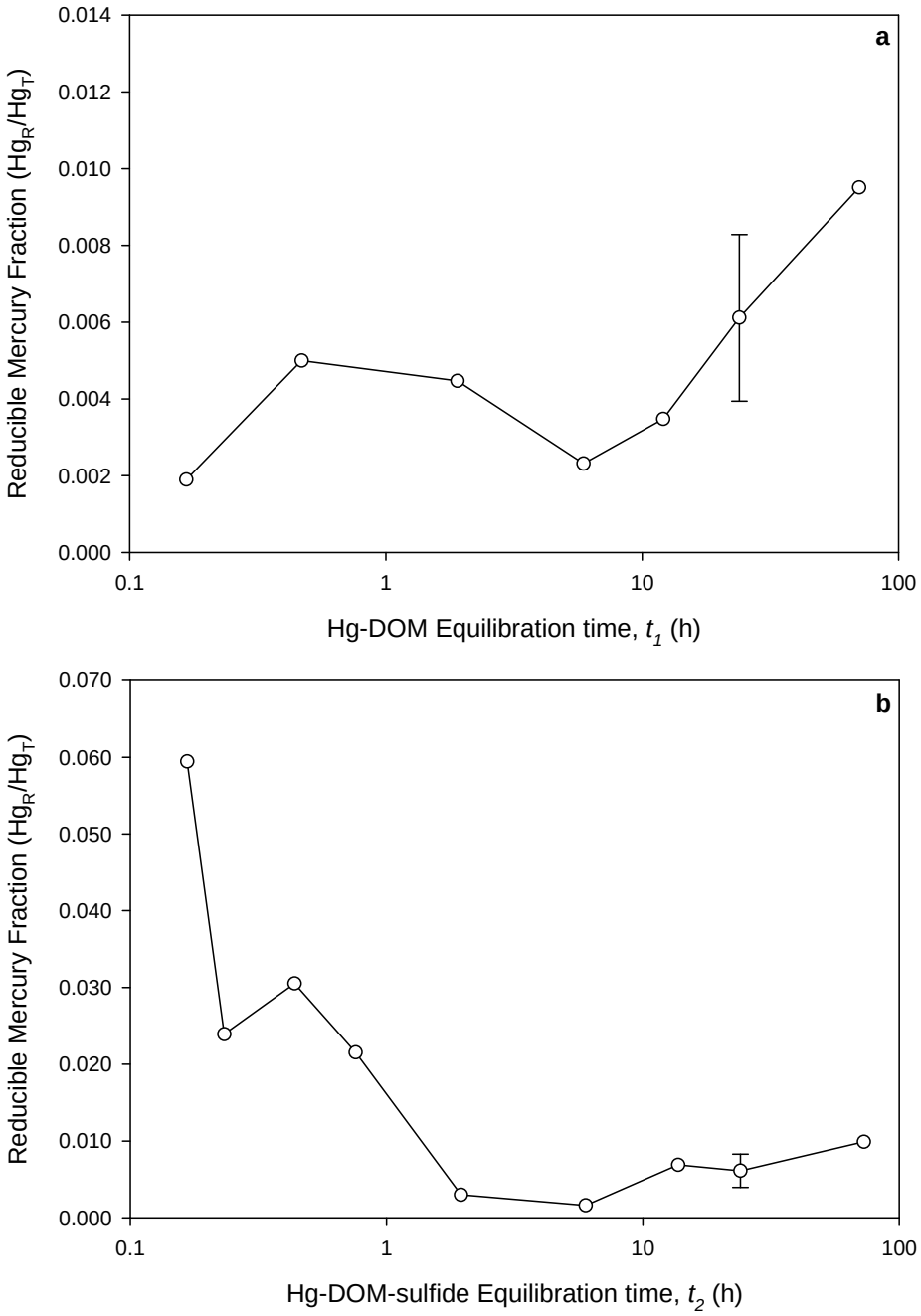

Figure 4.5. The effect of (a) Hg-DOM equilibration time (t_1) and (b) Hg-DOM-sulfide equilibration time (t_2) on the amount of reducible mercury in systems that contain 100 μM H_2S_T in phosphate buffer. Note the narrow range of the ordinate axis, especially in (a). When t_1 was varied, t_2 was held constant at 23.7-24.0 h; when t_2 was varied, t_1 was held constant at 23.8-24.0 h. DOM = 8.8-9.4 mg L^{-1} Everglades F1 HPoA. Hg_T = 2.3-3.3 nM. Error bars represent one standard deviation for four replicates.

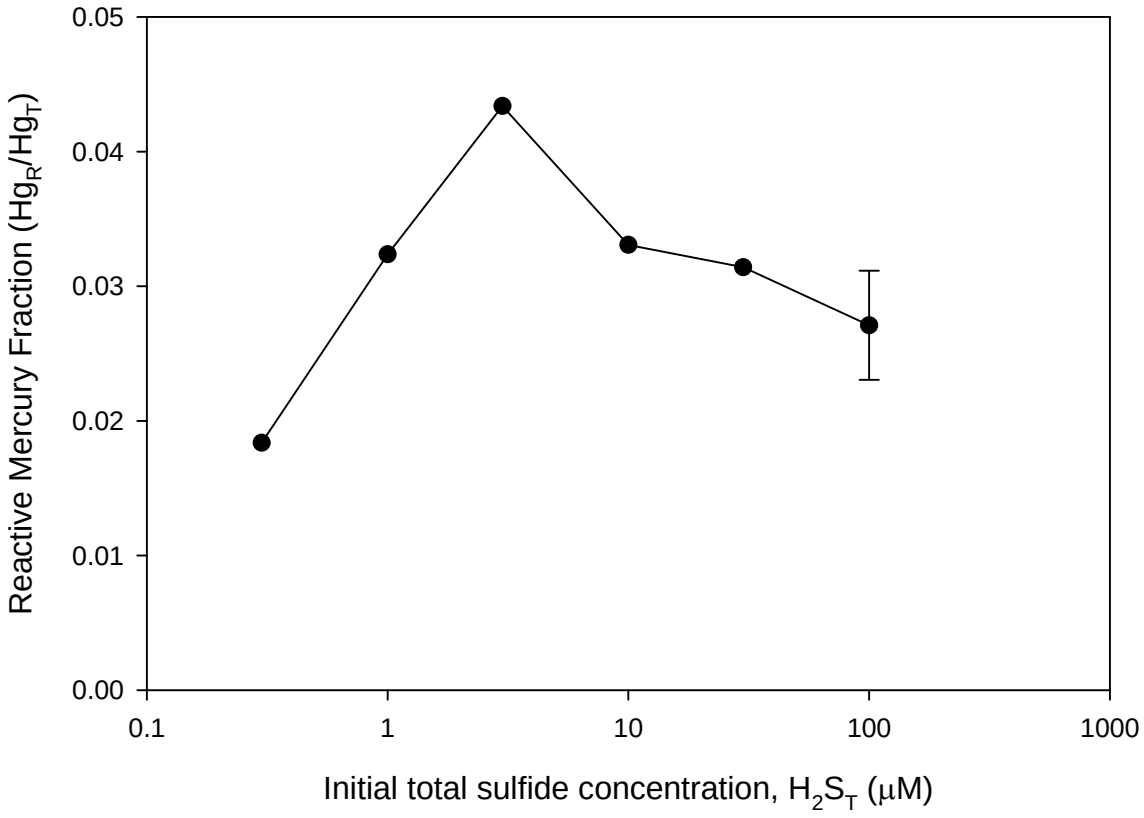

Figure 4.6. The effect of sulfide concentration on the reducible mercury fraction in systems that contain 8.8 mg L^{-1} F1 HPoA, and 2.3-2.5 nM Hg_T, where t_1 = 23.1-24.0 h and t_2 = 24.1-24.4 h. Error bars represent one standard deviation for two replicates.

capacity of organic matter to accept electrons through sulfide oxidation has been reported as about 1.3 μeq mgC^{-1} (Heitmann and Blodau, 2006). Most of the change in the Hg_R fraction occurs over a relatively short time (Figure 4.5b), but total sulfide concentrations are expected to change over this time as well. The effects of variable sulfide concentrations on the Hg_R fraction are generally too small to be meaningful.

4.5 DISCUSSION

Mercury and dissolved organic matter. The capacity of strong binding sites in the Everglades F1 HPoA, the primary DOM isolate used in this study, is about 4 nmol mg^{-1} (Haitzer et al., 2002). These binding sites are characterized by large conditional stability constants (on the order of 10^{23} L kg^{-1} at pH 7, I 0.1 M); hence, they are expected to be thiol-like. Above this strong binding capacity, the stability constants decrease to much smaller values (on the order of 10^{11} L kg^{-1} at pH 7, I 0.1 M) that are expected to represent mercury binding by oxygen-containing functional groups (carboxylic, phenolic). Other researchers have reached the same conclusion for mercury binding by organic matter from a wide variety of sources (Skyllberg et al., 2000; Haitzer et al., 2002, 2003; Hsu and Sedlak, 2003; Lamborg et al., 2003; Han and Gill, 2005; Skyllberg et al., 2006; Black et al., 2007; Tipping, 2007; Gerbig et al., 2011). We observed that the Hg_R fraction increased dramatically as the Hg:DOM ratio exceeded the 4 nmol mg^{-1} strong-binding capacity of the Everglades F1 HPoA (Figure 4.2). Mercury bound strongly to thiol-like sites at low Hg:DOM ratios was much less reactive with respect to tin reduction than mercury bound weakly to carboxyl- and phenol-like sites.

The Hg_R fraction appears to depend on the strength of Hg-DOM binding, but the reducibility of mercury bound to the organic ligands in this study (Table 4.2) and in another study (Lamborg et al., 2003) suggests that the strength of the actual binding site is of only minor significance to the reducibility of mercury. Glutathione, for example, is able to out-compete DOM for mercury, even at low Hg:DOM ratios (Hsu-Kim and Sedlak, 2005), but Hg-glutathione complexes are much more reactive with respect to tin reduction than Hg-DOM complexes. One explanation for the low reducibility of mercury bound to strong DOM binding sites is that the strong sites are slow to release mercury during tin reduction, whereas weaker sites exchange mercury rapidly.

In the reducible mercury measurement, the sample is exposed to the tin reductant for 15 min in an acidic, chloride-rich solution. Hg(II) and Hg-chloride complexes are readily reduced by tin (the total mercury analytical method relies on the rapid reduction of these species). Mercury bound to strong sites in the DOM may not be released quickly enough to be reduced during the 15 min of exposure to the tin reductant, even if the combination of proton competition for binding sites and chloride complexation for mercury is sufficient to desorb the mercury from the DOM. We can assume that these conditions are thermodynamically strong enough because the organic ligands, which have comparable binding sites to those observed in DOM, release mercury for reduction.

Metal binding by ligands is not necessarily a rapid process, especially when metals go through a series of binding arrangements before settling on the strongest sites (Hering and Morel, 1989a). Little is known about mercury release from DOM, but mercury binding takes a significant period of time – upwards of 24 h – to reach equilibrium with dissolved organic matter (Lamborg et al., 2003; Gasper et al., 2007; Miller et al., 2009). Stable Hg_R measurements were

not observed in this study until almost 10 h of Hg-DOM equilibration time had passed (Figure 4.3), presumably because mercury rapidly binds to more abundant but weaker sites, and slowly exchanges to less reactive strong sites over a period of time, as has been observed with copper and ligands in sea water (Hering and Morel, 1989b). If the release of mercury from the strong sites is also kinetically limited (in a way that the model ligands are not limited), we would see a substantial difference between the Hg_R fractions of DOM and organic ligands.

The explanation for the slow release kinetics is not entirely clear. All DOM isolates free of background mercury contamination have similar Hg_R fractions (Figure 4.4a), and the Hg_R fractions for the organic ligands are significantly greater than any DOM isolate (Table 4.2). The consistency in Hg_R across DOM samples from sulfide-free systems (Figure 4.4a) eliminates potential correlations with molecular weight, sulfur content, or other bulk characteristics of DOM (Appendix Table A3). The differences between the molecular weight of some of the smaller DOM isolates used in this study and some of the model compounds are not especially large. For example, Pacific Ocean fulvic acid has an average molecular weight of 532 g mol^{-1} (Appendix Table A3; Waples et al., 2005) and glutathione has a molecular weight of 307.3 g mol^{-1}. There isn't a single bulk property of DOM that explains the substantial difference between reducible mercury in solutions with model compounds and solutions with DOM, and also explains the consistent reducible mercury fractions across the various DOM isolates used in this study.

The slow release of mercury from DOM may partially explain observations of decreased mercury methylation rates in the presence of DOM (Barkay et al., 1997; Hammerschmidt et al., 2008). It has been demonstrated that microbial uptake of mercury is enhanced in the presence of simple organic ligands and when mercury is present as neutrally charged inorganic complexes

(Barkay et al., 1997; Schaefer and Morel, 2009; Schaefer et al., 2011). We clearly demonstrated that mercury bound to strong DOM sites and simple organic ligands have different reactivity with respect to tin reduction, even though both the DOM and the organic ligands contain functional groups that strongly bind mercury. While cysteine may rapidly exchange mercury with a microbial surface and promote methylation (Schaefer and Morel, 2009; Schaefer et al., 2011), DOM does not necessarily release bound mercury quickly, even when it comes into contact with surface sites on methylating microbes that present thermodynamically more favorable binding sites.

Mercury, dissolved organic matter, and sulfide. The mercury, DOM, and sulfide systems in this study are over-saturated with respect to metacinnabar under most circumstances (Appendix Figure A4). The solutions (~2.5 nM Hg_T) are only potentially under-saturated at high sulfide concentrations (100 μM H_2S_T) if a disputed aqueous mercury-sulfide complex (HgS^0) is included in equilibrium calculations (Skyllberg, 2008; Deonarine and Hsu-Kim, 2009), and the highest metacinnabar solubility product is chosen from the range of reported values (Appendix Figure A4). When these supersaturated conditions exist in a solution that also contains dissolved organic matter, very small (<10 nm) or poorly-crystallized metacinnabar-like particles will form and be stabilized by DOM (Chapter 3; Slowey, 2010; Gerbig et al., 2011). Figure 4.1 demonstrates that HgS(s) precipitated in the absence of DOM is not as reducible as the metacinnabar-like nanoparticles formed in the presence of DOM. Not all DOM isolates behave identically with respect to nanoparticulate metacinnabar formation. DOM isolates characterized by low $SUVA_{254}$ yield metacinnabar-like nanoparticles that are larger or more ordered than DOM isolates characterized by high $SUVA_{254}$ (Chapter 3).

In this study we show that the reducibility of the mercury in these metacinnabar-like nanoparticles is also related to the $SUVA_{254}$ of the DOM, which suggests there may be a relationship between particle size/crystallinity and the Hg_R fraction. For example, mercury from the larger or more crystalline nanoparticles formed in the presence of Pacific Ocean fulvic acid is significantly less reducible than mercury from the nanoparticles formed in the presence of Suwannee River hydrophobic acid or Ohio River humic acid (Figure 4.4b). Small particles have higher surface area-to-volume ratios, which would expose a greater fraction of the total mercury in the particle to the tin reductant. Small particles also tend to be easier to dissolve because high interfacial tension tends to destabilize the particles (Gilbert and Banfield, 2005). Poorly-crystallized materials are known to have different solubilities and dissolution rates than the bulk form of those materials (Shea and Helz, 1989; Stumm and Morgan, 1996). The poorly crystallized/smaller metacinnabar nanoparticles may be less stable, and therefore more susceptible to reduction by tin than the larger and well-crystallized metacinnabar particles.

It has been suggested that two distinct pools of dissolved organic matter interact with HgS(s) surfaces – one pool irreversibly adsorbs to the surface while the other pool readily exchanges to and from the surface (Waples et al., 2005). The irreversible pool is composed predominantly of DOM with low $SUVA_{254}$, while the opposite is true of the reversible pool (Waples et al., 2005). $SUVA_{254}$ is well correlated with both dissolved organic matter aromaticity and molecular weight (Chin et al., 1994; Weishaar et al., 2003), which indicates that either or both characteristic might be the driving force behind differences in particle interactions. Dissolved organic matter with high $SUVA_{254}$ is more effective at dissolving HgS(s), possibly because of the exchangeability of the DOM (Ravichandran et al., 1998). The exchangeability of dissolved organic matter may explain why metacinnabar-like nanoparticles formed with the

DOM of low $SUVA_{254}$ are also less reducible. Once the low-SUVA DOM adsorbs to the metacinnabar surface there is little exchange with the solution. The high-$SUVA_{254}$ DOM, however, promotes redissolution of the particles and readily leaves the surface after dissolving mercury. The systems still contains excess sulfide, so redissolved mercury precipitates again, perpetuating a cycle that yields smaller, less crystalline, and more reducible metacinnabar-like nanoparticles.

The redissolution/reprecipitation cycle is supported by the reducible mercury data for the Hg-DOM-sulfide system (Figure 4.5b). After sulfide exposure, the amount of reducible mercury drops as metacinnabar-like nanoparticles precipitate. The reducible mercury fraction is at a minimum at t_2 = 6 h, when only 0.2% of the total mercury is reducible by tin. After 6 h, the reducible mercury fraction rises again, eventually reaching 1.0% at t_2 = 73 h. The 95% confidence interval for the t_2 = 24 h point is ±0.2% (n=4). If we apply that interval to the other points in Figure 4, the increase in the Hg_R fraction with time after 6 h is significant. The cycling of mercury dissolution and precipitation in sulfide- and DOM-containing systems has been observed previously (Slowey, 2010). The cycling was most pronounced at the lowest mercury concentrations (~1 nM Hg_T), which are comparable to what was used for reducible mercury measurements in this study (~2.5 nM). No changes in metacinnabar size or crystallinity as a function of sulfide equilibration time (t_2) were observed in Chapter 3 with X-ray spectroscopy techniques. This is likely due to the higher total mercury concentration (~150 nM Hg_T), where cycling between dissolution and precipitation is less pronounced (Slowey, 2010).

The increase and subsequent decrease in the Hg_R fraction with increasing sulfide concentration (Figure 4.6) does not match the change in any known mercury species as a function of sulfide concentration. In general, metacinnabar becomes increasingly soluble with

increasing sulfide concentration, although it is likely over-saturated in all systems in this study, (Appendix Figure A4; Deonarine and Hsu-Kim, 2009). X-ray spectroscopy data suggests that the size/crystallinity of the metacinnabar-like nanoparticles likely present in these systems should increase as sulfide concentration increases from 1 to 100 μM (Chapter 3). Consequently, we would expect mercury reducibility to decline with increasing sulfide concentrations in that range. However, the reducible mercury fraction at 1 and 10 μM H_2S_T was about the same, and the reducible mercury fraction peaked at 3 μM H_2S_T (Figure 4.6). It is generally recognized that our understanding of mercury speciation at low sulfide and mercury concentrations is incomplete, especially when the unknown effects of DOM are considered (Miller et al., 2007; Skyllberg, 2008; Deonarine and Hsu-Kim, 2009). Furthermore, the loss of sulfide to the DOM may not be a trivial consideration in this system, especially at the lowest sulfide concentrations (Heitmann and Blodau, 2006; Einsiedl et al., 2008). The data in Figure 4.6 suggests there are changes in mercury species in this environmentally important range that we do not currently understand.

Environmental implications. Reducible mercury provides a useful tool to address changes in the form of mercury present in the environment. We have demonstrated that higher reactivity of unequillibrated mercury is related to the slow formation of equilibrium Hg-DOM species (Figure 4.3). These data explain the observation that mercury deposited in the Florida Everglades from the atmosphere is more reactive than mercury that has equilibrated in the system (Krabbenhoft et al., 1998). These results may also give insight into the forms of mercury available for methylation in environmental samples. The positive correlation between microbial methylation rate and the amount of reducible mercury in soil cores (Marvin-DiPasquale et al., 2009) suggests that we can use these data to characterize speciation relevant to microbes.

DOM and sulfide both effectively reduce the rate of microbial methylation, despite the fact that metacinnabar solubility increases with increasing sulfide concentration (Barkay et al., 1997; Hammerschmidt et al., 2008). Despite the inhibitory effects of DOM and sulfide, methylation continues to take place in organic matter-rich, sulfate-reducing environments (Gilmour et al., 1998; Morel et al., 1998; Fitzgerald et al., 2007). Microbes passively take up small neutrally-charged mercury species, and mercury bound to DOM is considered unavailable to microbes (Barkay et al., 1997). The fraction of mercury methylated in mining-affected environments is significantly lower than in environments with mercury from atmospheric deposition (Gilmour et al., 1998; Holloway et al., 2009), which suggests that large mercury-containing particles are also unavailable for methylation. This study has shown that the small, poorly crystallized, DOM-coated metacinnabar-like nanoparticles identified with X-ray spectroscopy techniques (Chapter 3; Gerbig et al., 2011) are significantly more reactive than metacinnabar precipitated without DOM. DOM with high $SUVA_{254}$ is more effective at maintaining the reactivity of metacinnabar-like nanoparticles than DOM with low $SUVA_{254}$. Future studies of methylation must consider small and poorly crystalline metacinnabar-like particles to be a significant pool of reactive mercury that may be substantially more available for methylation than previously considered.

Chapter 5

Conclusions and Summary

5.1 SUMMARY OF RESULTS

Direct determination of mercury speciation in natural environments is confounded by low mercury concentrations and poor analytical sensitivity. We were able to empirically examine mercury speciation in sulfide-containing and sulfide-free systems at mercury concentrations as low as 50 nm Hg_T, and Hg:DOM ratios less than 2 nmol mg^{-1} by combining solid phase extraction using C_{18} resin with extended X-ray absorption fine structure (EXAFS) spectroscopy. Minimizing mercury concentration and Hg:DOM ratio is important because the strong binding sites in DOM are in low abundance. This is the first study to empirically examine mercury speciation at concentrations and Hg:DOM ratios where the strong binding sites are relevant for mercury speciation.

In the absence of sulfide, mercury binding by DOM (hydrophobic acid isolate from the F1 site in the Florida Everglades) is characterized by 2.4 ± 0.2 sulfur atoms with a bond length typical of mercury-organic thiol ligands (2.35 Å). When mercury is equilibrated with DOM and sulfide the mercury species are distinctly different. The mercury–sulfur bond is significantly longer (2.51–2.53 Å) and is similar to the mercury–sulfur bond distance in metacinnabar (2.53 Å) (Chapter 2). Although the mercury-sulfur bond distance is representative of metacinnabar, there are fewer sulfur atoms binding mercury in Hg-DOM-sulfide systems than bind mercury in well crystallized metacinnabar. At a low Hg:DOM ratio where strong-binding DOM sites may control mercury speciation (1.9 nmol mg^{-1}) mercury was coordinated by 2.3±0.2 sulfur atoms, and the coordination number rose with increasing Hg:DOM ratio (Chapter 2). The less-than-ideal coordination numbers indicate metacinnabar-like species on the nanometer scale, and the positive correlation between Hg:DOM ratio and sulfur coordination number suggests

progressively increasing particle size or crystalline order with increasing abundance of mercury with respect to DOM.

In addition to Hg:DOM ratio, we examined several other parameters that were potentially important to the size or crystalline order of the metacinnabar-like nanoparticles in Hg-DOM-sulfide systems (Chapter 3). The amount of time that mercury equilibrated with DOM before sulfide exposure (12-142 h) and the amount of time that the Hg-DOM-sulfide system was allowed to equilibrate (4-121 h) did not significantly change the structure of the metacinnabar-like species at relatively high mercury concentrations (~150 nM Hg_T). Significant changes in the sulfur coordination number were observed with variable sulfide concentrations (1-100 μM). The changes in sulfur coordination number suggest that the metacinnabar-like nanoparticles were significantly smaller or more disordered at lower sulfide concentrations. The size or disorder of metacinnabar nanoparticles was also correlated with the specific ultraviolet absorbance (SUVA) of the DOM isolate in the system. DOM isolates of higher SUVA stabilized metacinnabar-like nanoparticles that were smaller or more disordered than those stabilized by DOM isolates of low SUVA.

The chemical reactivity of the Hg-DOM complexes and metacinnabar-like nanoparticles was examined with a tin-reducible mercury assay. Mercury bound to strong thiol binding sites in dissolved organic matter was less reducible than mercury bound by several organic ligands, including thiol ligands, and was also less reducible than mercury bound to carboxyl groups in DOM. Mercury precipitated with sulfide in the presence of DOM was less reducible than Hg-DOM complexes, but was more reducible than HgS(s) precipitated without DOM present. The reducibility of poorly crystallined metacinnabar-like HgS nanoparticles coated with DOM increased as the specific ultraviolet light absorbance (SUVA) of the DOM decreased. The

amount of reducible mercury decreased as the time of equilibration with sulfide increased, especially over the first 2 h of equilibration. The time that mercury equilibrated with DOM before sulfide addition affected the reducible mercury fraction but the amount of sulfide in solution had a nominal effect.

5.2 ENVIRONMENTAL IMPLICATIONS

This study is the first to examine the role of DOM in nanoparticle growth at low Hg:DOM ratios where the strong binding sites of the organic matter are relevant for mercury speciation. Metacinnabar-like particles formed at increasing Hg:DOM ratio are larger or more crystalline, which shows that minimizing the Hg:DOM ratio is a critical consideration when empirically determining metal speciation. The $SUVA_{254nm}$ of the DOM isolates is negatively correlated with the number of sulfur atoms coordinating mercury in metacinnabar-like nanoparticles. This suggests that bulk properties of the DOM isolates, namely aromaticity or molecular weight, are important for nanoparticle growth and aggregation at low Hg:DOM ratios. We can expect the form of mercury in sulfide-containing aquatic environments to be significantly different depending on the nature of the organic matter present. In waters containing DOM of low $SUVA_{254nm}$, mercury will precipitate as larger and more crystalline HgS(s) nanoparticles, and these particles will aggregate more readily into bulk HgS(s). Conversely, in waters containing DOM of high $SUVA_{254nm}$, mercury-sulfide nanoparticles will be smaller and less crystalline and the particles will be less likely to aggregate into bulk HgS(s).

Using the reducible mercury assay we have demonstrated that higher reactivity of unequillibrated mercury is related to the slow formation of equilibrium Hg-DOM species. These

data explain the observation that mercury deposited in the Florida Everglades from the atmosphere is more reactive than mercury that has equilibrated in the system (Krabbenhoft et al., 1998). These results may also give insight into the forms of mercury available for methylation in environmental samples. The positive correlation between microbial methylation rate and the amount of reducible mercury in soil cores (Marvin-DiPasquale et al., 2009) suggests that we can use these data to characterize speciation relevant to microbes.

DOM and sulfide both effectively reduce the rate of microbial methylation, despite the fact that metacinnabar solubility increases with increasing sulfide concentration (Barkay et al., 1997; Hammerschmidt et al., 2008). Despite the inhibitory effects of DOM and sulfide, methylation continues to take place in organic matter-rich, sulfate-reducing environments (Gilmour et al., 1998; Morel et al., 1998; Fitzgerald et al., 2007). Microbes passively take up small neutrally-charged mercury species, and mercury bound to DOM is considered unavailable to microbes (Barkay et al., 1997). The fraction of mercury methylated in mining-affected environments is significantly lower than in environments with mercury from atmospheric deposition (Gilmour et al., 1998; Holloway et al., 2009), which suggests that large mercury-containing particles are also unavailable for methylation. This study has shown that the small, poorly crystallized, DOM-coated metacinnabar-like nanoparticles are significantly more reactive than metacinnabar precipitated without DOM. DOM with high $SUVA_{254}$ is more effective at maintaining the reactivity of metacinnabar-like nanoparticles than DOM with low $SUVA_{254}$. Future studies of methylation must consider small and poorly crystalline metacinnabar-like particles to be a significant pool of reactive mercury that may be substantially more available for methylation than previously considered.

The results of this study also have broad implications for other nanoparticles in the environment. Organic matter may play a substantial role in stabilizing the nanoparticles and multinuclear clusters that natively form in many natural systems (Rozan et al., 2000; Moreau et al., 2007). The nature of organic matter may be an important factor when considering the stabilization, transport, and bioavialability of metal colloids from contaminated sites (Weber et al., 2009; Pédrot et al., 2011). Non-native nanocolloids introduced for engineering purposes (Liu et al., 2005) or as contaminants (Hyung et al., 2006) are also likely to be affected by organic matter. It is reasonable to expect that DOM will not act uniformly with respect to these nanocolloids, much as DOM did not act uniformly with respect to the size and crystallinity of the metacinnabar-like nanoparticles observed in this study.

5.3 FUTURE WORK

Previous empirical studies of mercury-sulfide precipitation in the presence of DOM have been conducted at relatively high mercury concentrations (Ravichandran et al., 1999; Deonarine and Hsu-Kim, 2009; Slowey, 2010). The lowest concentration in those studies where speciation was empirically determined, 10 μM Hg_T, is over two orders of magnitude more concentrated than the lowest mercury concentration used in this study (50 nM Hg_T). However, the lowest concentration used in this study is still 2-3 orders of magnitude higher than typical environmental concentrations (Grigal, 2002). We were able to extrapolate some of our empirical results to lower mercury concentrations based on the solid phase extraction characteristics of mercury or fraction of reducible mercury, but those extrapolations are not are precise as the definitive characterization of mercury speciation provided by X-ray spectroscopy. The studies that have

used higher mercury concentrations also extrapolated their results to lower concentrations (based on centrifugation or light scattering data), but we our empirical results at concentrations they extrapolated to, demonstrate that empirical observation provides a more nuanced understanding of speciation than extrapolation.

One of the most exciting tools for characterizing metal speciation at low metal concentrations is voltammetry. There is substantial debate about the application and interpretation of voltammetry data, particularly where naturally formed nanocolloids or clusters are concerned (Rozan et al., 2000; Ciglenecki et al., 2005), but when the tool is used appropriately it is capable of identifying metal speciation at total metal concentrations that are substantially lower than those used in this study. The presence of dissolved organic matter complicates volatammetric measurements, and typical hanging mercury drop electrodes are problematic for use in identifying mercury speciation, but those obstacles will be overcome.

In this study we used the specific ultraviolet absorbance of the dissolved organic matter as a proxy for chemical and physical properties (i.e., aromaticity and molecular weight) of the DOM because SUVA is generally well correlated to these properties (Chin et al., 1994; Weishaar et al., 2003). Aromaticity and molecular weight have not been reported elsewhere for all of the isolates used in this study and we lacked sufficient quantities of DOM isolate to make the measurements ourselves for some isolates. The relationship between SUVA and aromaticity is robust, but imperfect. Future studies should make direct measurement of the physical properties, if possible, rather than relying on a proxy measurement. Additionally, other tools to characterize DOM may be useful, including fluorescence spectroscopy, size exclusion chromatography, and spectral slope.

Furthermore, the DOM isolates used in this study were primarily hydrophobic acids or sub-fractions thereof. There are other portions of the DOM pool that comprise a significant amount of naturally occurring DOM (Thurman and Malcolm, 1981, Aiken et al., 1992) that we did not test. Previous studies have shown that the hydrophobic fraction of the organic matter is probably the most important fraction with respect to mercury-sulfide interactions. The growth of HgS(s) in systems with whole water (stripped of multivalent cations) or only the hydrophobic acid derived from the whole water showed effectively identical HgS(s) growth and aggregation behavior (Ravichandran et al., 1999). The hydrophobic acid fraction is also more practical because it is easier to isolate the large quantities of isolate required for these studies. Future studies should include whole water samples and non-hydrophobic acid fractions of DOM to fully characterize the role of DOM in mercury-sulfide geochemistry.

The experimental conditions in this study survey a wide range of variables that are potentially important to the formation of poorly crystalline metacinnabar-like nanoparticles, including DOM characteristics, sulfide concentration, Hg:DOM ratio, and equilibration times. We think that we surveyed some of the most important variables (and variables that are more difficult for other research groups to address), but we still neglected critical variables like pH and ionic strength. Ionic strength has a significant impact on the aggregation of DOM-coated metacinnabar particles (Deonarine and Hsu-Kim, 2009), and many of the pertinent mercury-sulfide and mercury-DOM interactions involve proton exchange (Appendix Table A2). For example, the metacinnabar-like particles that form in lower ionic strength systems (such as fresh water) will have substantially thicker electronic double layers, which may limit the adsorption of anionic DOM to the surface and may promote HgS particle growth and aggregation. However, this process may be balanced by increased electronic repulsion of negatively charged

metacinnabar-like particles, which will slow aggregation. The potential effects of extreme pH is somewhat more clear: extreme pH's tend to promote the solubilization of metacinnabar (as free mercury ions at low pH and as mercury-sulfide complexes at high pH). At circumneutral pH's the hydrophobicity of the DOM may change dramatically, especially around the pKa for the carboxyl groups in the DOM (typically 4-4.5). More protonated DOM will likely adsorb more readily to the metacinnabar particle surface, preventing growth and aggregation at earlier stages. A full accounting of mercury speciation in the presence of DOM and sulfide must account for the environmental ranges of pH and ionic strength.

We also intentionally kept all of our samples in the dark to prevent photoreactions. DOM reduction of mercury in dark systems is possible, but the effects can be neglected above about 0.5 mgC L^{-1} (Gu et al., 2011). In systems with light exposure, though, a whole suite of direct and indirect mechanisms can alter mercury geochemistry (Amyot et al., 1997; Krabbenhoft et al., 1998; Lalonde, 2001; Ravichandran, 2004; Garcia et al., 2005; O'Driscoll et al., 2006; Zhang, 2006). This is analogous to the role of photo-Fenton reactions in iron geochemistry in natural systems (Zepp et al., 1992), though precise mechanisms are not necessarily the same. How these mechanisms impact nanocolloidal metacinnabar-like particles, how various DOM characteristics change those interactions, and a suite of other important questions all require answers before a complete understanding of mercury biogeochemistry that includes the species identified in this study is possible.

The kinetics of the formation of metacinnabar-like particles in the presence of DOM is also likely to be an important parameter in environmental systems. We explore some kinetics issues in Chapters 3 and 4, but have done so primarily in a qualitative manner. No known studies have examined the kinetics of metacinnabar-like particle formation in a manner that would allow

for the rate of chemical reactions to be separated from the mixing scenario. However, some of the studies that have addressed Hg-DOM-sulfide systems used substantially different mixing regimes, but observed consistent kinetics. Slowey (2009) equilibrated the Hg-DOM-sulfide systems quiescently, whereas Miller et al. (2007) mixed their systems in a manner consistent with our method. Despite the differences in mixing scenarios, the two studies have similar kinetics results. In both studies the Hg-DOM-sulfide system equilibrated in 4-8 hours, which is also consistent with the equilibration kinetics we observed. The observation that reaction kinetics are generally independent of mixing suggests that the reaction is slow relative to the transport of reactants, even in unmixed scenarios, and that variations in mixing rate will have a nominal effect on the reaction rate. A thorough analysis of mass action and kinetics is warranted, but current studies suggest that the reaction rate is slow relative to external mass transfer.

Of course, this is all academic if the most important sensor of mercury speciation in the environment, microbes, show that nanocolloidal forms of metacinnabar are just as inert as large particles. Studies need to be conducted to determine the availability of these poorly-crystallized metacinnabar nanoparticles for methylation. The reducible mercury data shows that under some circumstances (e.g., DOM of high $SUVA_{254}$) there are large increases in the susceptibility of mercury to chemical reduction by tin. Although a good correlation between the reducible mercury fraction and methylation rates has been observed (Marvin-DiPasquale et al., 2009), the biogeochemical framework that explains this correlation is not complete. The ultimate test of the importance of DOM-stabilized nanocolloidal metacinnabar-like particles (DOMSNCMCLP, for short) is how microbes perceive them, and most importantly, if they play an important role in mercury methylation.

References

Aiken, G., Cotsaris, E., 1995. Soil and hydrology: Their effect on NOM. *Journal of the American Water Works Association* **87**, 36-45.

Aiken, G.R., 1984. Evaluation of ultrafiltration for determining molecular weight of fulvic acid. *Environmental Science & Technology* **18**, 978-981.

Aiken, G.R., Hsu-Kim, H., Ryan, J.N., 2011. Influence of dissolved organic matter on the environmental fate of metals, nanoparticles, and colloids. *Environmental Science & Technology* **45**, 3196-3201.

Aiken, G.R., Leenheer, J.A., 1993. Isolation and chemical characterization of dissolved and colloidal organic matter. *Chemistry and Ecology* **8**, 135-151.

Aiken, G.R., McKnight, D.M., Thorn, K.A., Thurman, E.M., 1992. Isolation of hydrophilic organic-acids from water using nonionic macroporous resins. *Organic Geochemistry* **18**, 567-573.

Amirbahman, A., Reid, A.L., Haines, T.A., Kahl, J.S., Arnold, C., 2002. Association of methylmercury with dissolved humic acids. *Environmental Science & Technology* **36**, 690-695.

Amyot, M., Mierle, G., Lean, D., Mc Queen, D.J., 1997. Effect of solar radiation on the formation of dissolved gaseous mercury in temperate lakes. *Geochimica et Cosmochimica Acta* **61**, 975-987.

Andren, A.W., Harriss, R.C., 1975. Observations on the association between mercury and organic matter dissolved in natural waters. *Geochimica et Cosmochimica Acta* **39**, 1253-1258.

Babiarz, C.L., Hurley, J.P., Hoffmann, S.R., Andren, A.W., Shafer, M.M., Armstrong, D.E., 2001. Partitioning of total mercury and methylmercury to the colloidal phase in freshwaters. *Environmental Science & Technology* **35**, 4773-4782.

Balogh, S.J., Nollet, Y.H., Swain, E.B., 2004. Redox chemistry in Minnesota streams during episodes of increased methylmercury discharge. *Environmental Science & Technology* **38**, 4921-4927.

Balogh, S.J., Swain, E.B., Nollet, Y.H., 2006. Elevated methylmercury concentrations and loadings during flooding in Minnesota rivers. *Science of the Total Environment* **368**, 138-148.

Barkay, T., Gillman, M., Turner, R.R., 1997. Effects of dissolved organic carbon and salinity on bioavailability of mercury. *Applied and Environmental Microbiology* **63**, 4267-4271.

Barnett, M.O., Harris, L.A., Turner, R.R., Stevenson, R.J., Henson, T.J., Melton, R.C., Hoffman, D.P., 1997. Formation of mercuric sulfide in soil. *Environmental Science & Technology* **31**, 3037-3043.

Barnett, M.O., Turner, R.R., Singer, P.C., 2001. Oxidative dissolution of metacinnabar (β-HgS) by dissolved oxygen. *Applied Geochemistry* **16**, 1499-1512.

Basinger, M.A., Casas, J.S., Jones, M.M., Weaver, A.D., 1981. Structural requirements for Hg(II) antidotes. *Journal of Inorganic and Nuclear Chemistry* **43**, 1419-1425.

Beldowski, J., Pempkowiak, J., 2003. Horizontal and vertical variabilities of mercury concentration and speciation in sediments of the Gdansk Basin, Southern Baltic Sea. *Chemosphere* **52**, 645-654.

Bell, A.M.T., Charnock, J.M., Helz, G.R., Lennie, A.R., Livens, F.R., Mosselmans, J.F.W., Pattrick, R.A.D., Vaughan, D.J., 2007. Evidence for dissolved polymeric mercury(II)-sulfur complexes? *Chemical Geology* **243**, 122-127.

Benner, R., Biddanda, B., Black, B., McCarthy, M., 1997. Abundance, size distribution, and stable carbon and nitrogen isotopic compositions of marine organic matter isolated by tangential-flow ultrafiltration. *Marine Chemistry* **57**, 243-263.

Benoit, J.M., Gilmour, C.C., Heyes, A., Mason, R.P., Miller, C.L., 2003. Geochemical and biological controls over methylmercury production and degradation in aquatic ecosystems, in: Cai, Y., Braids, O.C. (Eds.), *Biogeochemistry of Environmentally Important Trace Elements, ACS Symposium Series v. 835*. American Chemical Society, Washington, pp. 262-297.

Benoit, J.M., Gilmour, C.C., Mason, R.P., Heyes, A., 1999a. Sulfide controls on mercury speciation and bioavailability to methylating bacteria in sediment pore waters. *Environmental Science & Technology* **33**, 951-957.

Benoit, J.M., Mason, R.P., Gilmour, C.C., 1999b. Estimation of mercury-sulfide speciation in sediment pore waters using octanol-water partitioning and implications for availability to methylating bacteria. *Environmental Toxicology and Chemistry* **18**, 2138-2141.

Benoit, J.M., Mason, R.P., Gilmour, C.C., Aiken, G.R., 2001. Constants for mercury binding by dissolved organic matter isolates from the Florida Everglades. *Geochimica et Cosmochimica Acta* **65**, 4445-4451.

Black, F.J., Bruland, K.W., Flegal, A.R., 2007. Competing ligand exchange-solid phase extraction method for the determination of the complexation of dissolved inorganic mercury(II) in natural waters. *Analytica Chimica Acta* **598**, 318-333.

Bloom, N.S., Preus, E., Katon, J., Hiltner, M., 2003. Selective extractions to assess the biogeochemically relevant fractionation of inorganic mercury in sediments and soils. *Analytica Chimica Acta* **479**, 233-248.

Boszke, L., Kowalski, A., Astel, A., Barański, A., Gworek, B., Siepak, J., 2008. Mercury mobility and bioavailability in soil from contaminated area. *Environmental Geology* **55**, 1075-1087.

Brigham, M.E., Duris, J.W., Wentz, D.A., Button, D.T., Chasar, L.C., 2008. Total mercury, methylmercury, and ancillary water-quality and streamflow data for selected streams in Oregon, Wisconsin, and Florida, 2002-06, *U.S. Geological Survey Data Series 341*, p. 11.

Brigham, M.E., Wentz, D.A., Aiken, G.R., Krabbenhoft, D.P., 2009. Mercury cycling in stream ecosystems. 1. Water column chemistry and transport. *Environmental Science & Technology* **43**, 2720-2725.

Burkstaller, J.E., McCarty, P.L., Parks, G.A., 1975. Oxidation of cinnabar by Fe(III) in acid mine waters. *Environmental Science & Technology* **9**, 676-678.

Cai, Y., Jaffe, R., Jones, R.D., 1999. Interactions between dissolved organic carbon and mercury species in surface waters of the Florida Everglades. *Applied Geochemistry* **14**, 395-407.

Calvin, S., Luo, S.X., Caragianis-Broadbridge, C., McGuinness, J.K., Anderson, E., Lehman, A., Wee, K.H., Morrison, S.A., Kurihara, L.K., 2005a. Comparison of extended x-ray absorption fine structure and Scherrer analysis of x-ray diffraction as methods for determining mean sizes of polydisperse nanoparticles. *Applied Physics Letters* **87**, 1-3.

Calvin, S., Miller, M.M., Goswami, R., Cheng, S.F., Mulvaney, S.P., Whitman, L.J., Harris, V.G., 2003. Determination of crystallite size in a magnetic nanocomposite using extended x-ray absorption fine structure. *Journal of Applied Physics* **94**, 778-783.

Calvin, S., Riedel, C.J., Carpenter, E.E., Morrison, S.A., Stroud, R.M., Harris, V.G., 2005b. Estimating crystallite size in polydispersed samples using EXAFS. *Physica Scripta* **2005**, 744.

Casagrande, D.J., Idowu, G., Friedman, A., Rickert, P., Siefert, K., Schlenz, D., 1979. H_2S incorporation in coal precursors: Origins of organic sulphur in coal. *Nature* **282**, 599-600.

Charnock, J.M., Moyes, L.N., Pattrick, R.A.D., Mosselmans, J.F.W., Vaughan, D.J., Livens, F.R., 2003. The structural evolution of mercury sulfide precipitate: An XAS and XRD study. *American Mineralogist* **88**, 1197-1203.

Cheam, V., Gamble, D.S., 1974. Metal-fulvic acid chelation equilibrium in aqueous $NaNO_3$ solution - Hg(II), Cd(II), and Cu(II) fulvate complexes. *Canadian Journal of Soil Science* **54**, 413-417.

Chin, Y.P., Aiken, G., Oloughlin, E., 1994. Molecular-weight, polydispersity, and spectroscopic properties of aquatic humic substances. *Environmental Science & Technology* **28**, 1853-1858.

Choe, K.-Y., Gill, G.A., 2001. Isolation of colloidal monomethyl mercury in natural waters using cross-flow ultrafiltration techniques. *Marine Chemistry* **76**, 305-318.

Ciglenecki, I., Krznaric, D., Helz, G.R., 2005. Voltammetry of copper sulfide particles and nanoparticles: Investigation of the cluster hypothesis. *Environmental Science & Technology* **39**, 7492-7498.

Combes, J.M., Manceau, A., Calas, G., Bottero, J.Y., 1989. Formation of ferric oxides from aqueous solutions: A polyhedral approach by X-ray absorption spectroscopy: I. Hydrolysis and formation of ferric gels. *Geochimica et Cosmochimica Acta* **53**, 583-594.

Compeau, G.C., Bartha, R., 1985. Sulfate-reducing bacteria - principal methylators of mercury in anoxic estuarine sediment. *Applied and Environmental Microbiology* **50**, 498-502.

Cory, R.M., McKnight, D.M., 2005. Fluorescence spectroscopy reveals ubiquitous presence of oxidized and reduced quinones in dissolved organic matter. *Environmental Science & Technology* **39**, 8142-8149.

Cronan, C.S., Aiken, G.R., 1985. Chemistry and transport of soluble humic substances in forested watersheds of the Adirondack Park, New York. *Geochimica et Cosmochimica Acta* **49**, 1697-1705.

Deonarine, A., Hsu-Kim, H., 2009. Precipitation of mercuric sulfide nanoparticles in NOM-containing water: Implications for the natural environment. *Environmental Science & Technology* **43**, 2368-2373.

Deonarine, A., Lau, B.L.T., Aiken, G.R., Ryan, J.N., Hsu-Kim, H., 2011. Effects of humic substances on precipitation and aggregation of zinc sulfide nanoparticles. *Environmental Science & Technology* **45**, 3217-3223.

Dittman, J.A., Shanley, J.B., Driscoll, C.T., Aiken, G.R., Chalmers, A.T., Towse, J.E., Selvendiran, P., 2010. Mercury dynamics in relation to dissolved organic carbon concentration and quality during high flow events in three northeastern U.S. streams. *Water Resources Research* **46**, W07522.

Dittmar, T., Koch, B., Hertkorn, N., Kattner, G., 2008. A simple and efficient method for the solid-phase extraction of dissolved organic matter (SPE-DOM) from seawater. *Limnology and Oceanography: Methods* **6**, 230-235.

Drexel, R.T., Haitzer, M., Ryan, J.N., Aiken, G.R., Nagy, K.L., 2002. Mercury(II) sorption to two Florida Everglades peats: Evidence for strong and weak binding and competition by

dissolved organic matter released from the peat. *Environmental Science & Technology* **36**, 4058-4064.
Dyrssen, D., Wedborg, M., 1991. The sulphur-mercury(II) system in natural waters. *Water, Air, and Soil Pollution* **56**, 507-519.
Einsiedl, F., Mayer, B., Schäfer, T., 2008. Evidence for incorporation of H_2S in groundwater fulvic acids from stable isotope ratios and sulfur K-edge x-ray absorption near edge structure spectroscopy. *Environmental Science and Technology* **42**, 2439-2444.
Fellman, J.B., Hood, E., Spencer, R.G.M., 2010. Fluorescence spectroscopy opens new windows into dissolved organic matter dynamics in freshwater ecosystems: A review. *Limnology and Oceanography* **55**, 2452-2462.
Findlay, S., 2003. Bacterial Response to Variation in Dissolved Organic Matter, in: Findlay, S.E.G., Sinsabaugh, R.L. (Eds.), *Aquatic Ecosystems: Interactivity of Dissolved Organic Matter*. Academic Press, Burlington, pp. 363-379.
Fitzgerald, W.F., Lamborg, C.H., Hammerschmidt, C.R., 2007. Marine biogeochemical cycling of mercury. *Chemical Reviews* **107**, 641-662.
Fitzgerald, W.F., Lyons, W.B., 1973. Organic mercury compounds in coastal waters. *Nature* **242**, 452-453.
Fleming, E.J., Mack, E.E., Green, P.G., Nelson, D.C., 2006. Mercury methylation from unexpected sources: Molybdate-inhibited freshwater sediments and an iron-reducing bacterium. *Applied and Environmental Microbiology* **72**, 457-464.
Frenkel, A., 2007. Solving the 3D structure of nanoparticles. *Zeitschrift fuer Kristallographie* **222**, 605-611.
Frenkel, A.I., Hills, C.W., Nuzzo, R.G., 2001. A view from the inside: Complexity in the atomic scale ordering of supported metal nanoparticles. *The Journal of Physical Chemistry B* **105**, 12689-12703.
Fulton, J.R., McKnight, D.M., Foreman, C.M., Cory, R.M., Stedmon, C., Blunt, E., 2004. Changes in fulvic acid redox state through the oxycline of a permanently ice-covered Antarctic lake. *Aquatic Sciences* **66**, 27-46.
Garcia, E., Amyot, M., Ariya, P.A., 2005. Relationship between DOC photochemistry and mercury redox transformations in temperate lakes and wetlands. *Geochimica et Cosmochimica Acta* **69**, 1917-1924.
Gasper, J.D., Aiken, G.R., Ryan, J.N., 2007. A critical review of three methods used for the measurement of mercury (Hg^{2+})-dissolved organic matter stability constants. *Applied Geochemistry* **22**, 1583-1597.
Gerbig, C.A., Kim, C.S., Stegemeier, J.P., Ryan, J.N., Aiken, G.R., 2011. Formation of nanocolloidal metacinnabar in mercury-DOM-sulfide systems. *Environmental Science & Technology* **45**, 9180-9187.
Gilbert, B., Banfield, J.F., 2005. Molecular-scale processes involving nanoparticulate minerals in biogeochemical systems. *Reviews in Mineralogy & Geochemistry* **59**, 109-155.
Gilmour, C.C., Riedel, G.S., Ederington, M.C., Bell, J.T., Benoit, J.M., Gill, G.A., Stordal, M.C., 1998. Methylmercury concentrations and production rates across a trophic gradient in the northern Everglades. *Biogeochemistry* **40**, 327-345.
Gondikas, A.P., Masion, A., Auffan, M., Lau, B.L.T., Hsu-Kim, H., 2011. Early-stage precipitation kinetics of zinc sulfide nanoclusters forming in the presence of cysteine. *Chemical Geology* in press, doi:10.1016/j.chemgeo.2011.06.009.

Green, S.A., Blough, N.V., 1994. Optical absorption and fluorescence properties of chromophoric dissolved organic matter in natural waters. *Limnology and Oceanography* **39**, 1903-1916.

Grigal, D.F., 2002. Inputs and outputs of mercury from terrestrial watersheds: A review. *Environmental Reviews* **10**, 1-39.

Gu, B., Bian, Y., Miller, C.L., Dong, W., Jiang, X., Liang, L., 2011. Mercury reduction and complexation by natural organic matter in anoxic environments. *Proceedings of the National Academy of Sciences*.

Gu, B.H., Schmitt, J., Chen, Z.H., Liang, L.Y., McCarthy, J.F., 1994. Adsorption and desorption of natural organic-matter on iron-oxide - mechanisms and models. *Environmental Science & Technology* **28**, 38-46.

Gustafsson, J.P., 2010. *Visual MINTEQ*, version 3.0; Stockholm, Sweden, 2007. http://www2.lwr.kth.se/English/OurSoftware/vminteq/ (accessed January 2010).

Haitzer, M., Aiken, G.R., Ryan, J.N., 2002. Binding of mercury(II) to dissolved organic matter: The role of the mercury-to-DOM concentration ratio. *Environmental Science & Technology* **36**, 3564-3570.

Haitzer, M., Aiken, G.R., Ryan, J.N., 2003. Binding of mercury(II) to aquatic humic substances: Influence of pH and source of humic substances. *Environmental Science & Technology* **37**, 2436-2441.

Hammerschmidt, C.R., Fitzgerald, W.F., 2006. Methylmercury cycling in sediments on the continental shelf of southern New England. *Geochimica et Cosmochimica Acta* **70**, 918-930.

Hammerschmidt, C.R., Fitzgerald, W.F., Balcom, P.H., Visscher, P.T., 2008. Organic matter and sulfide inhibit methylmercury production in sediments of New York/New Jersey Harbor. *Marine Chemistry* **109**, 165-182.

Han, F., Shiyab, S., Chen, J., Su, Y., Monts, D., Waggoner, C., Matta, F., 2008. Extractability and bioavailability of mercury from a mercury sulfide contaminated soil in Oak Ridge, Tennessee, USA. *Water, Air, and Soil Pollution* **194**, 67-75.

Han, S.H., Gill, G.A., 2005. Determination of mercury complexation in coastal and estuarine waters using competitive ligand exchange method. *Environmental Science & Technology* **39**, 6607-6615.

Hatcher, P.G., Dria, K.J., Kim, S., Frazier, S.W., 2001. Modern analytical studies of humic substances. *Soil Science* **166**, 770-794.

He, Z., Traina, S.J., Weavers, L.K., 2007. Sonochemical dissolution of cinnabar (α-HgS). *Environmental Science and Technology* **41**, 773-778.

Hedberg, Y., Herting, G., Wallinder, I.O., 2011. Risks of using membrane filtration for trace metal analysis and assessing the dissolved metal fraction of aqueous media - A study on zinc, copper and nickel. *Environmental Pollution* **159**, 1144-1150.

Heitmann, T., Blodau, C., 2006. Oxidation and incorporation of hydrogen sulfide by dissolved organic matter. *Chemical Geology* **235**, 12-20.

Helms, J.R., Stubbins, A., Ritchie, J.D., Minor, E.C., Kieber, D.J., Mopper, K., 2008. Absorption spectral slopes and slope ratios as indicators of molecular weight, source, and photobleaching of chromophoric dissolved organic matter. *Limnology and Oceanography* **53**, 955-969.

Helz, G.R., Horzempa, L.M., 1983. EDTA as a kinetic inhibitor of copper(II) sulfide precipitation. *Water Research* **17**, 167-172.

Hering, J.G., Morel, F.M.M., 1989a. Slow coordination reactions in seawater. *Geochimica et Cosmochimica Acta* **53**, 611-618.
Hering, J.G., Morel, F.o.M.M., 1989b. Slow coordination reactions in seawater. *Geochimica et Cosmochimica Acta* **53**, 611-618.
Hesterberg, D., Chou, J.W., Hutchison, K.J., Sayers, D.E., 2001. Bonding of Hg(II) to reduced organic, sulfur in humic acid as affected by S/Hg ratio. *Environmental Science & Technology* **35**, 2741-2745.
Hines, M.E., Faganeli, J., Adatto, I., Horvat, M., 2006. Microbial mercury transformations in marine, estuarine and freshwater sediment downstream of the Idrija Mercury Mine, Slovenia. *Applied Geochemistry* **21**, 1924-1939.
Hintelmann, H., Welbourn, P.M., Evans, R.D., 1995. Binding of methylmercury compounds by humic and fulvic acids. *Water, Air, and Soil Pollution* **80**, 1031-1034.
Hintelmann, H., Welbourn, P.M., Evans, R.D., 1997. Measurement of complexation of methylmercury(II) compounds by freshwater humic substances using equilibrium dialysis. *Environmental Science & Technology* **31**, 489-495.
Hinton, M.J., Schiff, S.L., English, M.C., 1998. Sources and flowpaths of dissolved organic carbon during storms in two forested watersheds of the Precambrian Shield. *Biogeochemistry* **41**, 175-197.
Hoch, A.R., Reddy, M.M., Aiken, G.R., 2000. Calcite crystal growth inhibition by humic substances with emphasis on hydrophobic acids from the Florida Everglades. *Geochimica et Cosmochimica Acta* **64**, 61-72.
Holley, E.A., James McQuillan, A., Craw, D., Kim, J.P., Sander, S.G., 2007. Mercury mobilization by oxidative dissolution of cinnabar (α-HgS) and metacinnabar (β-HgS). *Chemical Geology* **240**, 313-325.
Holloway, J.M., Goldhaber, M.B., Scow, K.M., Drenovsky, R.E., 2009. Spatial and seasonal variations in mercury methylation and microbial community structure in a historic mercury mining area, Yolo County, California. *Chemical Geology* **267**, 85-95.
Honeyman, B.D., Santschi, P.H., 1989. A Brownian-pumping model for oceanic trace metal scavenging: Evidence from Th isotopes. *Journal of Marine Research* **47**, 951-992.
Horzempa, L.M., Helz, G.R., 1979. Controls on the stability of sulfide sols: Colloidal covellite as an example. *Geochimica et Cosmochimica Acta* **43**, 1645-1650.
Howard, A.G., 2010. On the challenge of quantifying man-made nanoparticles in the aquatic environment. *Journal of Environmental Monitoring* **12**, 135-142.
Hsu-Kim, H., Sedlak, D.L., 2005. Similarities between inorganic sulfide and the strong Hg(II) -complexing ligands in municipal wastewater effluent. *Environmental Science & Technology* **39**, 4035-4041.
Hsu, H., Sedlak, D.L., 2003. Strong Hg(II) complexation in municipal wastewater effluent and surface waters. *Environmental Science & Technology* **37**, 2743-2749.
Hurley, J.P., Krabbenhoft, D.P., Cleckner, L.B., Olson, M.L., Aiken, G.R., Rawlik Jr, P.S., 1998. System controls on the aqueous distribution of mercury in the northern Florida Everglades. *Biogeochemistry* **40**, 293-311.
Hyung, H., Fortner, J.D., Hughes, J.B., Kim, J.-H., 2006. Natural organic matter stabilizes carbon nanotubes in the aqueous phase. *Environmental Science & Technology* **41**, 179-184.
Jay, J.A., Morel, F.M.M., Hemond, H.F., 2000. Mercury speciation in the presence of polysulfides. *Environmental Science & Technology* **34**, 2196-2200.

Jokic, A., Cutler, J.N., Anderson, D.W., Walley, F.L., 2004. Detection of heterocyclic N compounds in whole soils using N-XANES spectroscopy. *Canadian Journal of Soil Science* **84**, 291-293.

Karger, B.L., Snyder, L.R., Horvath, C., 1973. *An Introduction to Separation Science*, First ed. Wiley-Interscience, New York.

Karlsson, T., Skyllberg, U., 2003. Bonding of ppb levels of methyl mercury to reduced sulfur groups in soil organic matter. *Environmental Science & Technology* **37**, 4912-4918.

Khwaja, A.R., Bloom, P.R., Brezonik, P.L., 2006. Binding constants of divalent mercury (Hg^{2+}) in soil humic acids and soil organic matter. *Environmental Science & Technology* **40**, 844-849.

Khwaja, A.R., Bloom, P.R., Brezonik, P.L., 2010. Binding strength of methylmercury to aquatic NOM. *Environmental Science and Technology* **44**, 6151-6156.

Kim, C.S., Bloom, N.S., Rytuba, J.J., Brown Jr, G.E., 2003. Mercury speciation by X-ray absorption fine structure spectroscopy and sequential chemical extractions: A comparison of speciation methods. *Environmental Science & Technology* **37**, 5102-5108.

Kim, C.S., Brown, G.E., Rytuba, J.J., 2000. Characterization and speciation of mercury-bearing mine wastes using X-ray absorption spectroscopy. *Science of the Total Environment* **261**, 157-168.

Kodama, H., Schnitzer, M., 1977. Effect of fulvic acid on the crystallization of Fe(III) oxides. *Geoderma* **19**, 279-291.

Krabbenhoft, D., Hurley, J., Olson, M., Cleckner, L., 1998. Diel variability of mercury phase and species distributions in the Florida Everglades. *Biogeochemistry* **40**, 311-325.

Labrenz, M., Druschel, G.K., Thomsen-Ebert, T., Gilbert, B., Welch, S.A., Kemner, K.M., Logan, G.A., Summons, R.E., Stasio, G.D., Bond, P.L., Lai, B., Kelly, S.D., Banfield, J.F., 2000. Formation of sphalerite (ZnS) deposits in natural biofilms of sulfate-reducing bacteria. *Science* **290**, 1744-1747.

Lalonde, J.D., 2001. Photooxidation of Hg(O) in artificial and natural waters. *Environmental Science and Technology* **35**, 1367-1372.

Lamborg, C.H., Fitzgerald, W.F., Skoog, A., Visscher, P.T., 2004. The abundance and source of mercury-binding organic ligands in Long Island Sound. *Marine Chemistry* **90**, 151-163.

Lamborg, C.H., Tseng, C.M., Fitzgerald, W.F., Balcom, P.H., Hammerschmidt, C.R., 2003. Determination of the mercury complexation characteristics of dissolved organic matter in natural waters with "reducible Hg" titrations. *Environmental Science & Technology* **37**, 3316-3322.

Lau, B.L.T., Hsu-Kim, H., 2008. Precipitation and growth of zinc sulfide nanoparticles in the presence of thiol-containing natural organic ligands. *Environmental Science & Technology* **42**, 7236-7241.

Lechler, P.J., Miller, J.R., Hsu, L.-C., Desilets, M.O., 1997. Mercury mobility at the Carson River Superfund Site, west-central Nevada, USA: Interpretation of mercury speciation data in mill tailings, soils, and sediments. *Journal of Geochemical Exploration* **58**, 259-267.

Lennie, A.R., Charnock, J.M., Pattrick, R.A.D., 2003. Structure of mercury(II)-sulfur complexes by EXAFS spectroscopic measurements. *Chemical Geology* **199**, 199-207.

Liang, L., Morgan, J.J., 1990. Chemical aspects of iron oxide coagulation in water: Laboratory studies and implications for natural systems. *Aquatic Sciences* **52**, 32-55.

Lindström, M., 2001. Distribution of particulate and reactive mercury in surface waters of Swedish forest lakes - An empirically based predictive model. *Ecological Modelling* **136**, 81-93.

Liu, G., Cai, Y., Philippi, T., Kalla, P., Scheidt, D., Richards, J., Scinto, L., Appleby, C., 2008. Distribution of total and methylmercury in different ecosystem compartments in the Everglades: Implications for mercury bioaccumulation. *Environmental Pollution* **153**, 257-265.

Liu, J., Aruguete, D.M., Murayama, M., Hochella, M.F., 2009. Influence of size and aggregation on the reactivity of an environmentally and industrially relevant nanomaterial (PbS). *Environmental Science & Technology* **43**, 8178-8183.

Liu, Y., Majetich, S.A., Tilton, R.D., Sholl, D.S., Lowry, G.V., 2005. TCE dechlorination rates, pathways, and efficiency of nanoscale iron particles with different properties. *Environmental Science & Technology* **39**, 1338-1345.

Lovgren, L., Sjoberg, S., 1989. Equilibrium approaches to natural-water systems - 7. Complexation reactions of copper(II), cadmium(II) and mercury(II) with dissolved organic-matter in a concentrated bog-water. *Water Research* **23**, 327-332.

Lowry, G.V., Shaw, S., Kim, C.S., Rytuba, J.J., Brown, G.E., 2004. Macroscopic and microscopic observations of particle-facilitated mercury transport from New Idria and Sulphur Bank mercury mine tailings. *Environmental Science & Technology* **38**, 5101-5111.

Lu, X.Q., Maie, N., Hanna, J.V., Childers, D.L., Jaffe, R., 2003. Molecular characterization of dissolved organic matter in freshwater wetlands of the Florida Everglades. *Water Research* **37**, 2599-2606.

Ma, H., Allen, H.E., Yin, Y., 2001. Characterization of isolated fractions of dissolved organic matter from natural waters and a wastewater effluent. *Water Research* **35**, 985-996.

Maie, N., Jaffé, R., Miyoshi, T., Childers, D., 2006. Quantitative and qualitative aspects of dissolved organic carbon leached from senescent plants in an oligotrophic wetland. *Biogeochemistry* **78**, 285-314.

Manceau, A., Nagy, K.L., 2008. Relationships between Hg(II)-S bond distance and Hg(II) coordination in thiolates. *Dalton Transactions*, 1421-1425.

Marvin-DiPasquale, M., Lutz, M.A., Brigham, M.E., Krabbenhoft, D.P., Aiken, G.R., Orem, W.H., Hall, B.D., 2009. Mercury cycling in stream ecosystems. 2. Benthic methylmercury production and bed sediment-pore water partitioning. *Environmental Science & Technology* **43**, 2726-2732.

Mason, R.P., Reinfelder, J.R., Morel, F.M.M., 1995. Bioaccumulation of mercury and methylmercury. *Water Air and Soil Pollution* **80**, 915-921.

Mason, R.P., Sullivan, K.A., 1998. Mercury and methylmercury transport through an urban watershed. *Water Research* **32**, 321-330.

McKnight, D.M., Aiken, G.R., 1998. Sources and age of aquatic humic substances, in: Hessen, D.O., Tranvik, L.J. (Eds.), *Aquatic Humic Substances: Ecology and Biogeochemistry (Ecological Studies v. 133)*. Springer-Verlag, Berlin, Germany, pp. 9-40.

McKnight, D.M., Bencala, K.E., Zellweger, G.W., Aiken, G.R., Feder, G.L., Thorn, K.A., 1992. Sorption of dissolved organic-carbon by hydrous aluminum and iron-oxides occurring at the confluence of Deer Creek with the Snake River, Summit County, Colorado. *Environmental Science & Technology* **26**, 1388-1396.

Mierle, G., Ingram, R., 1991. The role of humic substances in the mobilization of mercury from watersheds. *Water, Air, and Soil Pollution* **56**, 349-357.
Mikac, N., Foucher, D., Niessen, S., Lojen, S., Fischer, J.C., 2003. Influence of chloride and sediment matrix on the extractability of HgS (cinnabar and metacinnabar) by nitric acid. *Analytical and Bioanalytical Chemistry* **377**, 1196-1201.
Miller, C.L., Mason, R.P., Gilmour, C.C., Heyes, A., 2007. Influence of dissolved organic matter on the complexation of mercury under sulfidic conditions. *Environmental Toxicology and Chemistry* **26**, 624-633.
Miller, C.L., Southworth, G., Brooks, S., Liang, L., Gu, B., 2009. Kinetic controls on the complexation between mercury and dissolved organic matter in a contaminated environment. *Environmental Science & Technology* **43**, 8548-8553.
Miskimmin, B.M., Rudd, J.W.M., Kelly, C.A., 1992. Influence of dissolved organic carbon, pH, and microbial respiration rates on mercury methylation and demethylation in lake water. *Canadian Journal of Fisheries and Aquatic Sciences* **49**, 17-22.
Moran, M.A., Covert, J.S., 2003. Photochemically mediated linkages between dissolved organic matter and bacterioplankton, in: Findlay, S.E.G., Sinsabaugh, R.L. (Eds.), *Aquatic Ecosystems: Interactivity of Dissolved Organic Matter*. Academic Press, Burlington, pp. 243-262.
Moreau, J.W., Weber, P.K., Martin, M.C., Gilbert, B., Hutcheon, I.D., Banfield, J.F., 2007. Extracellular proteins limit the dispersal of biogenic nanoparticles. *Science* **316**, 1600-1603.
Morel, F.M.M., Kraepiel, A.M.L., Amyot, M., 1998. The chemical cycle and bioaccumulation of mercury. *Annual Review of Ecology and Systematics* **29**, 543-566.
Nagy, K.L., Manceau, A., Gasper, J.D., Ryan, J.N., Aiken, G.R., 2011. Metallothionein-like multinuclear clusters of mercury(II) and sulfur in peat. *Environmental Science & Technology* **45**, 7298-7306.
NIST, National Institude of Standards and Technology, 2004. NIST Critically Selected Stability Constants of Metal Complexes Database, 8.0 ed. NIST, Gaithersburg, MD.
O'Driscoll, N.J., Evans, R.D., 2000. Analysis of methyl mercury binding to freshwater humic and fulvic acids by gel permeation chromatography/hydride generation ICP-MS. *Environmental Science & Technology* **34**, 4039-4043.
O'Driscoll, N.J., Siciliano, S.D., Lean, D.R.S., Amyot, M., 2006. Gross photoreduction kinetics of mercury in temperate freshwater lakes and rivers: Application to a general model of DGM dynamics. *Environmental Science and Technology* **40**, 837-843.
Paquette, K., Helz, G., 1995. Solubility of cinnabar (red HgS) and implications for mercury speciation in sulfidic waters. *Water Air and Soil Pollution* **80**, 1053-1056.
Paquette, K.E., Helz, G.R., 1997. Inorganic speciation of mercury in sulfidic waters: The importance of zero-valent sulfur. *Environmental Science & Technology* **31**, 2148-2153.
Pédrot, M., Boudec, A.L., Davranche, M., Dia, A., Henin, O., 2011. How does organic matter constrain the nature, size and availability of Fe nanoparticles for biological reduction? *Journal of Colloid and Interface Science* **359**, 75-85.
Perdue, E.M., 1998. Chemical composition, structure and metal binding properties, in: Hessen, D.O., Tranvik, L.J. (Eds.), *Aquatic Humic Substances: Ecology and Biogeochemistry (Ecological Studies v. 133)*. Springer-Verlag, Berlin, Germany, pp. 41-62.
Potter, R.W., Barnes, H.L., 1978. Phase relations in the binary Hg-S. *American Mineralogist* **63**, 1143-1152.

Prietzel, J., Thieme, J., Salome, M., Knicker, H., 2007. Sulfur K-edge XANES spectroscopy reveals differences in sulfur speciation of bulk soils, humic acid, fulvic acid, and particle size separates. *Soil Biology & Biochemistry* **39**, 877-890.

Qian, J., Skyllberg, U., Frech, W., Bleam, W.F., Bloom, P.R., Petit, P.E., 2002. Bonding of methyl mercury to reduced sulfur groups in soil and stream organic matter as determined by x-ray absorption spectroscopy and binding affinity studies. *Geochimica et Cosmochimica Acta* **66**, 3873-3885.

Qualls, R.G., Richardson, C.J., 2003. Factors controlling concentration, export, and decomposition of dissolved organic nutrients in the Everglades of Florida. *Biogeochemistry* **62**, 197-229.

Ravichandran, M., 2004. Interactions between mercury and dissolved organic matter - a review. *Chemosphere* **55**, 319-331.

Ravichandran, M., Aiken, G.R., Reddy, M.M., Ryan, J.N., 1998. Enhanced dissolution of cinnabar (mercuric sulfide) by dissolved organic matter isolated from the Florida Everglades. *Environmental Science & Technology* **32**, 3305-3311.

Ravichandran, M., Aiken, G.R., Ryan, J.N., Reddy, M.M., 1999. Inhibition of precipitation and aggregation of metacinnabar (mercuric sulfide) by dissolved organic matter isolated from the Florida Everglades. *Environmental Science & Technology* **33**, 1418-1423.

Rehr, J.J., Mustre de Leon, J., Zabinsky, S.I., Albers, R.C., 1991. Theoretical x-ray absorption fine structure standards. *Journal of the American Chemical Society* **113**, 5135-5140.

Rickard, D., Luther III, G.W., 2006. Metal sulfide complexes and clusters, in: Vaughan, D.J. (Ed.), *Sulfide Mineraology and Geochemistry*. Mineralogical Society of America, pp. 421-504.

Rossotti, F.J.C., Whewell, R.J., 1977. Structure and stability of carboxylate complexes. Part 16. Stability constants of some mercury(II) carboxylates. *Journal of the Chemical Society, Dalton Transactions* **12**, 1223-1229.

Rozan, T.F., Lassman, M.E., Ridge, D.P., Luther, G.W., 2000. Evidence for iron, copper and zinc complexation as multinuclear sulphide clusters in oxic rivers. *Nature* **406**, 879-882.

Rytuba, J.J., 2000. Mercury mine drainage and processes that control its environmental impact. *Science of the Total Environment* **260**, 57-71.

Saraceno, J.F., Pellerin, B.A., Downing, B.D., Boss, E., Bachand, P.A.M., Bergamaschi, B.A., 2009. High-frequency in situ optical measurements during a storm event: Assessing relationships between dissolved organic matter, sediment concentrations, and hydrologic processes. *Journal of Geophysical Research* **114**, G00F09.

Schaefer, J.K., Morel, F.M.M., 2009. High methylation rates of mercury bound to cysteine by *Geobacter sulfurreducens*. *Nature Geoscience* **2**, 123-126.

Schaefer, J.K., Rocks, S.S., Zheng, W., Liang, L., Gu, B., Morel, F.M.M., 2011. Active transport, substrate specificity, and methylation of Hg(II) in anaerobic bacteria. *Proceedings of the National Academy of Sciences* **108**, 8714-8719.

Schwarzenbach, G., Schellenberg, M., 1965. Die komplexchemie des methylquecksilber-kations. *Helvetica Chimica Acta* **48**, 28-46.

Shanley, J.B., Alisa Mast, M., Campbell, D.H., Aiken, G.R., Krabbenhoft, D.P., Hunt, R.J., Walker, J.F., Schuster, P.F., Chalmers, A., Aulenbach, B.T., Peters, N.E., Marvin-DiPasquale, M., Clow, D.W., Shafer, M.M., 2008. Comparison of total mercury and methylmercury cycling at five sites using the small watershed approach. *Environmental Pollution* **154**, 143-154.

Shea, D., Helz, G., 1989. Solubility product constants of covellite and a poorly crystalline copper sulfide precipitate at 298 K. *Geochimica et Cosmochimica Acta* **53**, 229.
Skyllberg, U., 2008. Competition among thiols and inorganic sulfides and polysulfides for Hg and MeHg in wetland soils and sediments under suboxic conditions: Illumination of controversies and implications for MeHg net production. *Journal of Geophysical Research-Biogeosciences* **113**, 14.
Skyllberg, U., Bloom, P.R., Qian, J., Lin, C.M., Bleam, W.F., 2006. Complexation of mercury(II) in soil organic matter: EXAFS evidence for linear two-coordination with reduced sulfur groups. *Environmental Science & Technology* **40**, 4174-4180.
Skyllberg, U., Qian, J., Frech, W., Xia, K., Bleam, W.F., 2003. Distribution of mercury, methyl mercury and organic sulphur species in soil, soil solution and stream of a boreal forest catchment. *Biogeochemistry* **64**, 53-76.
Skyllberg, U., Xia, K., Bloom, P.R., Nater, E.A., Bleam, W.F., 2000. Binding of mercury(II) to reduced sulfur in soil organic matter along upland-peat soil transects. *Journal of Environmental Quality* **29**, 855-865.
Sleighter, R.L., Liu, Z., Xue, J., Hatcher, P.G., 2010. Multivariate statistical approaches for the characterization of dissolved organic matter analyzed by ultrahigh resolution mass spectrometry. *Environmental Science & Technology* **44**, 7576-7582.
Slowey, A.J., 2010. Rate of formation and dissolution of mercury sulfide nanoparticles: The dual role of natural organic matter. *Geochimica et Cosmochimica Acta* **74**, 4693-4708.
Slowey, A.J., Johnson, S.B., Rytuba, J.J., Brown, G.E., 2005a. Role of organic acids in promoting colloidal transport of mercury from mine tailings. *Environmental Science & Technology* **39**, 7869-7874.
Slowey, A.J., Rytuba, J.J., Brown, G.E., 2005b. Speciation of mercury and mode of transport from placer gold mine tailings. *Environmental Science & Technology* **39**, 1547-1554.
Solomon, D., Lehmann, J., Martinez, C.E., 2003. Sulfur K-edge XANES spectroscopy as a tool for understanding sulfur dynamics in soil organic matter. *Soil Science Society of America Journal* **67**, 1721-1731.
Spencer, R.G.M., Aiken, G.R., Butler, K.D., Dornblaser, M.M., Striegl, R.G., Hernes, P.J., 2009. Utilizing chromophoric dissolved organic matter measurements to derive export and reactivity of dissolved organic carbon exported to the Arctic Ocean: A case study of the Yukon River, Alaska. *Geophysical Research Letters* **36**, L06401.
Spencer, R.G.M., Baker, A., Ahad, J.M.E., Cowie, G.L., Ganeshram, R., Upstill-Goddard, R.C., Uher, G., 2007. Discriminatory classification of natural and anthropogenic waters in two U.K. estuaries. *Science of the Total Environment* **373**, 305-323.
Stein, E.D., Cohen, Y., Winer, A.M., 1996. Environmental distribution and transformation of mercury compounds. *Critical Reviews in Environmental Science and Technology* **26**, 1-43.
Stenson, A.C., Marshall, A.G., Cooper, W.T., 2003. Exact masses and chemical formulas of individual Suwannee River fulvic acids from ultrahigh resolution electrospray ionization Fourier transform ion cyclotron resonance mass spectra. *Analytical Chemistry* **75**, 1275-1284.
Stubbins, A., Hubbard, V., Uher, G., Law, C.S., Upstill-Goddard, R.C., Aiken, G.R., Mopper, K., 2008. Relating carbon monoxide photoproduction to dissolved organic matter functionality. *Environmental Science & Technology* **42**, 3271-3276.
Stumm, W., Morgan, J.J., 1996. *Aquatic Chemistry*, 3rd ed. Wiley-Interscience, New York.

Thurman, E.M., Malcolm, R.L., 1981. Preparative isolation of aquatic humic substances. *Environmental Science & Technology* **15**, 463-466.
Tiller, C.L., O'Melia, C.R., 1993. Natural organic matter and colloidal stability: Models and measurements. *Colloids and Surfaces A: Physicochemical and Engineering Aspects* **73**, 89-102.
Tipping, E., 2007. Modelling the interactions of Hg(II) and methylmercury with humic substances using WHAM/Model VI. *Applied Geochemistry* **22**, 1624-1635.
Tossell, J.A., 2001. Calculation of the structures, stabilities, and properties of mercury sulfide species in aqueous solution. *The Journal of Physical Chemistry A* **105**, 935-941.
Town, R.M., Filella, M., 2000. Dispelling the myths: Is the existence of L1 and L2 ligands necessary to explain metal ion speciation in natural waters? *Limnology and Oceanography* **45**, 1341-1357.
Tranvik, L.J., 1998. Degradation of dissolved organic matter in humic waters by bacteria, in: Hessen, D.O., Tranvik, L.J. (Eds.), *Aquatic Humic Substances: Ecology and Biogeochemistry (Ecological Studies v. 133)*. Springer-Verlag, Berlin, Germany, pp. 259-283.
Vairavamurthy, A., Wang, S., 2002. Organic nitrogen in geomacromolecules: Insights on speciation and transformation with K-edge XANES spectroscopy. *Environmental Science & Technology* **36**, 3050-3056.
Vairavamurthy, M.A., Maletic, D., Wang, S., Manowitz, B., Eglinton, T., Lyons, T., 1997. Characterization of sulfur-containing functional groups in sedimentary humic substances by X-ray absorption near-edge structure spectroscopy. *Energy and Fuels* **11**, 546-553.
Wang, L., Chin, Y.-P., Traina, S.J., 1997. Adsorption of (poly)maleic acid and an aquatic fulvic acid by goethite. *Geochimica et Cosmochimica Acta* **61**, 5313-5324.
Wang, Q., Kim, D., Dionysiou, D.D., Sorial, G.A., Timberlake, D., 2004. Sources and remediation for mercury contamination in aquatic systems - A literature review. *Environmental Pollution* **131**, 323-336.
Waples, J.S., Nagy, K.L., Aiken, G.R., Ryan, J.N., 2005. Dissolution of cinnabar (HgS) in the presence of natural organic matter. *Geochimica et Cosmochimica Acta* **69**, 1575-1588.
Webb, S.M., 2005. SIXpack: a graphical user interface for XAS analysis using IFEFFIT. *Physica Scripta* **2005**, 1011.
Weber, F.A., Voegelin, A., Kaegi, R., Kretzschmar, R., 2009. Contaminant mobilization by metallic copper and metal sulphide colloids in flooded soil. *Nature Geoscience* **2**, 267-271.
Weishaar, J.L., Aiken, G.R., Bergamaschi, B.A., Fram, M.S., Fujii, R., Mopper, K., 2003. Evaluation of specific ultraviolet absorbance as an indicator of the chemical composition and reactivity of dissolved organic carbon. *Environmental Science & Technology* **37**, 4702-4708.
Wetzel, R.G., 2001. *Limnology: Lake and River Ecosystems, Third edition*. Academic Press, Orlando, FL.
Xia, K., Skyllberg, U.L., Bleam, W.F., Bloom, P.R., Nater, E.A., Helmke, P.A., 1999. X-ray absorption spectroscopic evidence for the complexation of Hg(II) by reduced sulfur in soil humic substances. *Environmental Science & Technology* **33**, 257-261.
Yin, Y.J., Allen, H.E., Huang, C.P., Sanders, P.F., 1997. Interaction of Hg(II) with soil-derived humic substances. *Analytica Chimica Acta* **341**, 73-82.

Yoon, S.J., Diener, L.M., Bloom, P.R., Nater, E.A., Bleam, W.F., 2005. X-ray absorption studies of CH_3Hg^+-binding sites in humic substances. *Geochimica et Cosmochimica Acta* **69**, 1111-1121.

Zepp, R.G., Faust, B.C., Hoigne, J., 1992. Hydroxyl radical formation in aqueous reactions (pH 3-8) of iron(II) with hydrogen peroxide: the photo-Fenton reaction. *Environmental Science & Technology* **26**, 313-319.

Zhang, H., 2006. Photochemical redox reactions of mercury, *Structure and Bonding*, pp. 37-79.

Appendix

Appendix Table A1. Solution composition and Hg L_{III}-EXAFS fitting results for Hg-S coordination numbers (CN), interatomic distances (R), and Debye-Waller factors (σ^2)

	Experimental Parameters				EXAFS Results for Hg-S Bonds		
Figure[a]	$[Hg]_T$ (nM)	[DOM] (mg L^{-1})	Hg:DOM (nmol:mg)	$[H_2S]_T$ (μM)	CN	R (Å)	σ^2 ($Å^2$)[b]
2.3a	180	45.4	4.0	0	2.4±0.2	2.35±0.01	0.007
2.3b	94	50[c]	1.9	100	2.3±0.2	2.51±0.02	0.007
2.3c	50	10.3	4.9	100	2.9±0.2	2.52±0.01	0.007
2.3d	415	12.1	34	100	3.3±0.2	2.53±0.01	0.007

Note: EXAFS fitting errors represent 95% confidence levels (±2σ).
[a] refers to EXAFS spectra in Figure 2.3.
[b] value fixed.
[c] approximate; calculated from mass of isolate used in preparation.

Appendix Table A2. Thermodynamic constants used for mercury speciation modeling (25°C, ionic strength = 0 M).

Reactions	log K	Source
$HgS_{(s)} + H^+ = Hg^{2+} + HS^-$	-38 ± 2	(NIST, 1993)
$Hg^{2+} + HS^- = HgSH^+$	30.2	(Benoit et al., 1999b)
$Hg^{2+} + HS^- = HgS^0 + H^+$	26.5	(Benoit et al., 1999b)
$Hg^{2+} + 2HS^- = Hg(HS)_2{}^0$	37.7	(Dyrssen and Wedborg, 1991)
$Hg^{2+} + 2HS^- = HgHS_2{}^- + H^+$	31.5	(Dyrssen and Wedborg, 1991)
$Hg^{2+} + 2HS^- = HgHS_2{}^{-2} + 2H^+$	23.2	(Dyrssen and Wedborg, 1991)
$Hg^{2+} + RS_2{}^{-2} = Hg(RS_2)$	34.9	(Haitzer et al., 2003)
$RS_2{}^{-2} + H^+ = RS_2H^-$	8.4	(Khwaja et al., 2006)
$RS_2{}^{-2} + 2H^+ = RS_2H_2{}^0$	16.8	(Khwaja et al., 2006)
$Hg^{2+} + H_2O = HgOH^+ + H^+$	-3.4	(NIST, 1993)
$Hg^{2+} + 2H_2O = Hg(OH)_2{}^0 + 2H^+$	-6.2	(NIST, 1993)
$Hg^{2+} + 3H_2O = Hg(OH)_3{}^- + 3H^+$	-21.1	(NIST, 1993)

The constants used in this study are the same as those used by Deonarine et al. (2009) with one exception; they are reproduced here with their primary reference. The one exception is the constant for HgS^0, which was not used in Deonarine et al. (2009). The constants for hydroxide complexes and DOM binding are included only for completeness; they do not play a significant role in mercury speciation in the presence of sulfide. All speciation calculations were done with Visual MINTEQ (Gustafsson, 2010) and the standard library of constants, except for those noted in the table. Visual MINTEQ uses $Hg(OH)_2$ as the mercury component, which required all equations to be written in terms of $Hg(OH)_2$. The simpler, Hg^{2+}-based equations are reproduced here.

Table A3. Site descriptions for DOM isolates.[a]

DOM Sample	Site Description
Everglades F1 hydrophobic acid (F1 HPoA) Everglades F1 transphilic acid (F1 TPiA)	Eutrophied marshland located in Water Conservation Area 2A in the Everglades. Vegetation dominated by cattails. (26°21'35" N; 80°22'14" W)
Everglades 2BS hydrophobic acid (2BS HPoA)	Relatively pristine marshland located in Water Conservation Area 2B in the northern Everglades. Vegetation dominated by saw grass. (26°09'00" N; 82°22'30" W)
Ogeechee River fulvic acid Ogeechee River humic acid	Small river draining the Piedemeont in Eastern Georgia. Sampled at Grange, Georgia. Vegetation types: Oak-Hickory-Pine forest (Quercus, Carya, Pinus)
Ohio River fulvic acid (OhR FA) Ohio River humic acid (OhR HA) Ohio River hydrophobic acid (OhR HPoA)	Marjor river drainging east-central United States. Sampled at Cincinatti, Ohio. Vegetation types: Appalachian Oak Forest, Mixed Mesophytic Forest, Oak Hickory Forest.
Pacific Ocean fulvic acid (PO FA)	Sample collected from 100 m depth, 170 km southwest of Honolulu, Hawaii, marine organic matter
Suwannee River fulvic acid (SR FA) Suwannee River humic acid (SR HA) Suwannee River hydrophobic acid (SR HPoA)	Black water river draining the Okeefenokee Swamp. Sampled at Fargo, Georgia. Vegetation types: Souther Floodplain Forest (Quercus, Nyassa, Taxodium). Humic and fulvic acids are International Humic Substances Society standards.
Williams Lake hydrophobic acid (WL HPoA)	Seepage lake in north-central Minnesota. Organic matter dominated by autochthonous sources (algae, bacteria, emergent

[a]Site descriptions reproduced from Waples et al. (2005).

Table A4. Chemical characteristics of dissolved organic matter isolates.[a]

	Elemental Composition						Molecular	^{13}C-NMR (% of total area)						Reduced S	$SUVA_{280nm}$
DOM	C (wt%)	H (wt%)	O (wt%)	N (wt%)	S (wt%)	Ash (wt%)	Weight (Da)	Aliphatic I (0-62 ppm)	Aliphatic II (62-90 ppm)	Acetal (90-110 ppm)	Aromatic (110-160 ppm)	Carboxyl (160-190 ppm)	Ketone (190-230 ppm)	(mol% total S)	($L\ mgC^{-1}\ m^{-1}$)
Everglades F1 hydrophobic acid (F1 HPoA)	52.2	4.64	39.9	1.53	1.73	9.37	1031	33.1	8.9	2.3	25.4	23.1	7.2	28.7	3.09
Everglades 2BS hydrophobic acid (2BS HPoA)	52.3	4.79	40.2	1.58	1.23	7.31	953	39.5	9.2	1.6	21.3	22.2	6.3	30.4	2.27
Ogeechee River fulvic acid (OgR FA)	54.0	4.02	38.5	0.93	1.27	0.39	1021	33	13.9	6.8	24.7	18.3	3.3	22.6	2.89
Ogeechee River humic acid (OgR HA)	54.6	4.9	36.8	1.6	1.8	3.9	1906	24.7	10.4	7.3	40.8	15.1	1.6	19.5	5.28
Ohio River fulvic acid (OhR FA)	55.5	5.4	35.9	1.5	1.28	0.57	705	33.6	15.2	5.6	24.3	19.3	1.6	22.4	2.17
Ohio River humic acid (OhR HA)[b]	57.4	4.73	34.1	2.31	1.49	n.a.	2544	n.a.	n.a.	n.a.	n.a.	n.a.	n.a.	n.a.	4.9
Pacific Ocean fulvic Acid (PO FA)	56.2	6.0	36.3	1.1	0.4	0.36	532	56.9	13.4	1.2	7.3	19.5	1.6	12.5	0.44
Suwannee River fulvic acid (SR FA)	54.2	3.92	38.0	0.72	0.35	0.19	1360	35	10.1	5	22.9	21.3	5.6	16.6	3.01
Suwannee River humic acid (SR HA)	53.4	3.9	40.9	1.1	0.68	4.13	1399	21.3	7.3	6.6	35.1	20.7	9	18.3	5.47
Williams Lake hydrophobic acid (WL HPoA)[c]	52.7	5.2	36.6	1.7	0.72	2.98	772	50	15	5.8	13.8	13.9	1.5	n.a.	1.32
Williams Lake hydrophobic acid (WL HPoA)[d]	55.2	5.73	36.5	1.76	0.75	2.1	n.a.	n.a.	n.a.	n.a.	n.a.	n.a.	n.a.	n.a.	1.40

[a]Data from Waples et al. (2005) and citations therein, unless otherwise noted. No published data available for Everglades F1 transphilic acid (F1 TPiA), Ohio River hydrophobic acid (OhR HPoA), or Suwannee River hydrophobic acid (SR HPoA). [b]Data from Deonarine et al. (2011). [c]WL HPoA isolate reported in Waples et al. (2005) and used in the reducible mercury study (Chapter 4). [d]WL HPoA isolate used for EXAFS study (Chapter 3), reported on an ash-free basis. Not reported in Waples et al. (2005).

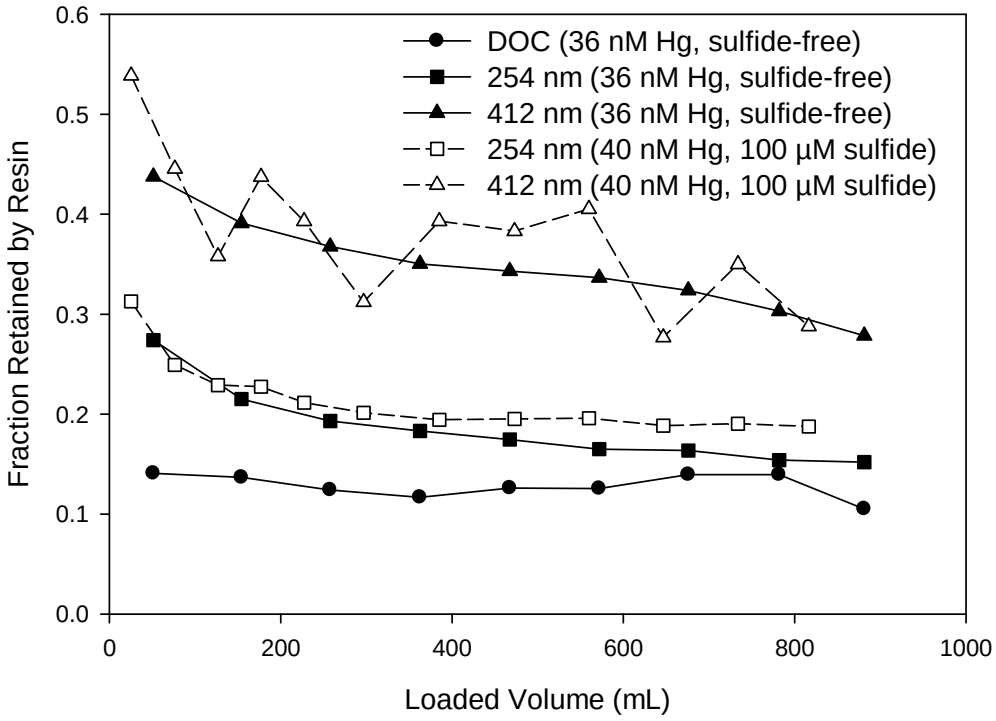

Appendix Figure A1. The fraction of DOC and UV-vis-absorbing components retained by the chromatography resin as a function of loaded volume for a sulfide-free (filled symbols) and a sulfide-containing (open symbols) system. The DOM adsorption for the range of mercury concentrations (0.35 nM – 1.4 µM) is represented well by the two systems depicted.

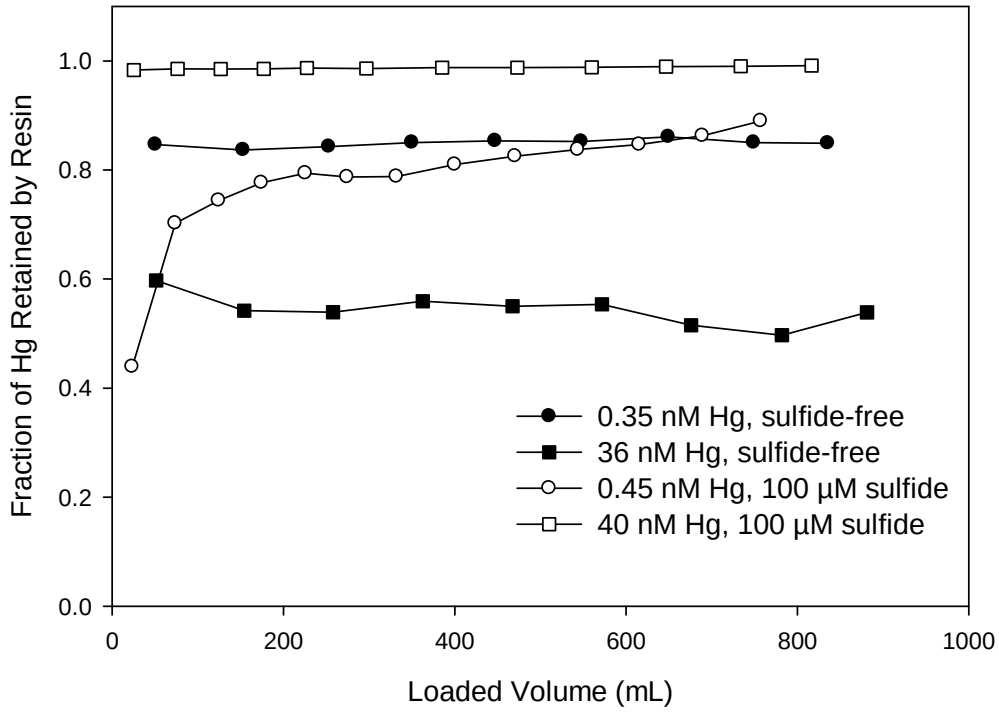

Appendix Figure A2. The fraction of mercury retained by the chromatography resin as a function of loaded volume for four representative solutions. The 0.35 nM Hg sulfide-free data are typical of 0.35 nM – 3.4 nM Hg sulfide-free systems. The 36 nM Hg sulfide-free data are typical of 13 nM – 1.4 µM Hg sulfide-free systems. The 40 nM Hg sulfide-containing data are typical of all sulfide-containing systems (1.5 – 490 nM Hg) except for the 0.45 nM Hg sulfide-containing system.

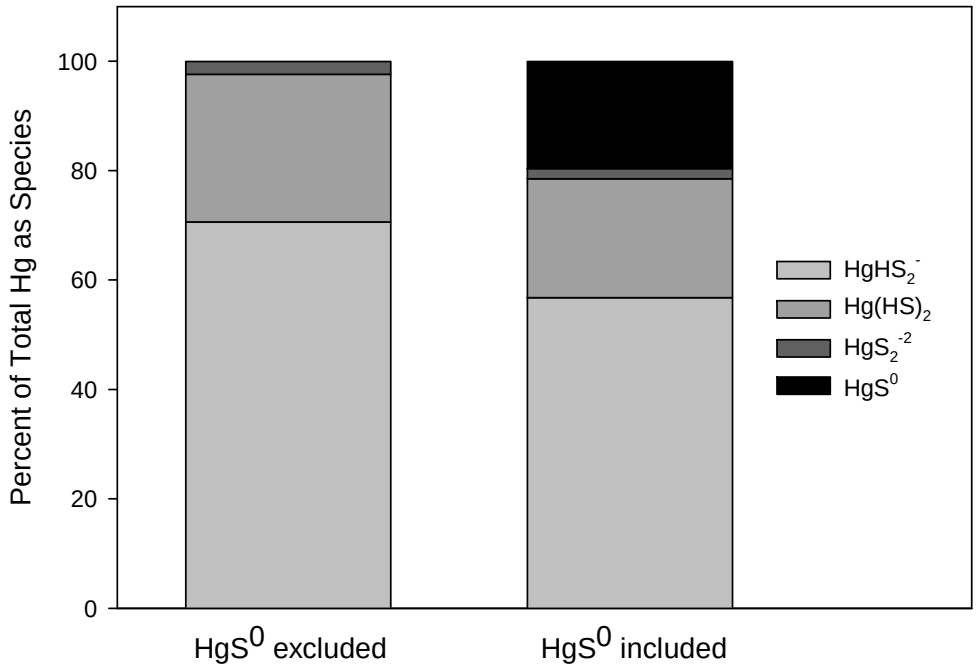

Appendix Figure A3. The speciation of mercury (2 nM total) in the presence of sulfide (100 μM total), and DOM (10 mg L^{-1}, modeled as 40 nM $RS_{2,T}$) at pH 6.5 and I 0.1 M as calculated using Visual MINTEQ (Gustafsson, 2010) using the constants in Appendix Table A2 and the highest metacinnabar solubility product.

The uncertainty in the metacinnabar solubility product gives rise to uncertain mercury speciation in our sulfidic systems below approximately 4 nM total mercury. When the solubility product is lowest (log K_{s0} = -40), precipitation of metacinnabar is predicted. When the solubility product is highest (log K_{s0} = -36), the model predicts several mercury-sulfide complexes dominate mercury speciation. Of the possible species, the presence of HgS^0 is debated (Deonarine and Hsu-Kim, 2009). Regardless of the inclusion of HgS^0, mercury speciation would be dominated by charged mercury sulfide complexes if metacinnabar has not precipitated (73% charged when HgS^0 is excluded and 59% charged when HgS^0 is included).

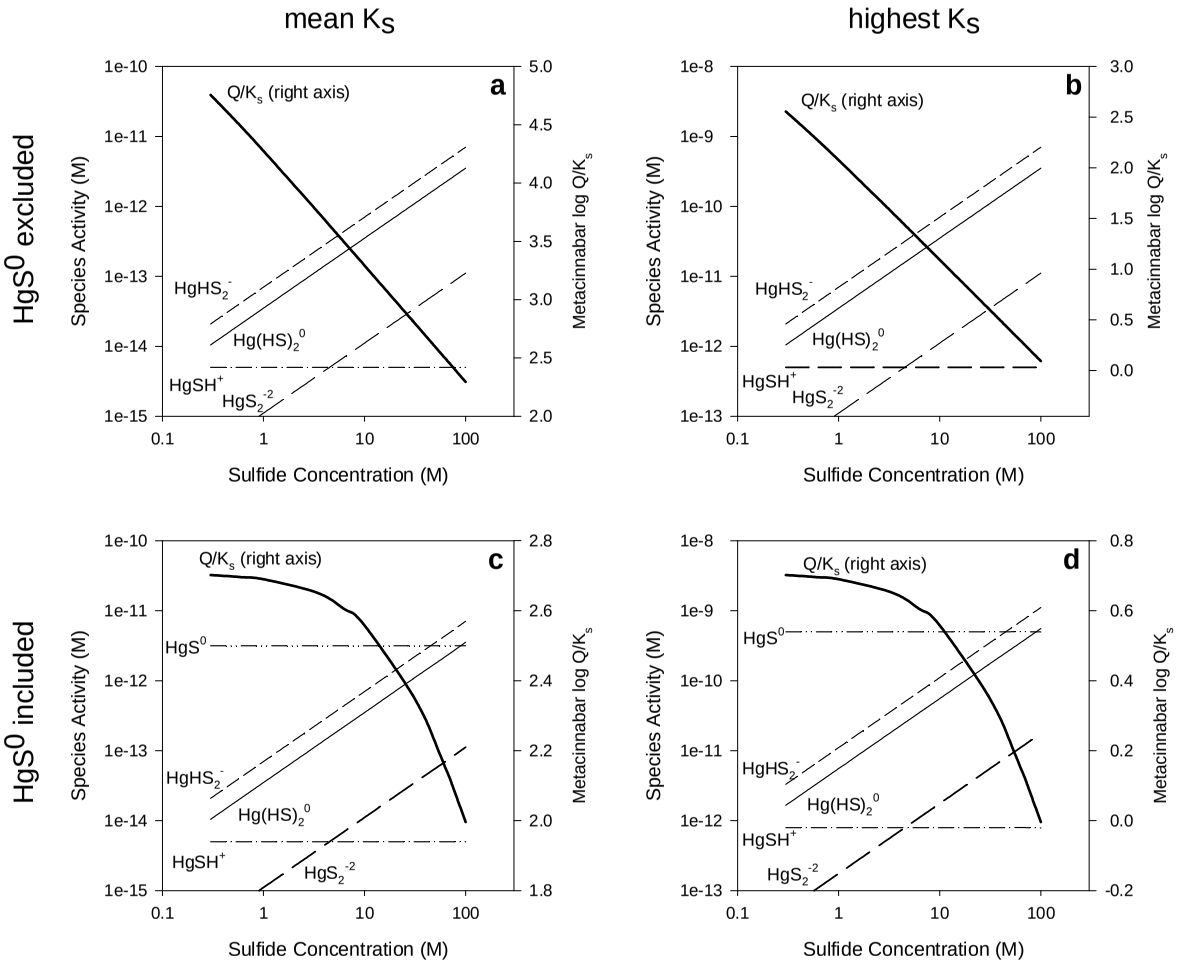

Appendix Figure A4. The speciation of mercury (2.5 nM) with sulfide and DOM (10 mg L^{-1} DOM modeled as $RS_{2,T}$ = 40 nM) at pH 6.5, I 0.1M as calculated by Visual MINTEQ (Gustafsson, 2010) using the constants in Apendix Table A2. The metacinnabar solubility product (K_s) was varied between the mean reported value and the highest end of the solubility constant range. Calculations were done with and without HgS^0 as a possible complex. The solubility quotient, Q, was calculated before metacinnabar precipitation, and the species concentrations are calculated in equilibrium with any potential metacinnabar. DOM was included in the calculations, but the activity of the Hg-DOM complex is too small to appear on the scale.

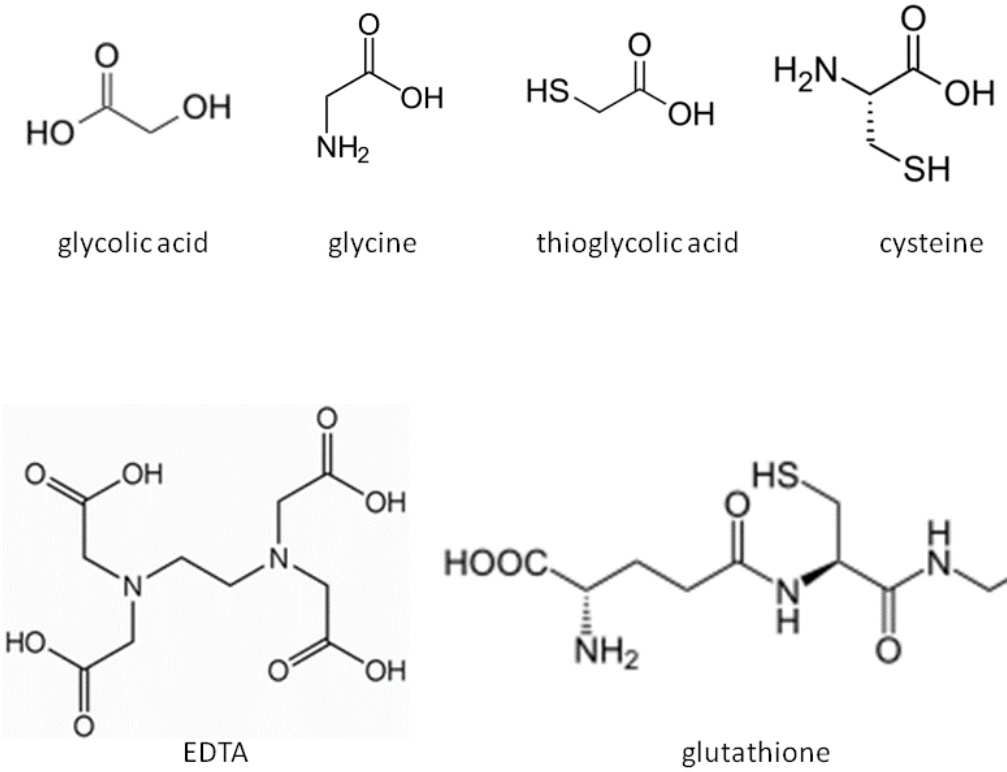

Appendix Figure A5. Structures of the model ligands used in reducible mercury experiments.

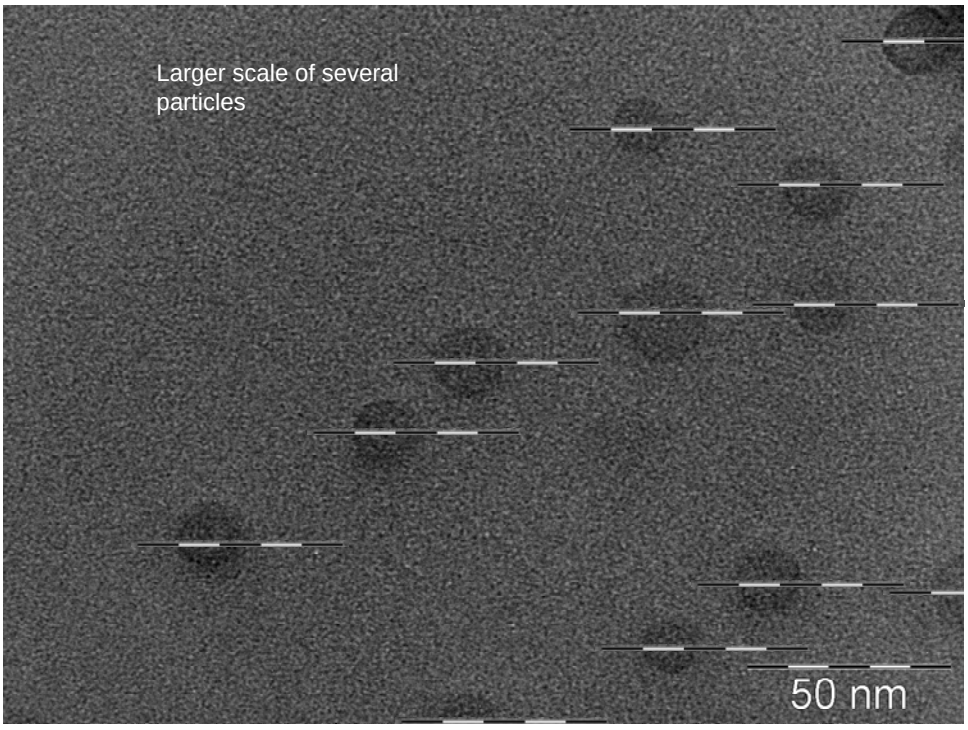

Appendix Figure A6. Transmission electron microscope image of several mercury-containing particles. The mercury in the particles was identified with energy dispersive spectroscopy. Mercury and sulfur were identified in the particles, but the relative quantities could not be reliably measured. The particles were not stable in the electron beam. They enlarged and disappeared within one minute. The solution that was dried on to the microscopy grid contained 50 nM Hg_T, 100 μM H_2S_T, and 20 mg L^{-1} F1 HPoA at pH 6.5 and I 0.0024 M.